DELIVERABLE

WP7 - Deliverable 7.4: Towards improvement of site condition indicators

Work package	WP7/NA5 – Task 7.4: Towards improvement of site characterization indicators
Lead	SED-ETHZ
Authors	Paolo Bergamo, Conny Hammer, Donat Fäh. SED, ETH Zurich
Reviewers	C. Cornou, CNRS
Approval	Management Board
Status	Final
Dissemination level	Public
Delivery deadline	[31.10.2019]
Submission date	[31.10.2019]
Intranet path	DOCUMENTS/DELIVERABLES/SERA_D7.4_IMPROVEMENT_SITE_INDICATORS.pdf

Table of Contents

Summary

This report summarizes the research undertaken by ETH in the framework of WP7/NA5 – Task 7.4 of SERA project ("Towards improvement of site characterization indicators"), in collaboration with partners AUTH, INGV, CNRS. We have addressed the broad topic of site condition indicators, or proxies, with a comprehensive work: i) firstly, we have reviewed the state of the art and tracked the present research trends in the use of proxies; ii) secondly, to test their applicability at a wide scale, we have compiled an extensive database of site condition parameters, covering more than 1000 instrumented sites in Switzerland and Japan, and paired it with a companion dataset of empirically-derived local amplification functions. In this phase of data collection, particular attention was dedicated to the harmonization of information derived from disparate sources and referring to different geological and geographical contexts; iii) in a third step, we have systematically assessed the sensitivity of site condition indicators towards local seismic amplification, ranking and collating their behaviour, also in different environments; iv) lastly, we have attempted to assess their potential for the prediction of local site response, resorting to a neural-network structure. The results we have obtained from the two latter stages offer an interesting insight on the varied correlations between local amplification and various typologies of site condition indicators. Furthermore, the findings gained by the neural-network analysis allow us to determine a 'best' set of site condition parameters appropriate to predict local site amplification.

1 Introduction

The concept of site characterization indicator is found quite frequently in literature on seismic soil response, and therefore it has acquired a rather broad meaning. After an extensive review of the scientific production on the topic, we can summarize the definition of site characterization/site condition indicator, or proxy, as a parameter (in scalar or vector form) aiming at representing in a concise way the local seismic response, possibly at a reduced cost of estimation. In this sense, the notion of proxy is common also to other fields of research, such as, for instance, medical science, where a number of tests have been developed to assess in a quick and inexpensive way the health of patients, in place of invasive and costly analyses (e.g. Peel et al., 2013, Bo et al., 2019).

The idea of using a term to "summarize" the site amplification behaviour arises in the 90's within the development of ground motion prediction equations (GMPEs). The first parameter to be employed was V_S30 (travel-time averaged V_S for the shallowest 30 m; Borcherdt 1994), achieving quite rapidly a wide diffusion (e.g. Martin and Dobry, 1994, Rodriguez-Marek et al., 2001, Pitilakis et al., 2001, Abrahamson 2008). V_S30 was later accompanied by other parameters, such as the fundamental frequency of resonance (f_0, e.g. Cadet et al., 2012), or the depth to the upper interface of a layer exceeding a pre-set V_S value (Ancheta et al., 2014). The same site condition parameters were also adopted by normative building codes (see for instance Eurocode 8, EC8 2004), when defining soil classes with consistent response behaviour. It should be highlighted that, since their early development, site condition parameters do not derive necessarily from in situ measurements, but they can also be indirectly inferred (Borcherdt, 1994). In fact, much of the scientific literature about site characterization indicators from the 2000s and 2010s focuses on identifying parameters of "cheap" availability (e.g. topographic slope) that correlate more or less robustly with established proxies with a geo-mechanical "meaning" (generally V_S30; see for instance Wald and Allen, 2007). In this sense, the first indicator becomes a proxy for another (higher-order) proxy. Another established approach involves the use of proxies in the form of layers of diffuse information (continuous topographical parameters, geological maps) as the basis for the extrapolation of local, higher quality data (again, in general, measured V_S30) to areal extents (e.g. Willis et al., 2000, Vilanova et al., 2018).

In the framework of WP7/NA5 – Task 7.4 of SERA project, we have aimed at addressing the topic of site condition indicators with a broad and comprehensive work: i) firstly, we have reviewed the state of the art and tracked the present research trends in the use of proxies ; ii) secondly, to test their applicability at a wide scale, we have compiled an extensive database of site condition parameters, covering more than 1000 instrumented sites, and paired it with a companion dataset of empirically-derived local amplification functions. In this phase of data collection, particular attention was dedicated to the harmonization of information derived from disparate sources and referring to different geological and geographical contexts; iii) in a third step, we have systematically assessed the sensitivity of site condition indicators towards local seismic amplification, ranking and collating their behaviour (also in different environments); iv) lastly, we have attempted to assess their potential for the prediction of local site response, resorting to a neural-network structure.

This report describes in detail the work we have carried out for Task 7.4. Chapter 2 presents the first stage of the workflow, a revision of literature on the subject of site condition proxies, with a systematic coverage of various sources and categories of indicators, as well as their applications. Basing on the outcome of this preliminary phase, we have compiled a considerable database of site condition indicators, comprising more than 1000 instrumented sites in Switzerland and Japan; for each station we collected a wide gamut of indicators, from measured V_S profile- or H/V_{noise}-derived parameters to topographical quantities and geological information (chapter 3). A particular effort was put in place to ensure a homogeneous characterization of Swiss and Japanese stations. This proxy database is accompanied by a set of empirically-obtained Fourier amplification functions for the free-field sites (around 800) of our list of stations (chapter 4). In chapter 5 we use these parallel datasets of indicators and amplification functions to conduct a systematic assessment of the sensitivity of the various site

condition indicators towards local amplification at 10 selected frequency abscissae in the range 0.5 – 20 Hz. For continuous-variable proxies (e.g. V_S30) the analysis is performed through a series of linear regressions; as for classification proxies (e.g. geological categorizations), we evaluate their ability to group sites with a homogenous amplification behaviour. This methodical appraisal allows determining which parameters show a higher sensitivity towards site amplification, and at which frequency abscissae; besides, we also checked whether the same proxies "work" in a similar manner in Switzerland and Japan. Finally, in chapter 6, we evaluate the potential use of site characterization indicators for the prediction of local seismic response with a neural network approach. Based on the results from regression analysis we merge the Swiss and Japanese data set in order to provide a sufficiently large data set to reliably learn the neural network parameters. We systematically assess the prediction performance of various sets of site condition parameters by comparing the frequency-dependent site amplification with predictions obtained from the neural network. The comparison is based on measuring the deviation between the true binned amplification and the predicted amplification bin at a specific frequency. In that way we are able to rank various site condition parameter sets according to their frequency-dependent prediction performance.

2 Literature review

Considering the broadness of the "site characterization indicators" topic, the first step carried out for the completion of task 7.4 was a systematic literature review. The review was conducted in year 1 of activity, also with contributions from the other partners (AUTH, ISTerre, INGV) who were solicited to suggest relevant material (papers, reports). Furthermore, additional input was provided by A. Yong (Caltech) and S.K. Ahdi (UCLA) during and after the COSMOS-SERA workshop held at the 2018 ESC in Malta, September 2018.

After a first phase of collection and documentation, the compiled material was then classified according to the source and/or use of the proxies. We therefore defined the following five lines of research within the scientific literature on site condition indicators:

1. Works dedicated to *proxies related to stratigraphic amplification in 1D environment*. This first category deals with parameters derived from the estimated V_S profile or H/V_{noise} curve (Nakamura, 1989), in turn obtained from in-situ geophysical measurements; these parameters are evaluated in their ability to succinctly portray or predict local site amplification. This type of proxies comprises f_0 (fundamental frequency of resonance, corresponding to a peak in the H/V_{noise} curve , A_{0HV} (amplitude of H/V_{noise} curve at f_0), V_{SZ} (travel-time averaged V_S down to a depth *z*, e.g. V_{S30}, V_{S20}), $V_{Sberock}$ (S-wave velocity of the shallowest layer exceeding a threshold V_S value, generally 800 m/s), V_{Sm} (travel-time averaged V_S above the bedrock), C_V (velocity contrast, defined as V_{Ssurf} or V_{Smin} / $V_{Sbedrock}$), H_{800} (depth to the shallowest layer exceeding V_S = 800 m/s), V_{SQWL} I_{CQWL} (quarter-wavelength velocity and impedance contrast). Table 1 contains a list of the most significant works we retrieved, alongside the treated proxies and their main conclusions; for an extended definition of the parameters listed above, we refer to these publications.

Table 1: Most significant works collected for category (1)

PUBLICATIONS	PARARMETERS	MAIN CONCLUSIONS
Cadet et al., 2010. **Defining a Standard Rock Site: proposition based on the KiK-net database.** BSSA	V_{S30}, f_0	Good performance of couple V_{S30}-f_0 in defining soil types with consistent behaviour
Cadet et al., 2011. **Site effect assessment using kik-net data: part2 – site amplification prediction equation based on f0 and Vsz.** BEE	V_{Sz} (z=5,10,20,30 m), f_0	V_{S30} performs better than V_{Sz} (z=5-20 m) in predicting site amplification, f_0 performs better than V_{S30}, f_0-V_{s30} performs better than single proxy
Derras et al., 2017. **Vs30, slope, H800 and f0: performance of various site-condition proxies in reducing ground-motion aleatory variability and predicting nonlinear site response.** Earth, planets and space.	V_{S30}, H_{800}, f_0, slope	Among single proxies, slope performs worst. Any pair performs better than any single proxy
Salameh et al., 2016. **Using ambient vibration measurements for risk assessment an urban scale: from numerical proof of concept to a case study in Beirut.** IASPEI 2016	f_0, A_{0HV}	f_0 and A_{0HV} from H/V are good proxies in predicting site amplification; A_{0HV} is satisfactory proxy for impedance contrast sediment/bedrock=> hence for site amplification
Boughdene Stambouli et al., 2017. **Deriving amplification factors from simple site parameters using generalize regression neural networks: implications for relevant site proxies.** Earth, planet and space.	f_0, V_{S30}, C_v, $V_{Sbedrock}$, V_{Sm}	Sets (4-6) of proxies are effective in predicting amplification factors: the best single proxy is C_v (V_{Smin}/ $V_{sbedrock}$), the best pair V_{S30}-f_0
Poggi et al., 2011. **Derivation of a reference V_S model from empirical site amplification**. BSSA Poggi et al., 2012b. **The quarter-wavelength average velocity: a review of some past and recent application developments.** 15th WCEE, Lisbon	Vs^{QWL},IC^{QWL} (quarter-wavelength velocity and impedance contrast)	Vs^{QWL} physically relates the resolution on ground parameters with the characteristics of the propagating wave-field at the discrete frequencies. IC^{Qwl} is a powerful tool to assess influence of resonance phenomena in soft sediment sites

2. Works dedicated to *proxies attempting to portray topographical effect*. This set of publications comprises both case studies and systematic studies, attempting to identify local amplification phenomena linked to marked topographical features (e.g. pinnacles, ridges), and to relate them to measurable topographical parameters. These parameters include: height and/or width of a relief, topographical slope, topographical smoothed curvature, topography position index (TPI, Burjánek et al., 2014), EC8 topographic class (CEN, 2004). Table 2 reports two example of case-study publications and some systematic studies which we have considered among the most relevant.

Table 2: Most significant works collected for category (2)

	PUBLICATION	PARAMETERS	MAIN CONCLUSIONS
CASE STUDIES	Lovati et al., 2011. **Estimation of topographical effects at Narni ridge (central Italy): comparisons between experimental results and numerical modelling,** BEE.	l=semi-width of mountain	Experimental evidence of topographical effect in SSR and HVSR at crest of ridge $f_{res}= V_S/ l$ x (0.4)
	Stolte et al., 2017. **An experimental topographic amplification study at Los Alamos National Laboratory using ambient vibrations.** BSSA	Height of topographical feature	Empirical evidence of topographical effects from SSR, HVSR , MRM
	Geli L at al., 1988. **The effect of topography on earthquake ground motion: a review and new results**, BSSA	Relief shape ratio = h (height)/l	Topographic effect difficult to separate from surface layering; topographical amplification cannot be explained with SH-waves alone
SYSTEMATIC STUDIES	Pessina & Fiorini, 2014. **A GIS procedure for fast topographic characterization of seismic recording stations**. SDEE	Slope, ridge, EC8 topographic classes	GIS procedure using DEM to classify sites according to the topographic classes of EC8 (T1-T4)
	Burjanek et al. 2014. **Empirical evidence of local seismic effects at sites with pronounced topography: a systematic approach**. GJI	Slope, topography position index **TPI**(x,y)=H(x,y)-mean(H)$_A$	Scale-dependent ($A^{1/2}$=120-2020 m) topographical classification of sites using slope and TPI. Observed amplifications are linked with ground motion directionality estimated by polarization analysis. No clear relation between local topographic features and observed amplification
	Maufroy et al., 2015. **Frequency-scaled curvature as a proxy for topographic site-effect amplification and ground-motion variability**.BSSA Hollender et al., 2017. **Characterization of site conditions for 33 stations from French permanent network using surface wave methods**. BEE	**FSC_A** =smoothed curvature ($d^2H/dx,y$) over area A	Correlation between topographical amplification at frequency f (corresponding to V_S wavelength λ_S) and $A^{1/2}$ $\lambda_S=4A^{1/2,}$

3. Works dedicated to *proxies related to basin, 2D/3D resonance effects*. A wide variety of studies describe peculiar local response behaviors (edge-generated surface waves, 2/3D resonances) arising at sedimentary sites with 2 or 3D topographical configuration (e.g. sedimentary basins, thick alluvial sediments covering the bottom of valleys; see Joyner, 2000; Bindi et al., 2009; Ermert et al., 2014). The task to capture these phenomena with simple parameters or proxies is quite challenging, due to the high degree of complexity of the sites where these effects occurs. Therefore, scientific publications have generally proposed simplistic proxies (e.g. the valley shape ratio, Bard & Bouchon, 1985). Only recently, within NERA project (JRA1/WP11: "Waveform modeling and site coefficients for basin response and topography"), a systematic assessment of the influence of sedimentary basin geometry and properties has been carried out, conveyed in Boughdene Stambouli et al. (2018).

4. Works dedicated to *indirect proxies*, i.e. indirect parameters that are used to estimate other proxies that are more closely related to the local site response; the most well know example is

that of topographical slope used to predict V_{S30} (Wald and Allen, 2007). In the context of indirect proxies, we further distinguish:

4.1 Works proposing a "simple" or direct correlation between one or few indirect proxies and the target parameter. Exemplificative works are the paper of Boore et al. (2011), presenting a correlation study to predict V_{S30} from V_{S20}, V_{S10}, and the work of Wald and Allen (2007), mentioned above. Table 3 below presents a more complete list of notable examples.

Table 3 – Works illustrating a direct correlation between one or more indirect proxies and the inferred parameter

PUBLICATIONS	INPUT PROXIES	INFERRED PROXIES
Boore et al., 2011. **Regional correlations of Vs30 and velocities averaged over depths less than and greater than 30 m**. BSSA	Measured V_{Sz} (z<30 m)	Vs30, soil class
Kuo et al., 2012. **Site classification and Vs30 estimation of free field TSMIP stations using the logging data of EGDT**. Engineering geology Kwok et al., 2018. **Taiwan-specific model for Vs30 prediction considering between-proxy correlation**s. Earthquake spectra.	In situ geotechnical tests (SPT), Vsz (z<30 m)	
Ahdi et al., 2017. **Development of vs profile database and proxy-based models for vs30 prediction in the pacific northwest region of North America**. BSSA	Measured Vs30, geology, topography	Vs30
Wald & allen2007**. Topographic slope as a proxy for seismic site condition and site amplification**. BSSA Lemoine et al., 2012. **Testing the applicability of correlation between topographic slope and Vs30 for europe**. BSSA, Rey et al., 2011. **Cartographie automatique des classes de sol à l'échelle régionale à partir d'un modèle numérique de surface**.	Topographic slope	Vs30, soil class
Savvaidis et al., 2018. **Comparison of vs30 using measured, assigned and proxy values in three Cities of northern Greece**. Engineering Geology	Topographic slope+ geological info.	Vs30
Hassani et al., 2016. **Applicability of the site fundamental frequency as a vs30 proxy for central and eastern North America**. BSSA	f_0	Vs30

4.2 Works describing attempts to extrapolate to areal extents a set of high quality local measures (e.g. of S-wave velocity), by correlating the latter to other diffuse layers of information (e.g. geology, topography). These publications typically make use of measured, spatially-referenced V_S profile, CPT, SPT or geotechnical information databases. The local measures are then correlated with diffuse layers of information (e.g. the surficial formation from geological or geotechnical maps, and/or topography); the robustness and statistical significance of the correlation are evaluated. In the final step local information are extrapolated to areal surfaces using the geological and/or topographical map as subproxy; possible strategies for extrapolation are kriging or the use of neural network. Table 4 lists some notable examples.

Table 4 – Publications assigned to category 4.2

PUBLICATION	INPUT DATA	EXTRAPOLATION/CORRELATION STRATEGY	INFERRED PROXIES
Willis et al., 2000. **Site-condition map for California based on geology and shear wave velocity**, BSSA	Measured Vs profiles + surficial cover map	Statistical correlation	Soil class
Holzer et al., 2005. **Mapping NEHRP Vs30 site classes**. Earthquake Spectra.	SCPT data+surficial cover map	Statistical correlation	V_{S30}, soil class
Kwak et al., 2015. **Prediction equations for estimating shear-wave velocity from combined geotechnical and geomorphic indexes based on Japanese data set**. BSSA	SPT, geology, slope	Kriging	V_{S30}
Xie et al., 2016. **Vs30 empirical prediction relationships based on a new soil-profile database for the Beijing plain area, China**. BSSA	Measured V_S profiles, topography, geology	Statistical correlation	V_{S30}
Yong et al., 2012. **A terrain-based site-conditions map of California with implications for the contiguous united states.** BSSA	Measured Vs30, Topographic slope+convexity+texture, geology	Statistical correlation	V_{S30}
Thompson et al., 2014. **A Vs30 map for California with geologic and topographic constraints**. BSSA	Measured Vs30, topography, geology	Kriging	V_{S30}
Vilanova et al., 2018. **Developing a geologically based Vs30 map for Portugal: methodology and assessment of the performance of proxie**s. BSSA	Measured Vs profiles + surficial cover map	Statistical correlation, kriging	V_{S30}
Motalleb Nejad et al., 2018. **Shear wave velocity and soil type microzonation using neural network and geographic information system**. SDEE	SPT, Downhole profiles, geotechnical lab tests	Neural network	V_{S30}, soil type

5. Works dedicated to proxies used to identify sites prone to earthquake-induced phenomena, such as liquefaction or mass movements, or to non-linear soil response.

Table 5: Examples of publications dealing with proxies related to earthquake-induced phenomena

PHENOMENON	PUBLICATION	PROXY
Nonlinear soil response	Réigner et al., 2018. **Non-linear modulation of site response: sensitivity to various loading parameters and site proxies using a neural network approach**. ESC Malta 2018.	Vs30, f0 (site proxies) PGA, PGV/Vs30 (strain proxies)
liquefaction	Zhu et al, 2015. **A Geospatial Liquefaction Model for Rapid Response and Loss Estimation**. Earthquake Spectra Zhu et al., 2017. **An Updated Geospatial Liquefaction Model for Global Application**. BSSA. Cauzzi et al., 2018. **Calibration of global empirical model for real-time liquefaction prediction in Switzerland**. 16th ECEE	Slope as proxy for V_{S30} Topographical roughness Distance from coast/river as proxy for water table depth Slope as proxy for granulometry, saturation Soil class Hydrogeological map Yearly precipitation as proxy for water table depth
mass movements (rockfalls, landslides, avalanches)	Cauzzi et al., 2018. **ShakeMap-based prediction of earthquake-induced mass movements in Switzerland calibrated on historical observations**. Natural Hazards	Topographical slope Map of susceptibility to landslides/avalanches/rockfalls

The publications mentioned so far in this section might not be entirely exhaustive, as we have reported the most significant works according to our judgement. Nevertheless, to our knowledge the main lines of research in the use of soil condition parameters are covered by the categories we have here identified (1-5)

2.1 Conclusions

The analysis of the collected material, and in particular the collation of works belonging to the same field of research, enabled us to define common aspects of interest and findings for each category of publications. We report here these conclusions for classes 1-4, of greater interest for the global development of our study; in fact, considering the vastness of the subject (see section above), we focus henceforth on proxies related to local site amplification, leaving the study of earthquake-induced phenomena and non-linear behaviour (category 5 above) to future work.

1. Works dedicated to proxies related to stratigraphic amplification in 1D environment
    - Several publications highlight the importance of the fundamental frequency of resonance f_0, when defining internally-consistent soil classes or predicting soil amplification.
    - Some site condition parameters perform better than others, i.e. they are better correlated with the local site response. For instance, Boughdene-Stambouli et al. (2017) identify C_V (velocity constrast, defined as $V_{Smin}/V_{Sbedrock}$) as the best performing single proxies; Salameh (2016) underline the role of A_{0HV} as a good proxy for the sediments-to-bedrock impedance contrast, hence for site amplification.
    - Pairs or sets of site condition parameters perform better than individual proxies, when defining internally-consistent soil classes or predicting soil amplification.
    - In several works, site condition parameters are fed as input to a neural network structure to predict site amplification factors; the relevance of each proxy for the prediction can be evaluated by the neural network.

2. Works dedicated to proxies attempting to portray topographical effect.
   - Evidence of resonance effects related to marked topographical features can be found in empirical (e.g. Stolte et al., 2017) and numerical (e.g. Maufroy et al., 2015) studies, although with simplified V_S structure; more difficult is separating topographical amplification from stratigraphic amplification when both are present (i.e. complex V_S structures; Burjanek et al., 2014). Stratigraphic amplification can reach higher amplification factors than topographical amplification (Lee et al. 2009; Burjanek et al., 2014).
   - The way topography affects amplification is inherently scale- (i.e. wavelength-) dependent**,** and wavelengths are determined by local stratigraphy. Therefore, topographical proxies too can be defined as scale-dependent: examples are the frequency-scaled curvature (FSC, Maufroy et al., 2015), and the multi-scale topography position index (TPI, Burjanek et al., 2014).
3. Works dedicated to proxies related to basin, 2D/3D resonance effects.
   - As already mentioned in the first part of this section, the desire to capture these phenomena with succinct parameters is quite challenging, due to the high degree of complexity of the sites where these effects occur; the shape of the longitudinal and transversal section of the basins, as well as the impedance contrast between sediments and bedrock, all play a role in driving the local site response. In this sense, remarkable is the work of Boughdene Stambouli et al. (2018), tackling this complexity.
   - Basin, 2D/3D amplification effects are often coupled with lengthening of ground motion (e.g. Beauval et al., 2003).
4. Works dedicated to *indirect proxies.*
   - Focusing on group 4.1, (direct correlation among proxies), it is worth remarking that the use of direct correlations between lower (e.g. slope) and upper level (e.g. V_{S30}) proxies, when proposed as global model, might not necessarily hold true in all environments; as example, the global slope-to-V_{S30} correlation proposed by Wald and Allen (2007) has been proven to produce mixed results when applied to datasets other than those it was developed upon (Lemoine et al., 2012). Nevertheless, similar models have proven to perform quite well when developed and applied locally at city or regional scale (e.g. Savvaidis et al., 2018), on more homogeneous geological environments.
   - In our judgement, the approach of group 4.2 (extrapolation of local high-quality data through the use of layers of diffuse information) appears as the most promising method for an indirect estimate of proxies closely related to site amplification (e.g. V_{S30}; see Vilanova et al., 2018) or, in perspective, to site response itself. Of interest are also the correlation/extrapolation methods used in works of class 4.2, including statistical tests, kriging, and neural network structures.

The work of literature review described in this section was a necessary preliminary step in our study; its outcomes were kept as reference in the following stages, i.e. the preparation of the site condition parameter database (for the selection of proxies to be retrieved), and for its use.

3 Compilation of a database of site condition parameters

Following the indications from the previous stage of literature review, we prepared a database of site condition parameters.

3.1 Sites selection

We focused on two geographical areas, Switzerland and Japan. Switzerland was selected because of the direct availability to the SED-ETHZ group of

- earthquake recordings from the Swiss national networks,
- site characterization data from the SED site characterization database (https://stations-intranet.ethz.ch/en/home/ , including circa 250 active and passive surface wave surveys, and more than 6000 H/V_{noise} measurement);
- a wide range of geological/geotechnical datasets provided by the Swiss Federal Office of Topography (Swisstopo) and the Swiss Geophysical Commission (SGPK).

Alongside Switzerland, Japan was considered:

- for data completion, as the earthquake recordings from the Japanese monitoring network KiK-net (publicly available, Aoi et al., 2004) constitute at the moment an unparalleled database in terms of magnitude - distance range coverage and site condition variability;
- for the availability of direct site characterization information at all instrumented sites of the mentioned network;
- for comparison with Switzerland, to determine to what extent the behavior of the same proxies is similar in very different geological environments.

Since the final target of our study is relating site condition parameters to site response, we decided to collect proxies at sites where the latter can be estimated empirically, i.e. instrumented sites.

For Switzerland, we considered all the stations of the Swiss national networks SSMNet (strong motion) and SDSNet (broadband), presently active or having worked for more than 6 months since 2009 (www.seismo.ethz.ch/en/earthquakes/monitoring). The final list of sites amounts to 398 stations (Figure 1). As for Japan, we included in our search all the stations of the KiK-net network (698 sites as of August 2018, Figure 2).

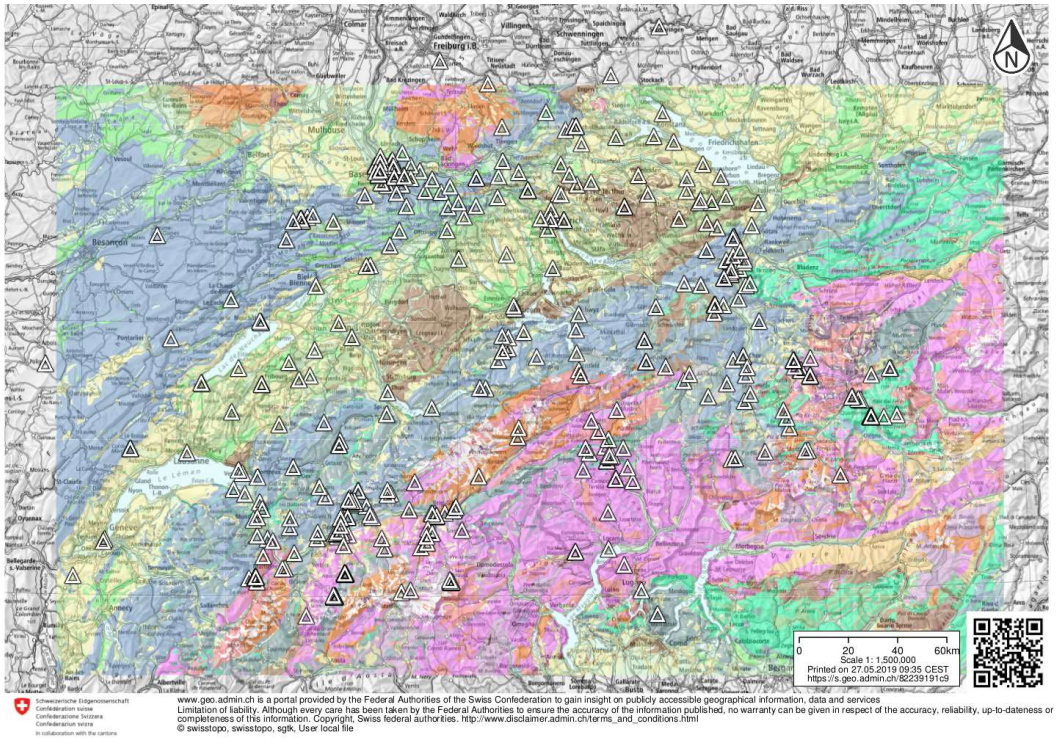

Figure 1: Geographical distribution of Swiss instrumented sites (white triangles). © Swisstopo, 2019.

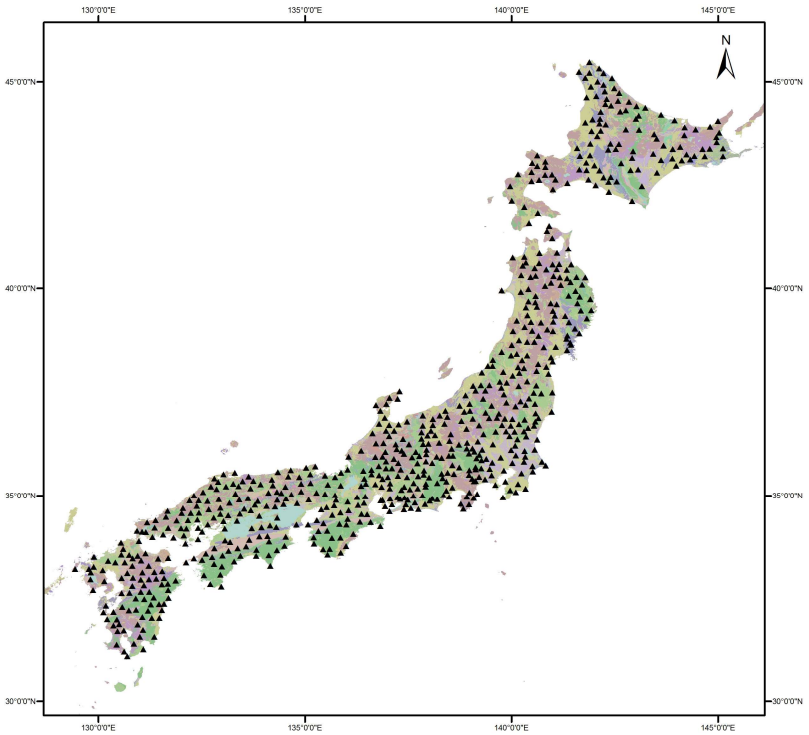

Figure 2: Geographical distribution of considered Japanese instrumented sites (black triangles).

3.2 Site condition parameters selection and data sources

Following the outcome of the literature review phase, we identified four categories of proxies to be retrieved – when possible - at all considered sites:

- Proxies directly derived from measured V_S profile;
- Proxies directly derived from H/V_{noise} measurements (Nakamura, 1989);
- Topographical proxies, derived from the analysis of digital elevation models (DEM) datasets;
- Common (for Switzerland and Japan) dataset of Indirect proxies derived from layers of diffuse information (e.g. geological maps).
- Indirect proxies specific to either Switzerland or Japan.

Particular effort was devoted to obtain homogeneous proxy datasets for Swiss and Japanese stations. Whenever available, the measure of the uncertainty on the proxy value was retained and stored in the database.

3.2.1 Proxies directly derived from measured V_S profile

A set of proxies obtained from the measured V_S profile was computed for each Swiss or Japanese site where the latter is available. The sources of information (V_S profile databases) are the following:

- Switzerland. Swiss Seismological Service (SED) Site Characterization Database (https://stations-intranet.ethz.ch/en/home/). The database contains data and results of site characterization surveys carried out over the past decades by SED (GeoExpert, 2009, Cauzzi et al. 2015, Michel et al. 2014, Poggi et al. 2017). For Swiss SSMNet and SDSNet stations, the database provides the measured V_S profile for 104 (out of 399) sites (as of September 2018). The V_S profiles are generally derived from non-invasive geophysical surveys, i.e. active or passive seismic measurements, or a combination of both. At very few stations the surficial portion of the velocity profile was constrained by SCPT data as well. Considering the non-uniqueness of the solution of non-invasive surveys, the Site Characterization database usually provides for each site a set of equally-feasible V_S profiles. The central value for each proxy was hence determined as the mean of the proxies derived from each feasible profile; the uncertainty measure is the standard deviation.
- Japan. For KiK-net sites the source is the KiK-net site characterization database (www.kyoshin.bosai.go.jp/kyoshon/db/index_en.html?all). The database provides for each station a V_S,V_P velocity profile derived from down-hole surveys, reaching the depth of the borehole seismometer (as each site of the KiK-net network is composed of a surface and a borehole receiver, located at a depth of 100 m or more). As a single profile is provided for each site, no uncertainty measure for the central value of the proxies is available.

The set of scalar proxies retrieved for each site are the following: V_{S10}, V_{S20}, V_{S30} (travel-time averaged S-wave velocity down to 10, 20, 30 m depth), $V_{Sbedrock}$ (velocity of the shallowest layer exceeding V_S = 800 m/s), V_{Sm} (travel-time average V_S above the shallowest layer exceeding V_S = 800 m/s), H800 (depth to the shallowest layer exceeding V_S = 800 m/s), C_V (velocity contrast, defined as $V_{Smin}/V_{Sbedrock}$), and C_{V10} (V_{S10} velocity contrast, defined as $V_{S10}/V_{Sbedrock}$). The latter was introduced as the definition of C_V appeared to us as too dependent on the adopted subsoil parameterization (V_{Smin} being the minimum S-wave velocity recorded along entire profile), while V_{SZ} (with respect to V_{Smin}) should be a more robust estimate. Secondly, in a test we conducted on KiK-net data, C_{V10} appeared to be better correlated to the ratio PGA recorded at surface seismometer / PGA recorded at borehole seismometer, when compared to C_{V20} or C_{V30} (Figure 3).

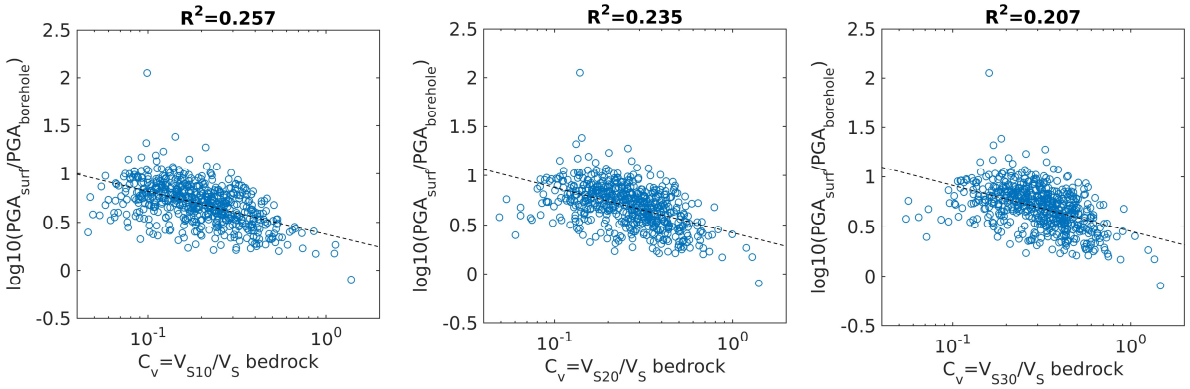

Figure 3: From left to right, correlation between C_{Vz} (=$V_{Sz}/V_{Sbedrock}$, with z = 10, 20, 30 m) and average ratio (at each station) between PGA recorded at surface seismometer / PGA recorded at borehole seismometer, for KiK-net sites. The linear regression achieving the maximum coefficient of determination R^2 is the first on the left (C_{V10}).

Besides scalar proxies, we also determined two additional site condition parameters in vector form, quarter-wavelength velocity (Vs^{QWL}) and quarter-wavelength impedance contrast (IC^{QWL}, Poggi et al. 2012a, 2012b, 2013). Vs^{QWL} and IC^{QWL} are both continuous functions of the frequency; we retained in our database their values at 0.5, 1, 1.67, 2.5, 3.33, 4, 5, 6.67, 10 and 20 Hz.

Figure 4 offers some examples of comparison between the Swiss and Japanese proxy populations. The two environments show some differences in the distribution of soil condition parameters; velocities appear to be slower in Japan, particularly for the weathering, unconsolidated sediments, and the engineering bedrock is generally located at shallower depths at Japanese sites.

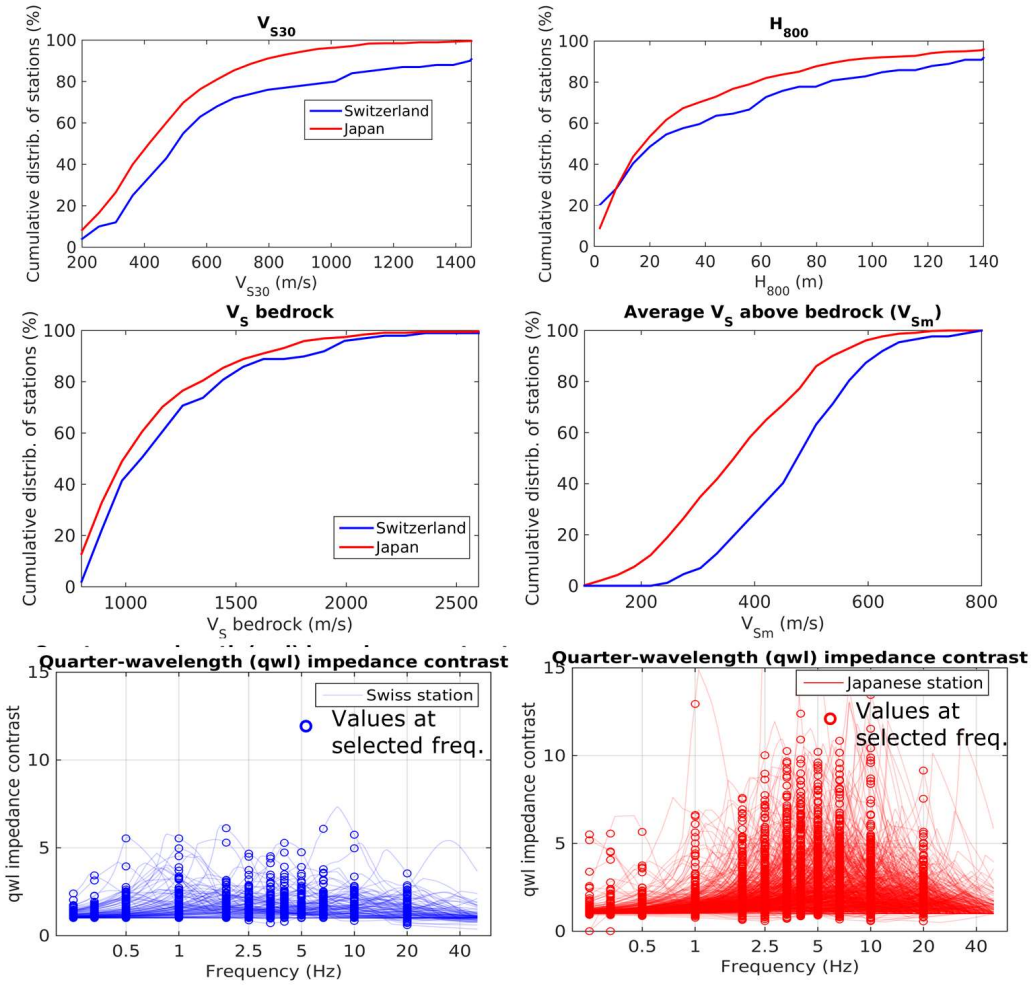

Figure 4: Top and central row: comparison between the cumulative distributions of V_{S30}, H800, $V_{Sbedrock}$ and V_{Sm} for Switzerland and Japan. Bottom: quarter-wavelength impedance contrasts at Swiss (left) and Japanese (right) stations.

3.2.2 Proxies directly derived from H/V_{noise} measurements

The SED Site Characterization Database (https://stations-intranet.ethz.ch/en/home/) was also (see previous subsection) used as source for the H/V_{noise}-related proxies at Swiss sites (Nakamura, 1989) . As anticipated, the database includes more than 6000 three-component, single-station ambient noise measurements. The first action we undertook was a general review of the database, to ensure homogeneity of data recordings (e.g. we excluded all measurements shorter than 30 minutes) and consistency in their H/V processing (e.g. applying the same methods, with the same processing parameters). Secondly, we identified the ambient noise measurement closest to each free-field or urban free-field Swiss station (the reason for this sub-selection will be explained later in chapter 4). We considered a station characterized by H/V_{noise} measurement when its distance from the nearest measuring point is < 50 m; this way, we cover 117 out of 145 free-field or urban free-field stations. When this was not already available in the database, a manual picking for the identification of the fundamental (f_0) and higher-order peaks was performed.

At each Swiss station, we determined the following H/V_{noise}-related proxies:

- Frequencies (f_n) of the manually identified fundamental and 1st,2nd order peaks of the H/V curve as obtained from the time-frequency method of Poggi and Fäh (2010). A measure of the

uncertainty for the peak frequency central value is also available, as determined by the manual picker (Fäh et al., 2001).

- Amplitudes (A_n) of the H/V_{noise} curve from Poggi and Fäh (2010) at the manually-identified peaks. The uncertainty on the central A_n value corresponds to the uncertainty interval of the curve (Poggi and Fäh 2010). It should be noted that not for all measurements peaks up to the 2nd order were identified (at few stations, the H/V_{noise} curve was considered flat, i.e. entirely devoid of peaks).
- The amplitudes of the H/V curve from Poggi and Fäh (2010) at this set of fixed frequencies: 0.5, 1, 1.67, 2.5, 3.33, 4, 5, 6.67, 10 and 20 Hz.

Figure 5 offers an overview of the H/V_{noise}-derived proxies

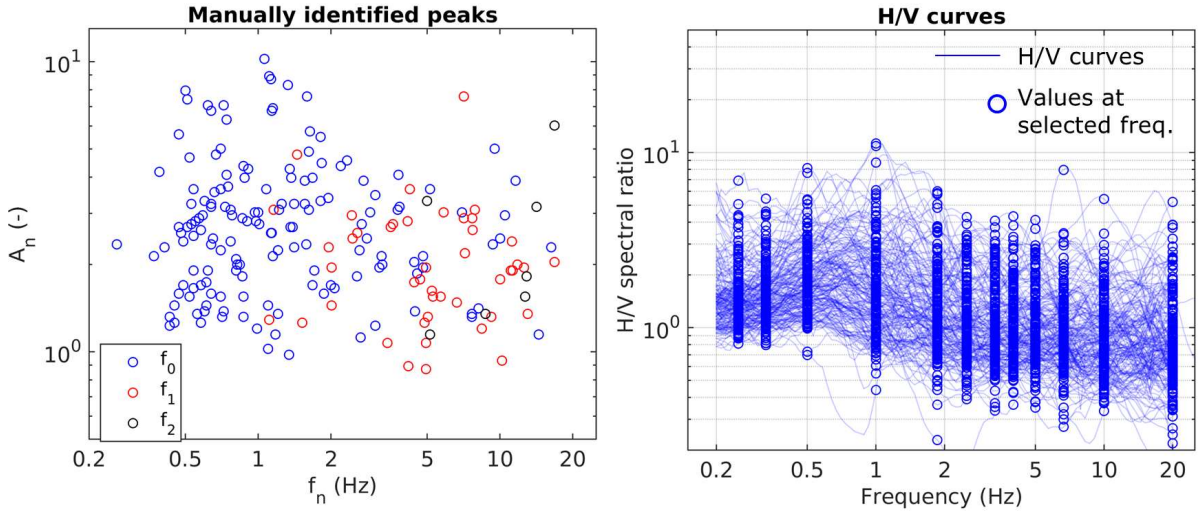

Figure 5: H/V_{noise} -related proxies at Swiss stations. Left: frequency (f_n) and amplitude (A_n) of manually identified peaks. Right: the whole H/V_{noise} curves.

As for Japanese Kik-net sites, to our knowledge there are no systematic ambient noise recordings available at the moment; therefore, we were not able to build a database of H/V proxies.

3.2.3 Topographical parameters

From the systematic analysis of digital elevation model (DEM datasets) we obtained a comprehensive database of topographical proxies for Swiss and Japanese sites. We highlight that we did not compile this database to specifically target the so-called topographical amplification, but rather to have a complete morphological description of our stations. In fact, as anticipated in chapter 2 (literature review), the topographical morphology of a site is indeed related to its geology (e.g. depositional environment), hence to its local amplification (see for instance Wald and Allen, 2007, and Yong et al., 2012).

The sources we selected for the compilation of this dataset are:

- For Japan, the Advanced Spaceborne Thermal Emission and Reflection Radiometer (ASTER) 'Global Digital Elevation Model Version 2' (GDEM V2). This digital elevation model is referenced in WGS84 coordinates with a posting interval of 1 arcsec, i.e. approximately 30 m. From this global dataset, we derived 698 10 x 10 km DEM tiles, re-sampled on a 20 m regular grid and referenced to projected UTM coordinates; each tile is centered on a particular KiK-net station (Figure 6, left column).
- For Switzerland, the DEMs DHM25 (spatial resolution of 25 m) and swissALTI3D (spatial resolution of 2 m), both referred to the projected Swiss coordinate system. Form the first dataset (DHM25), similarly to Japan, we derived 399 10 x 10 km DEM tiles, re-sampled on a 20

m regular grid, each centered on a particular Swiss station. From swissALTI3D, we derived 399 2.5 x 2.5 km high resolution DEM tiles (spatial resolution of 2 m), each centered on a particular Swiss station.

The DEMs we used for both Switzerland and Japan do not carry any information about the bathymetry of water bodies (sea, lakes), they simply report the altitude of the water surface. Since this feature might seriously affect the following stage of proxy extraction, we carved sea surfaces out of Japan DEM tiles, and lakes surfaces out of Swiss tiles.

We used this ad hoc dataset of DEM squares to determine for each station the following parameters:

- Topographical slope. We computed the value of topographic slope at the center of each DEM tile (i.e. the station location), following the definition of slope of Burjanek et al. (2014). The slope computation was repeated at 7 logarithmically-spaced spatial scales: 60, 100, 180, 340, 660, 1140, 2020 m.
- Normalized topography position index (TPI_{norm}), a multi-scale parameter proposed by Burjanek et al. (2014). It is the difference in elevation between the target site and the average of its surrounding area (whose size defines the scale of investigation), normalized as deviation from the mean TPI of a large population of terrain configurations and scaled by its standard deviation. High, positive values of TPI_{norm} characterize ridges, while negative values define concave basins or valley bottoms (Figure 6, third row). TPI_{norm} was evaluated at the 7 spatial scales already mentioned for slope (60 – 2020 m).
- Terrain class. We adopt the terrain classification scheme of Burjanek et al. (2014), that combines slope and TPI_{norm} to define 6 scale-dependent categories: valley bottom, flat area, lower/middle/upper slope, ridge (Figure 6, bottom row). The terrain classification was carried out at the 7 spatial scales 60 -2020 m.
- Smoothed topographical curvature (STC), proposed by Maufroy et al. (2015): it is the scale-dependent second derivative of terrain elevation. As original contribution for this study, we additionally retained the measures of curvature along the northing and easting axes ($STC_{N,E}$), in the attempt to identify sites with asymmetrical 2D/3D topographical configuration (Figure 6, two top rows). Due to restrictions related to the DEM resolution (Maufroy et al., 2015), we could use the 20 m-resolution tiles to determine the curvature for the spatial scales 180 – 2020 m only. At smaller scale (60 and 100 m), we had to rely on high-resolution DEM squares, available for Swiss sites only.

Figure 6 shows an example of DEM tile processing for a sample Japanese station, HRSH17, located on the sedimentary bottom of a deeply incised valley, approx. 400 m wide. The computation of directional smoothed curvatures (two topmost row, central and right column) is effective in retrieving elongated convex or concave structures, typical of a mountain environment. Similar results are obtained for normalized TPI (third row from bottom), although losing the directional information. Finally, the terrain classification (last row) adequately summarizes the complex structure of the topographical surface. We remark that, as the scale of analysis increases (compare second and third columns, referring to 340 and 1140 m scales respectively) smaller-extent features “disappear” and large-range patterns become evident.

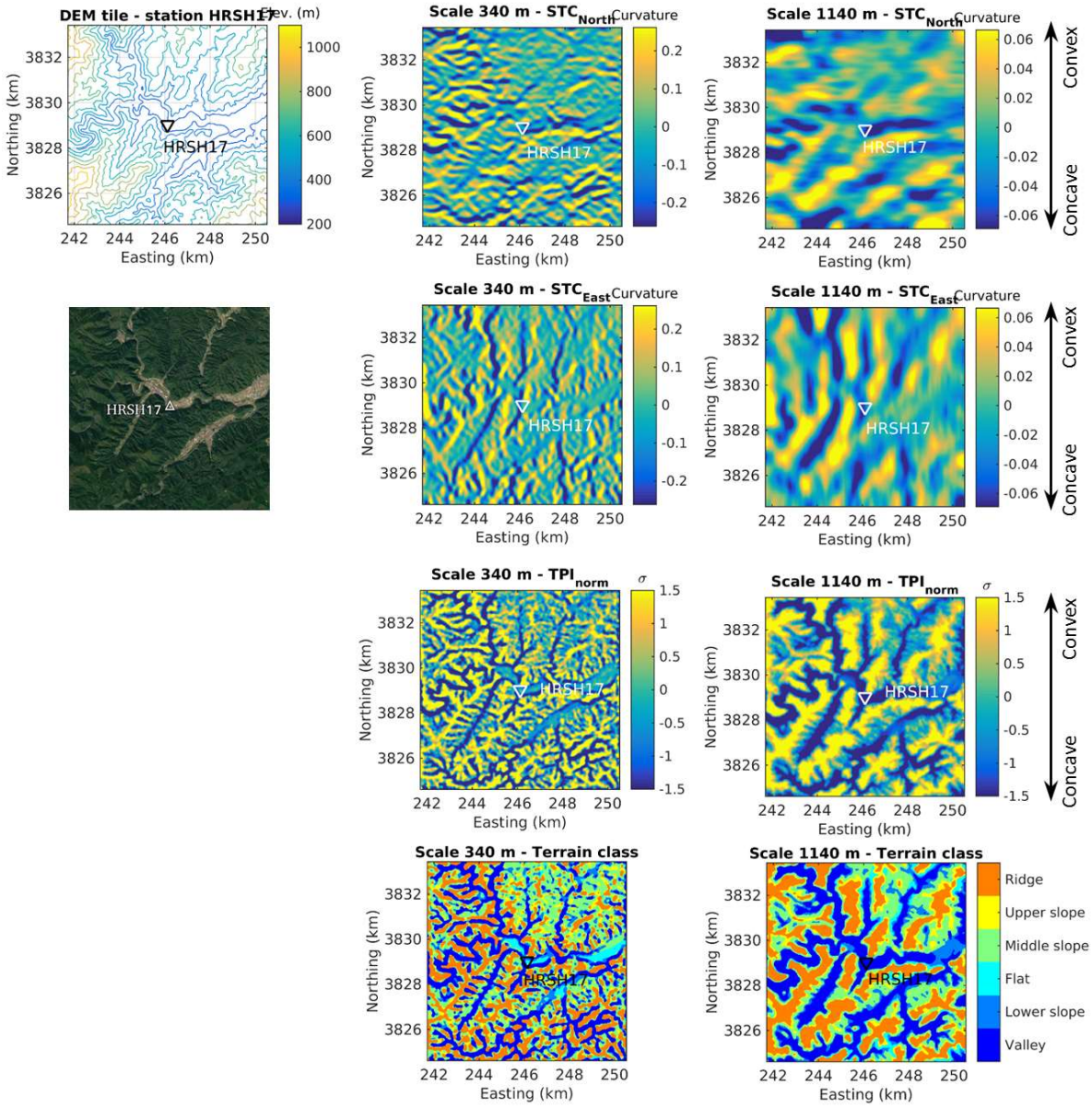

Figure 6: Example of DEM tile processing of a sample KiK-net station, HRSH17. Leftmost column: aerial image of the surrounding of the station (bottom) and corresponding DEM square (top). Central column, from top to bottom: smoothed topographic curvature along northing and then easting axis, normalized topographical index and terrain classification, all referred to 340 m scale. Rightmost column, from top to bottom: smoothed topographic curvature along northing and then easting axis, normalized topographical index and terrain classification, all referred to 1140 m scale.

Figure 7 displays some sample comparisons between the populations of topographical parameters for Switzerland and Japan, for two spatial scales (340 and 1140 m). It is evident that the two datasets show different distributions in their proxy values; Japanese stations are located at sites with generally gentler slope, and more frequently in flat or concave topographical structures (predominance of negative values for TPI_{norm} and curvature). Vice versa, in Switzerland a small but not insignificant fraction of stations is anyway placed on convex features (e.g. ridges, compare for instance the terrain classes). The effect of spatial scaling is evident in the change of relative distribution among the different terrain classes when moving towards larger spatial scales (Figure 7, third row); while at smaller scales the affiliation to flat areas is markedly predominant (in fact seismic stations are generally installed in flat spots), when the scale of observation is enlarged the

distribution among the various classes tends to be more homogeneous, i.e. the stations are more likely to appear included in a more varied topography.

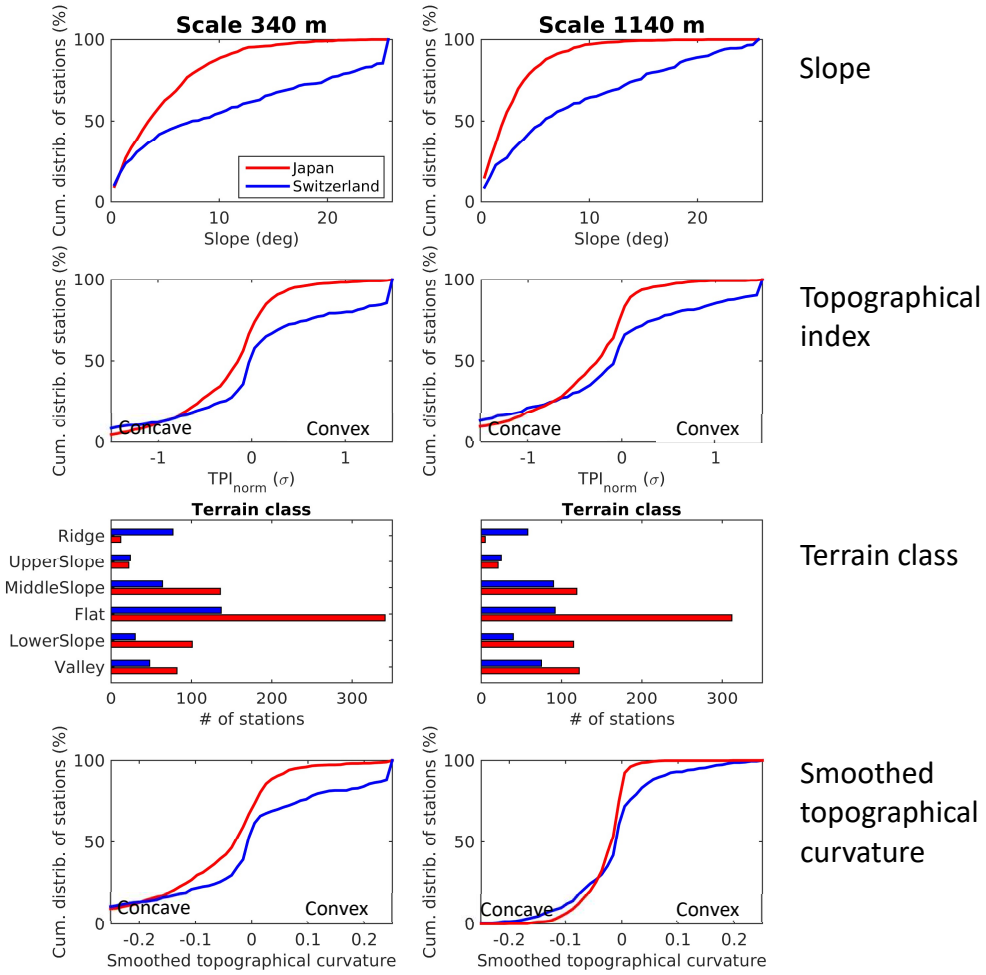

Figure 7: Comparison between Swiss and Japanese stations, in terms of slope (top row), normalized topography position index (second row), terrain class (third row) and smoothed topographic curvature (bottom row), for the spatial scales 340 m (left column) and 1140 m (right column).

3.2.4 Common indirect proxies derived from layers of diffuse information

The last category of site condition parameters relates to the extraction of information from layers of diffuse information (e.g. geological, geotechnical, lithological, pedologic maps), providing an indirect knowledge for the local site condition.

Considering the diversity of geological environment between Switzerland and Japan, as well as the heterogeneity of available data sources, a significant effort was put in place to derive a common, or at least reciprocally compatible, dataset for Swiss and Japanese sites.

The sources of information we used were:

- Regarding the geological description of the stations sites, we resorted to the Seamless Digital Geological Map of Japan (1:200000, detailed version), by the Geological Survey of Japan, and the Geological Map of Switzerland (1:500000), by the Federal Office of Topography (swisstopo). To our knowledge, the two maps are the most detailed sources of geological information covering homogeneously the entire territory of each of the two nations. Considering the marked difference between the geological environments of Switzerland and Japan, as well as

the different description offered by the two geological maps, we identified the rock age and genesis as the lowest common denominator features between the two countries.

- Regarding the information about the thickness of ice cover at the last glacial maximum, for Switzerland we referred to the vector map "Switzerland During the Last Glacial Maximum (LGM) 1:500000" by swisstopo. As for Japan, we resorted to the works of Ono et al. (2004, 2005).
- We referred to the world-wide pedologic database of SoilGrids250 (Hengl et al., 2017). This database provides predictions for a variety of soil properties on a global grid of 250 x 250 m. Such predictions are based on 150000 soil profiles for training and a stack of 158 remote sensing-based soil covariates.

Based on the aforementioned sources, at each Swiss or Japanese site we retrieved the following information:

- Age of the geological formation on which the station is sitting. The information was obviously derived from the geological maps of Switzerland and Japan. Aiming to further simplify, we classified the rock age into five categories, consistently with Wakamatsu et al. (2006): Holocene, Pleistocene, Quaternary (volcanic rocks), Tertiary, Pre-tertiary (Figure 8, top).
- Genesis of the geological formation on which the station is sitting. The information was derived from the geological maps of Switzerland and Japan. We defined two levels of classification (one coarse, one detailed), listed in Table 6. This classification was largely derived from the one already available in the Geological Map of Switzerland; as for Japan, we carefully attributed with expert judgement the 165 categories of the Japanese Geological Maps to the simplified classification of Table 6.
- Thickness of ice cover at the last glacial maximum. This information is directly provided for Swiss sites by the map "Switzerland During the Last Glacial Maximum (LGM) 1:500000" by Swisstopo (Figure 9). For Japan, we referred to the map of the elevation of the climatic snowline (ELA) at global LGM by Ono et al. (2004), concluding that all KiK-net sites are located below this line (i.e. no ice cover).
- From the global database SoilGrids250m we focused on two layers, which we argued to be more closely related to local amplification: the depth to the pedologic bedrock and the volumetric percentage of coarse fraction (grain size > 2 mm) at the largest depth available (2 m; Figure 10, top row). We underline that the SoilGrids250m database has been conceived as a collection of soil properties related to agricultural exploitation, not seismic soil response. For instance, the definition of pedologic bedrock, or R-horizon, does not fully coincide with that of engineering bedrock (although they refer to related concepts); this partial discrepancy might explain why the depth to R-horizon from SoilGrids250m database correlates only loosely to measured H800 (Figure 10, lower-right panel). Vice versa, it is worth observing that the % of coarse fraction shows a clear correlation with "higher-order" site amplification proxies such as H800 and V_{S30} (Figure 10, center and lower left plots; we highlight that the performance of coarse fraction % is comparable to that of another well-established indirect proxy, i.e. slope, see Figure 10 center right panel).

Table 6: rock genesis classification

COARSE CLASSIFICATION	DETAILED CLASSIFICATION (SUBCATEGORIES)
Rivers, lakes	Rivers, lakes
Glaciers, snowfields	Glaciers, snowfields
Magmatic rocks	Magmatic rocks in general Volcanic rocks Plutonic rocks
Metamorphic rocks	Metamorphic rocks in general Mainly metasedimentary rocks Mainly metamagmatic rocks
Coherent sedimentary rocks	Coherent sedimentary rocks in general Biogenic sedimentary rocks, evaporates Clastic sedimentary rocks Biogenic and clastic sedimentary rocks, possibly with evaporites
Tertiary sediments	Tertiary sediments
Incoherent quaternary sediments	Swamp deposits Reclaimed land Tephra Silt, clay (loess) Sand dune Marine and non-marine sediments Alluvia Terrace Volcanic debris Dejection cone Moraine Scree deposit Blocks (landslide) Incoherent quaternary rocks in general

Figure 8 below offers an overview of the distribution of Swiss and Japanese sites according to the age (top) and genesis (bottom) of the geological formation they are located upon. As already observed for V_S profile-related proxies (Figure 4) and topographical parameters (Figure 7), the two territories show significant differences. As for age, similar percentages of Swiss and Japanese sites belong to Holocene or Pleistocene classes; understandably, the Quaternary (volcanic) class is entirely dedicated to Japan; relatively fewer Swiss sites (compared to Japan) fall into Tertiary class, while the vice versa applies to Pre-tertiary category. As far as rock genesis is concerned, the "magmatic rocks" and "tertiary sediments" categories are dominated by Japanese sites; the opposite applies to coherent sedimentary and metamorphic rocks. Among the "incoherent quaternary sediments", few subclasses are relatively balanced between Swiss and Japanese stations: swamp deposits, alluvia, terrace and dejection cone. Other subclasses are entirely dedicated to Switzerland (e.g. moraine) or Japan (tephra, volcanic debris, marine and non-marine sediments).

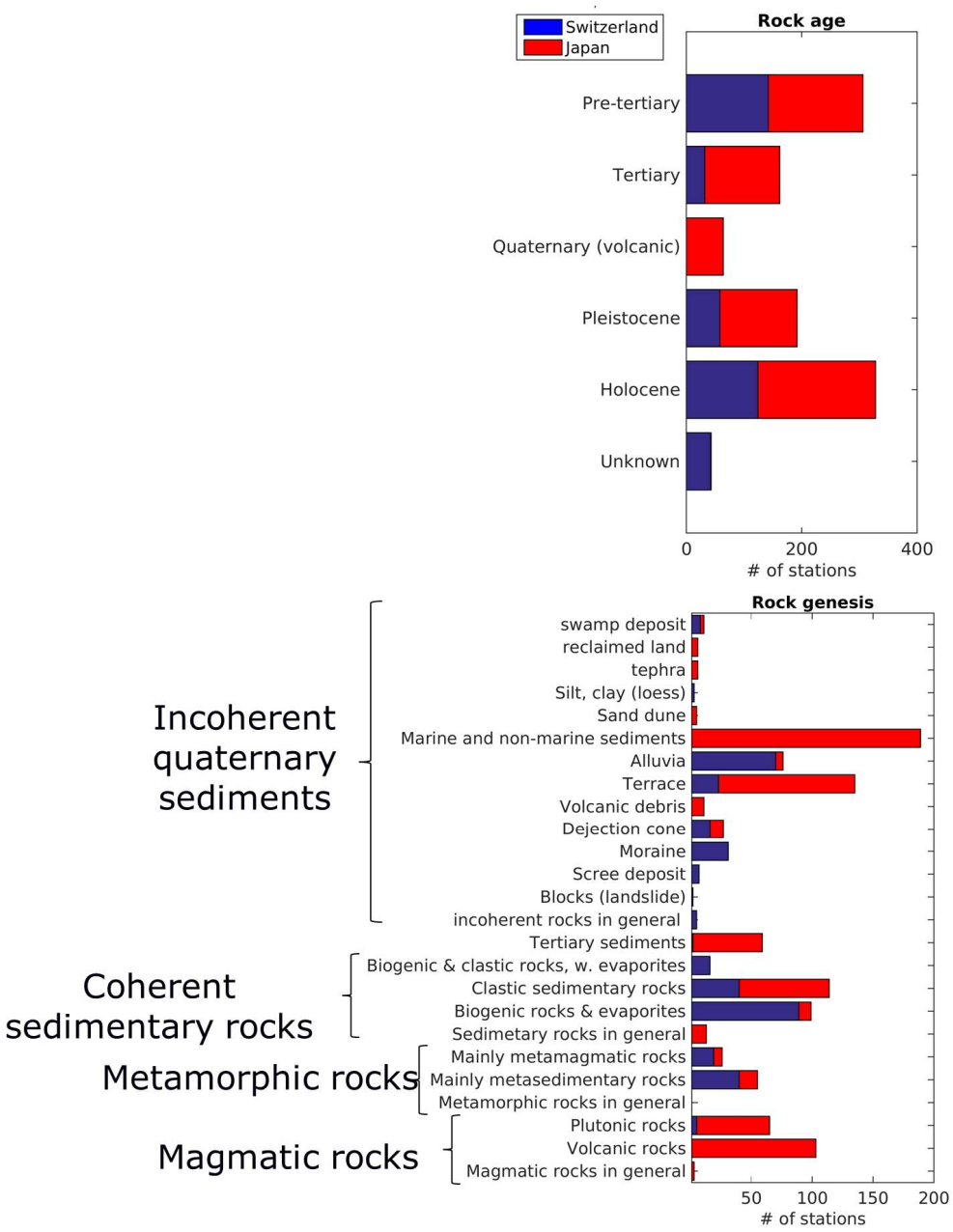

Figure 8: Top: Distribution of Swiss and Japanese stations in 5 age categories. Bottom: distribution of Swiss and Japanese stations in the categories of the detailed rock genesis classification

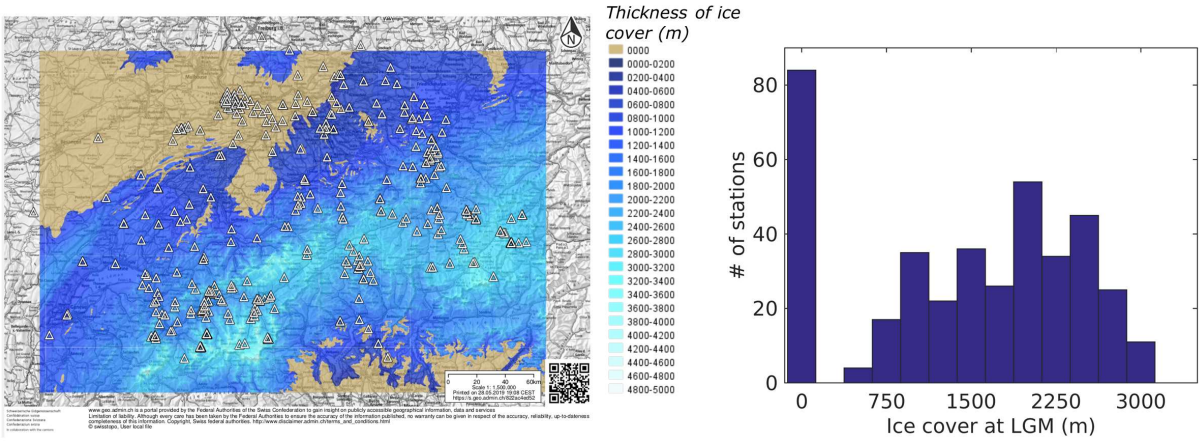

Figure 9: Thickness of ice cover at the last glacial maximum, Switzerland. Left: Map of ice cover in Switzerland at the last glacial maximum by Swisstopo (© Swisstopo). White triangles indicate the position of Swiss stations. Right: histogram of ice cover at LGM at stations locations.

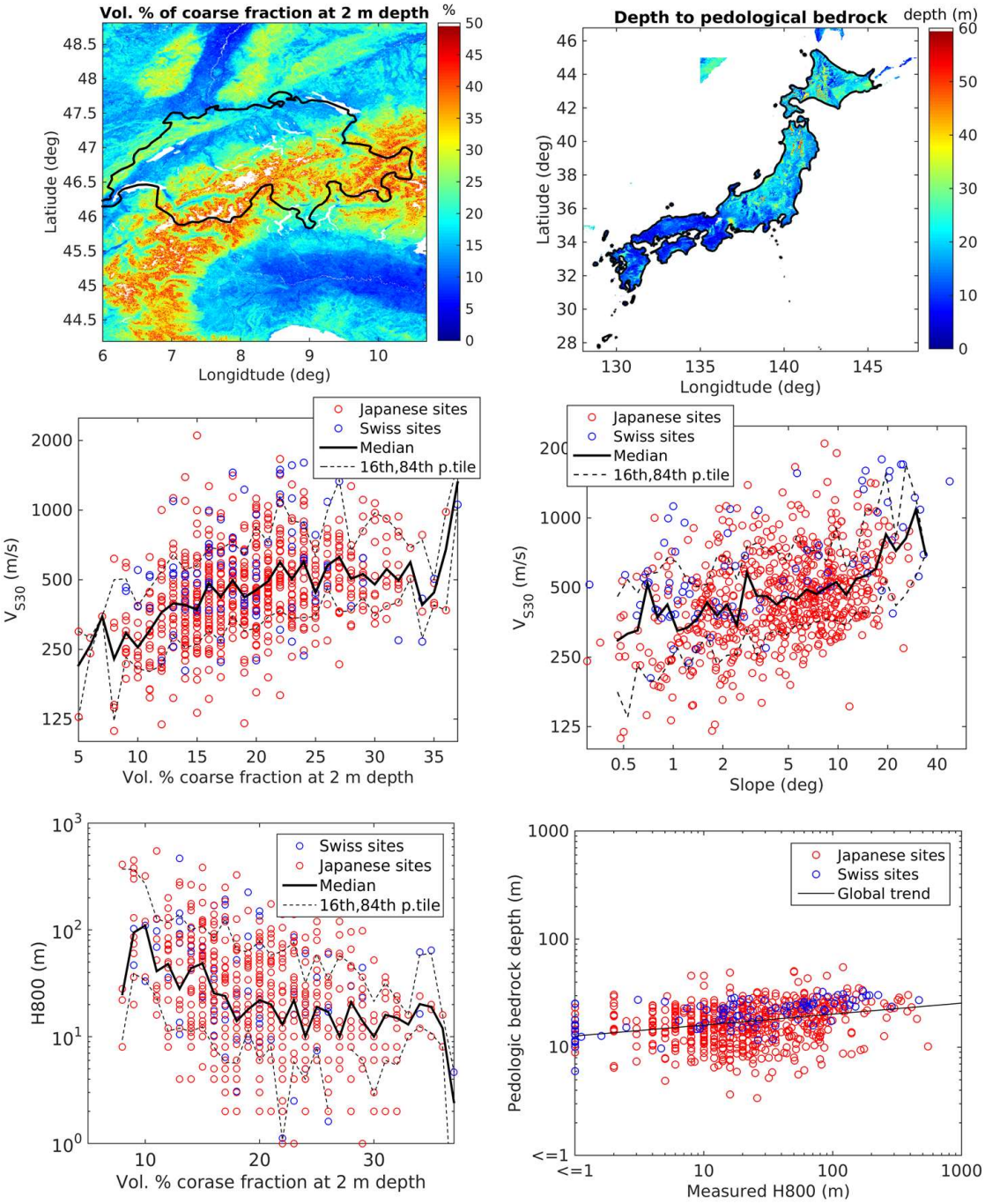

Figure 10: Proxies derived from SoilGrids250 pedologic database (Hengl et al., 2017). Top row: examples of input layers. Left: map of volumetric % of coarse fraction at 2 m depth for Switzerland; right: map of depth to pedologic bedrock for Japan. Central row, left: correlation between percentage of coarse fraction at 2 m depth and measured V_{S30} at Swiss and Japanese stations. Right: correlation between topographic slope (60 m scale) and measured V_{S30} at Swiss and Japanese stations. Bottom row, left: correlation between percentage of coarse fraction at 2 m depth and measured H800 at Swiss and Japanese stations; right: correlation between inferred pedologic bedrock depth and measured H800 at Swiss and Japanese stations.

3.2.5 Indirect proxies specific to either Switzerland or Japan

Besides the common dataset of indirect proxies illustrated in the previous subsection, we also collected site condition information from geological/lithological/geotechnical/geophysical layers, unfortunately available only for either Switzerland or Japan.

For Swiss sites, we collected the following information:

- The SIA 261 (2014) soil class (A-E) as inferred from the map of seismic subsoil categories (2017) prepared by the Swiss Federal office of environment (FOEN) and based on geological maps, drillings and geotechnical reports. The map covers only part of the Swiss territory (Figure 11). It should be noted that the soil classification from the geotechnical map does not necessarily agree with the affiliation determined by in-situ measurements (Figure 11), as already evidenced by Fäh & Gassner-Stamm (2014).
- The dominant geomorphological process (glacial, fluvial, denudativ, or karstic) as provided by the "Overview of geomorphology" layer by Swisstopo (2008), based on the Atlas of Switzerland, Sheet 8, Geomorphology (1975). See Figure 12
- The thickness of unconsolidated sediments, as inferred from the "Thickness model of unconsolidated deposits" (2019), by Swisstopo, based on the analysis of gravimetric and borehole data. The model does not cover the entire Switzerland (Figure 13). In the lower-right panel of Figure 13, the depths of the sediments-bedrock horizons from the Swisstopo layer are collated with the H800 values as measured from geophysical surveys at Swiss stations. At sites with shallow engineering bedrock (H800 < 20 m), the Swisstopo model underestimates the thickness of incoherent sediments; the correspondence between the two datasets improves for sites with a deeper bedrock (H800 > 20 m).
- The lithological classification of the underlying geological formation, as provided by the Swiss Atlas of the Physical Properties of Rocks (SAPHYR) database (Zappone and Bruijn, 2012). The database proposes a simplified classification of the 79 lithology types of the Geological Map of Switzerland, grouping them into 28 wider categories: Marls, Porous sandstones, Mudstones/shales/slates, Clac-shales/slates, Compact sandstones, Conglomerates/breccias, Calc-slates/schists, Marly limestone, Mixed carbonates, Sliceous limestones, Dolomites, Granitoids, Marbles, Radiolarites, Feldpar gneisses, Biotite micaschist/gneisses, Mica feldspar gneisses, Mica feldspar gneisses Mica schist gneisses, Quartzites, Serpentinites, Ultramafic, Volcanics, Metagabbro, Mafics, Water, Ice, Fine Grained deposits, Unconsolidated debris (Figure 14).
- The mean value of bulk density and P-wave velocity of the corresponding lithological group, attributed by SAPHYR combining the lithological map with a database of laboratory results from rock samples of geo-referenced origin (Zappone and Bruijn, 2012). Although the V_P values provided by SAPHYR appear as excessively high when collated with the V_S of the lower halfspace from geophysical measurements, they anyhow show a (weak) positive correlation with the latter (Figure 15).

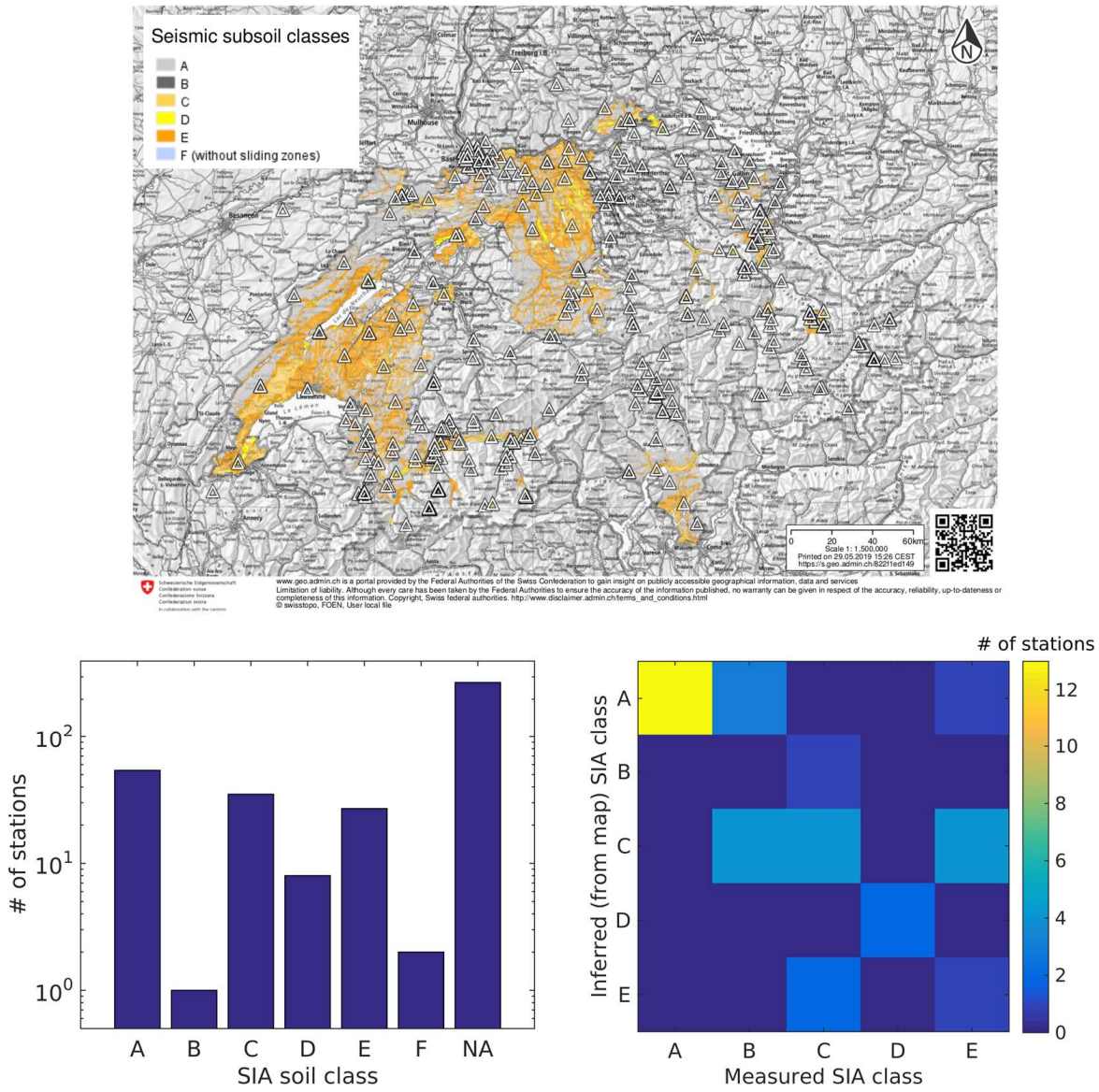

Figure 11: SIA 261 (2014) soil class map. Top: Map of seismic subsoil categories (2017) prepared by the Swiss Federal office of environment (FOEN), © Swisstopo. Bottom: soil class affiliation of Swiss stations according to the geotechnical map (NA = not available). Bottom right: comparison between soil classification as inferred from the geotechnical map and as determined by in-situ geophysical measurements (only for the stations when the latter is available).

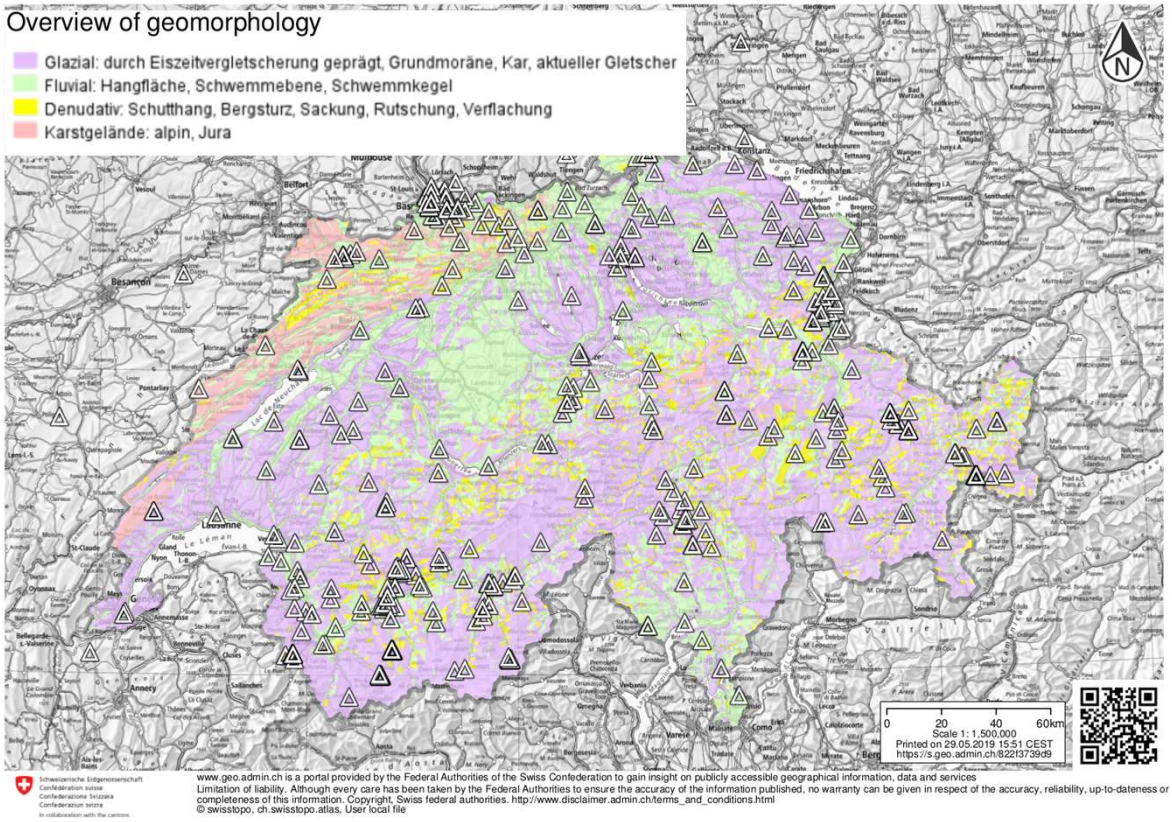

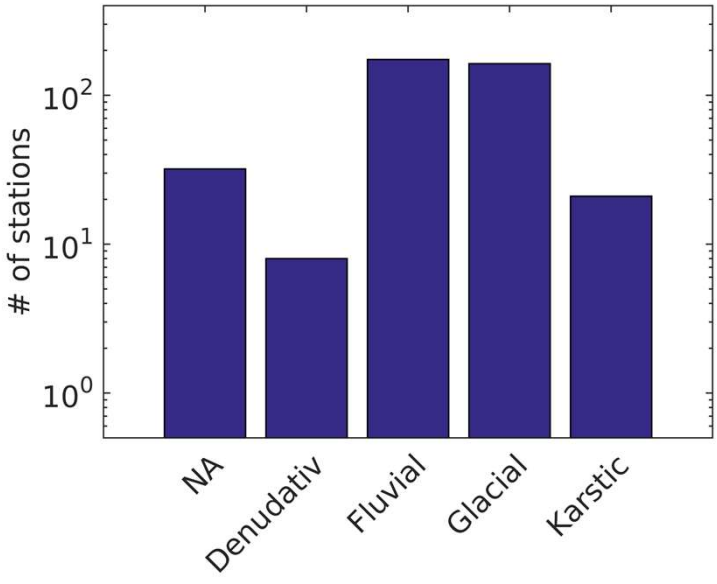

Figure 12: Geomorphologic classification for Swiss stations. Top: "Overview of geomorphology" map, © Swisstopo. Bottom: histogram of geomorphologic process at Swiss stations (NA = not available).

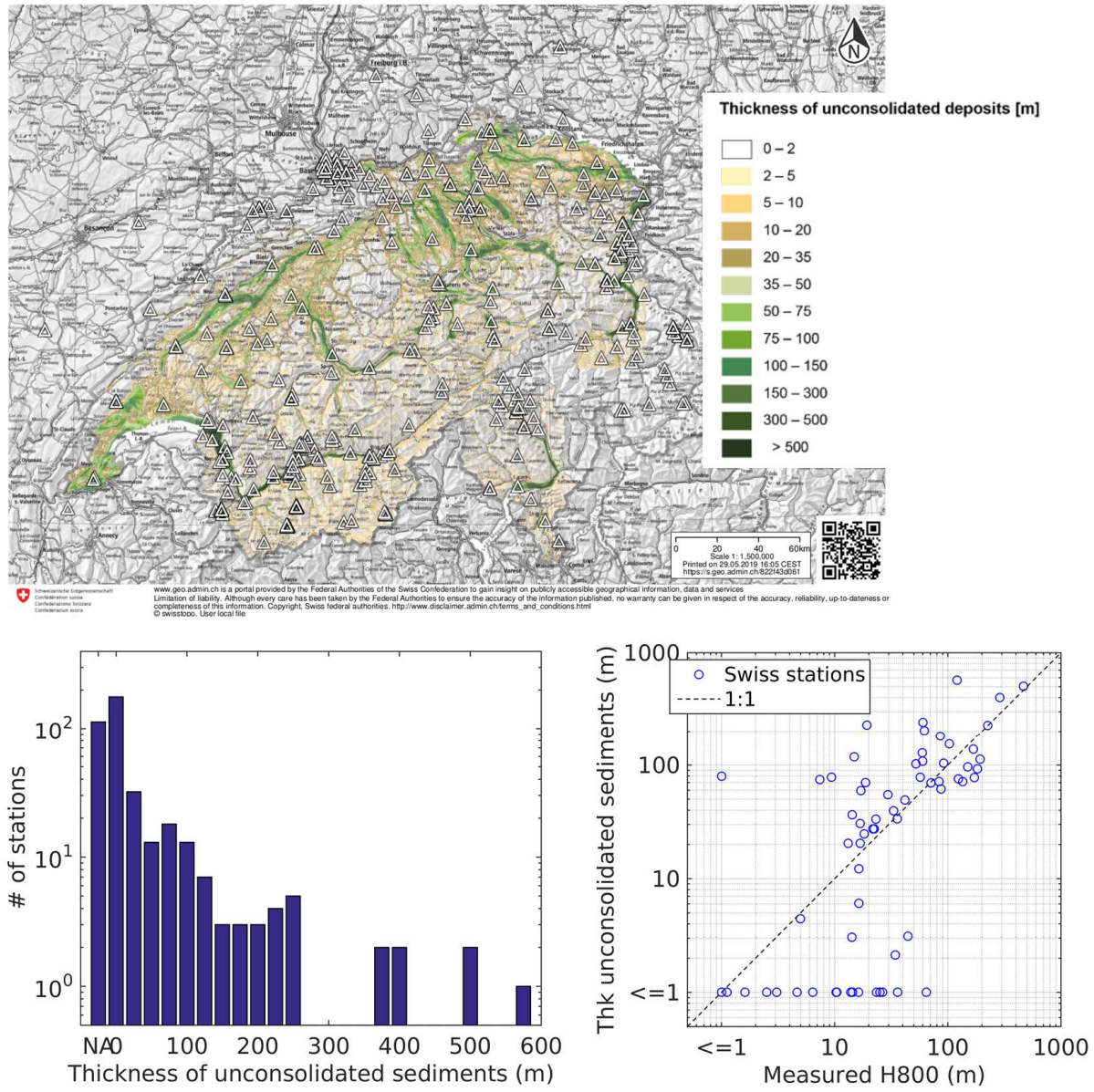

Figure 13: Thickness of unconsolidated sediments. Top: "Thickness of unconsolidated sediments" layer by Swisstopo, © Swisstopo. Bottom left: histogram of the inferred thickness of unconsolidated sediments at Swiss stations. Bottom right: comparison between the inferred thickness of unconsolidated sediments and measured H800 at Swiss stations (only for stations where a site characterization measurement is available).

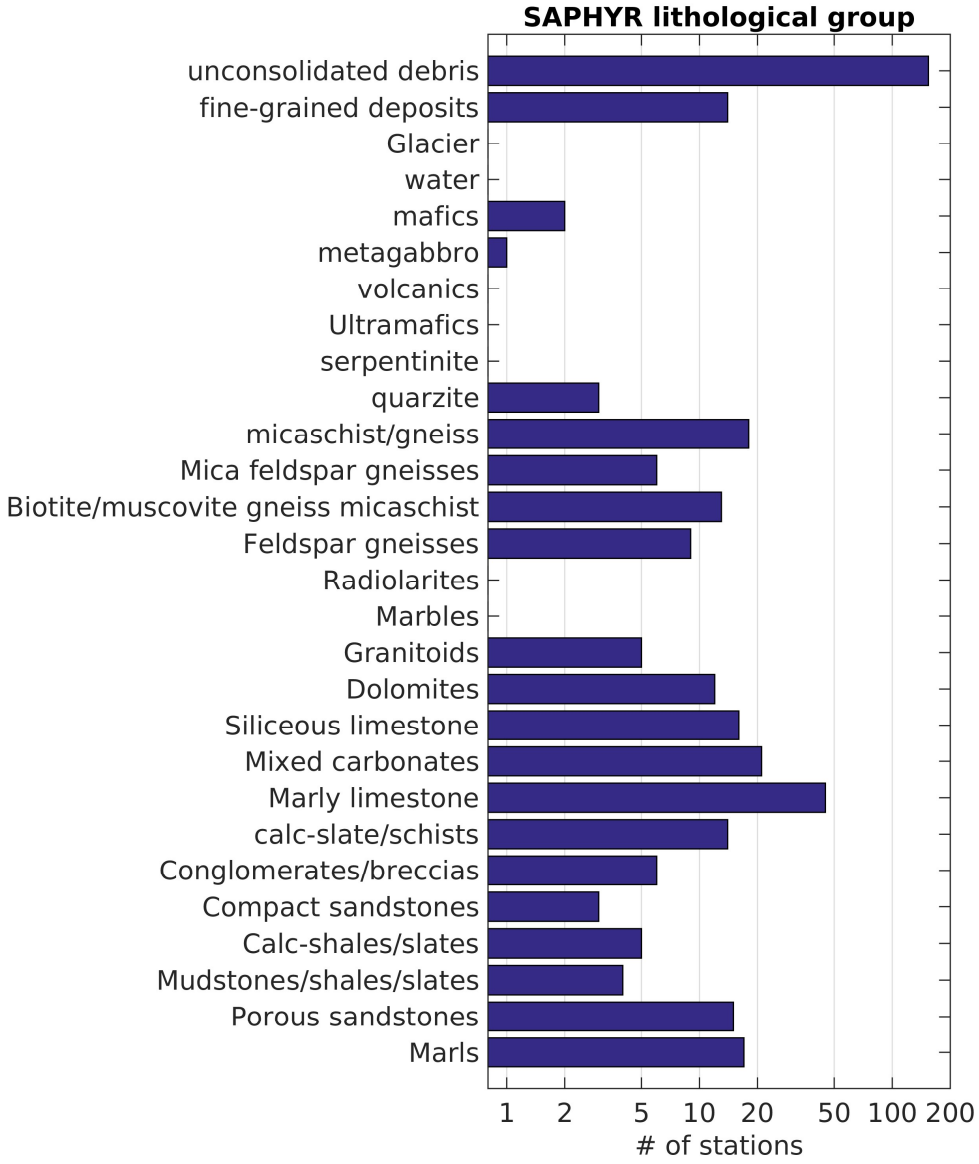

Figure 14: Distribution of Swiss stations among the 28 lithological groups of SAPHYR database.

Figure 15 below collates the V_S for the lower halfspace as estimated by site-characterization measurements and the average V_S for the suitable lithological groups as derived by SAPHYR (both values referring to Swiss stations sites). The V_S derived from SAPHYR was obtained by converting the average V_P value (directly provided by SAPHYR for each lithological group), assuming a likely Poisson's ratio of 0.17 (A. Zappone, 2018, personal communication). It is worth noting the two variables appear to be, although weakly, somehow correlated; most of the data points are comprised between 1:1 and 1:2 lines, the most occurring ratio being around 0.8.

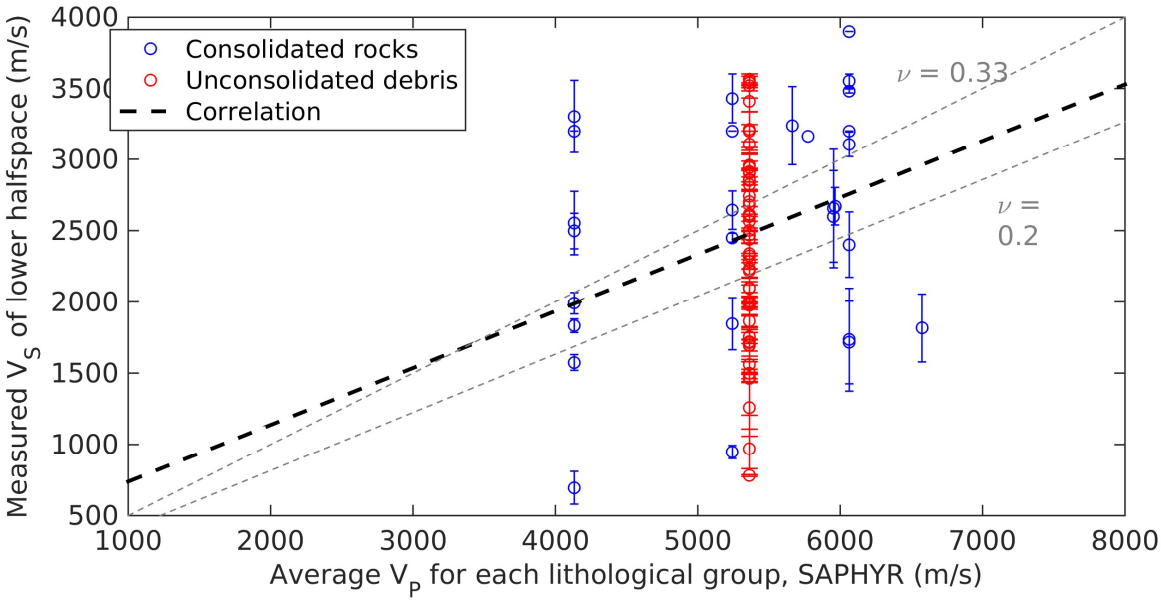

Figure 15: Collation between the P-wave velocity value inferred from SAPHYR and the V_S of the lower halfspace as estimated by in-situ geophysical measurement (for the Swiss stations where the latter is available). In red the sites belonging to the "unconsolidated debris" group, in blue the sites belonging to compact rocks lithological groups. The linear correlation between the two sets of values is represented with a dashed black line; grey lines indicated the V_P/V_S ratios corresponding to ν = 0.33 and 0.2,

As far as Japanese sites are concerned, we collected the following information:

- From the J-SHIS (Japan Seismic Hazard Information Station) database, we determined the engineering geomorphology class (Wakamatsu and Matsuoka, 2013) of each site. The J-SHIS engineering geomorphologic classification encompasses 24 different classes (see Figure 16).
- From the J-SHIS subsurface model for Japan (Fujiwara et al., 2009), we extracted the value of H800 (depth to the shallowest layer exhibiting V_S > 800 m/s) at all Japanese stations locations. Our intention was retrieving a dataset somehow similar to the "Thickness of unconsolidated sediments" available for Switzerland. Figure 17 shows the comparison between H800 as inferred from the J-SHIS subsurface model and as obtained from site-characterization measurements.
- From the Basic Geological Map of Japan 1:200000 (Geological Survey of Japan), we re-classified the 85 possible lithological types into 26 wider groups, according to our expert judgement. The intention is to provide for Japan a simplified lithological classification, similarly to what SAPHYR (Zappone and Bruijn, 2012) offers for Switzerland. See Figure 18 for the list of lithological groups and the corresponding distribution of Japanese stations.

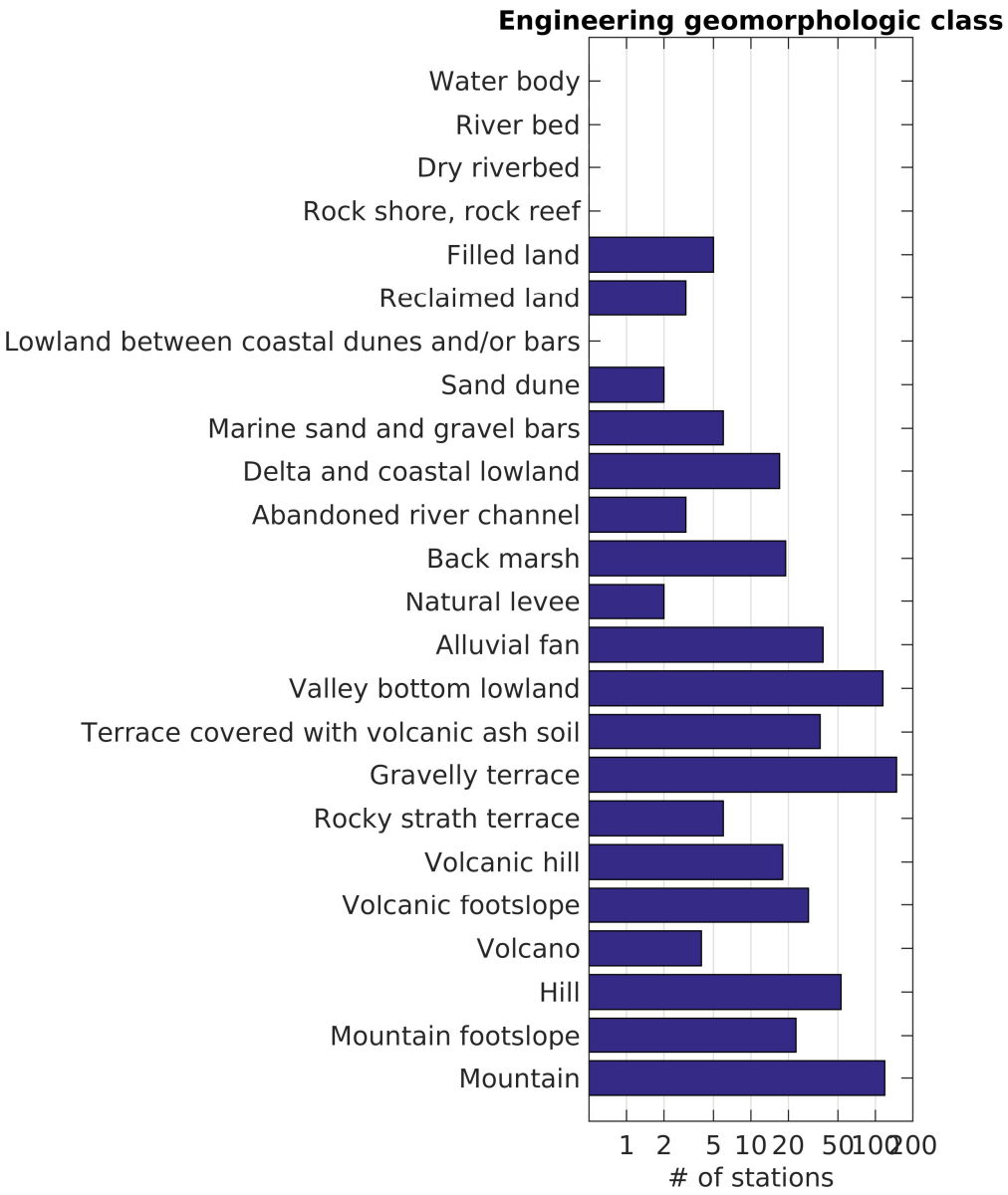

Figure 16: Distribution of Japanese stations among the engineering geomorphology classes of the J-SHIS database.

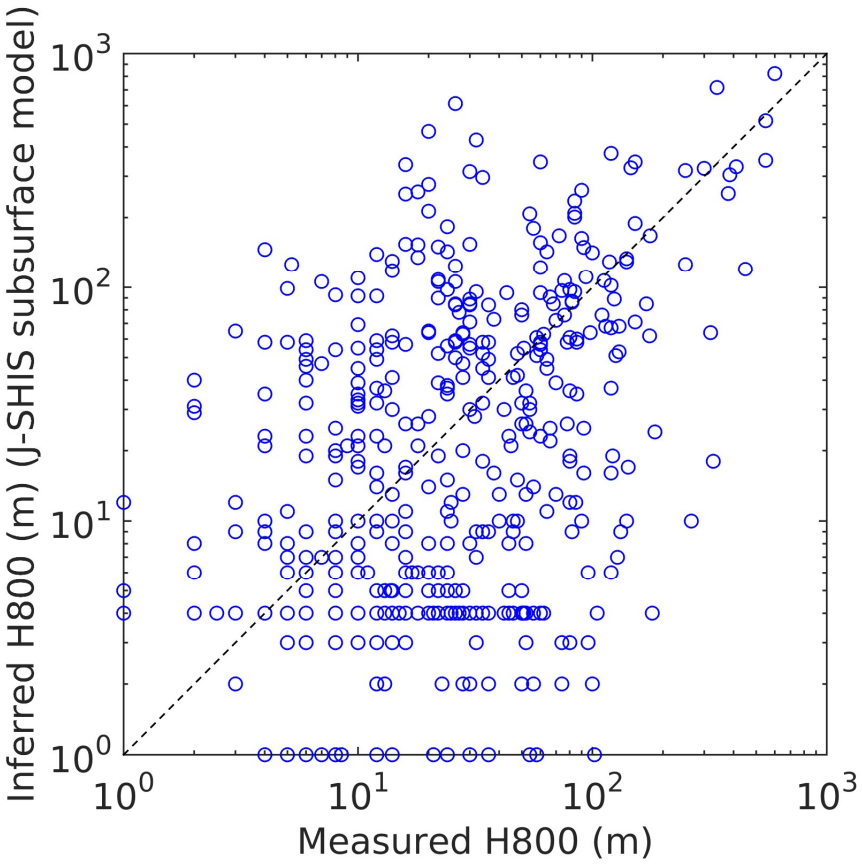

Figure 17: Comparison between measured and inferred (from J-SHIS subsurface model) H800 values at KiK-net stations.

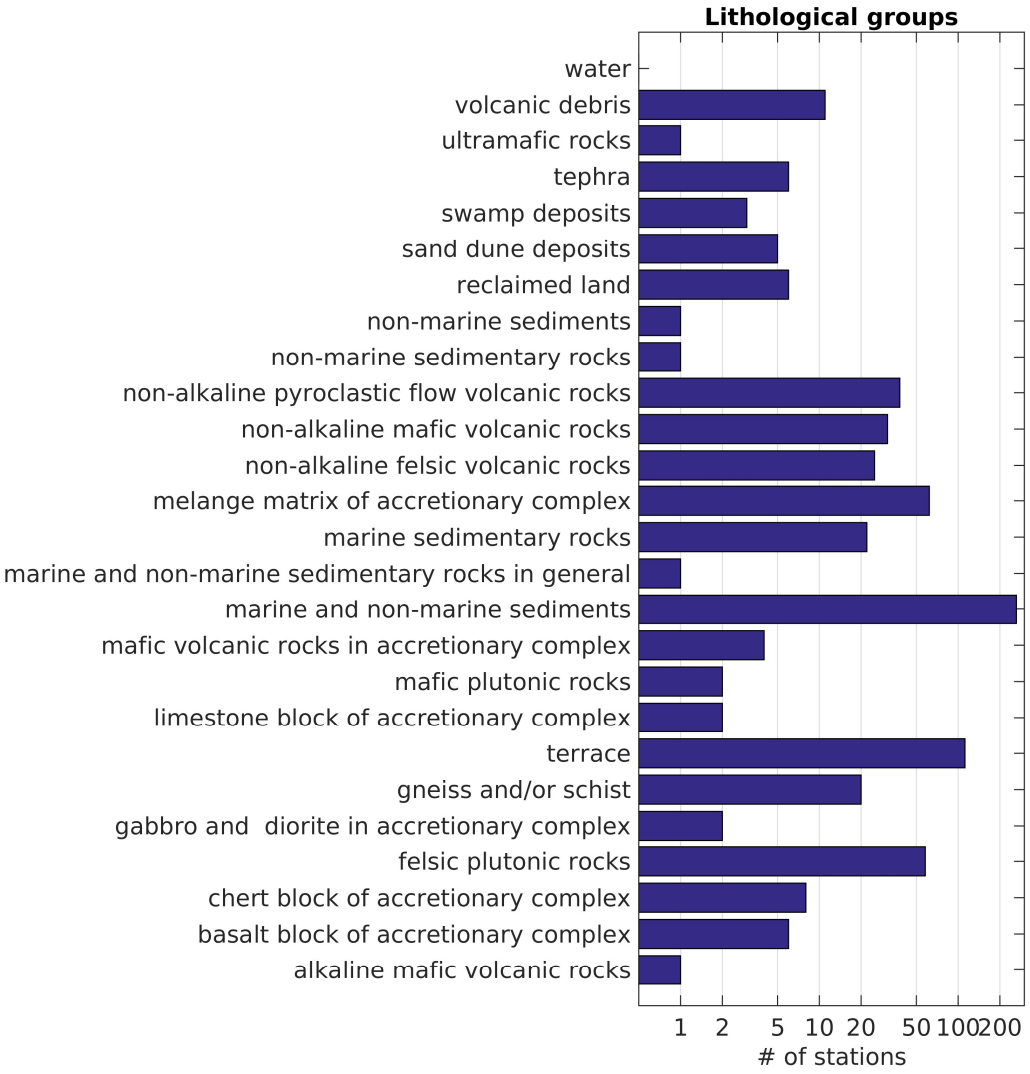

Figure 18: Distribution of Japanese Kik-net sites into the 26 lithological group we defined on the basis of the Basic Geological Map of Japan 1:20000.

To offer a synthetic overview of the entire database of site condition parameters we compiled, we present Table 7 below. The text in black in the two rightmost columns ("Collected proxies" and "Data sources") refers to both Switzerland and Japan, text in red refers to Japan only, text in blue to Switzerland only. * indicates that a measure of uncertainty for the corresponding proxy value was available and was included in the database.

Table 7: Overview of the compiled site condition parameters database. Text in black refers to both Switzerland and Japan, text in red refers to Japan only, text in blue to Switzerland only. * indicates that a measure of uncertainty for the corresponding proxy value was available and was included in the database.

TYPE OF INFORMATION		COLLECTED PROXIES	DATA SOURCES
Proxies directly derived from measured V_S profile		V_{S10}*, V_{S20}*, V_{S30}* ,$V_{Sbedrock}$*, V_{Sm}*, H800*, C_V*, C_{V10}*, Vs^{QWL}*, IC^{QWL}*	SED site characterization database Kik-net site characterization database
Proxies derived from H/V_{noise} measurements		f_n*, A_n* (n = 0-2), H/V amplitudes* at selected frequencies (0.5 – 20 Hz).	SED H/V_{noise} database
Topographical parameters		Topographical slope, TPI_{norm}, terrain class at scales 60, 100, 180, 340, 660, 1140, 2020 m Smoothed topographical curvature (total, along easting and northing axes) at scales 180, 340, 660, 1140, 2020 m Smoothed topographical curvature (total, along easting and northing axes) at scales 60 and 100 m	ASTER GDEM V2 DHM25, swissALTI3D
Common (for Switzerland and Japan) dataset of indirect proxies		Rock age class Rock genesis classification, coarse and detailed	Geological Map of Switzerland 1:500000 Detailed Geological Map of Japan 1:200000
		Ice cover thickness at LGM*	Switzerland During the Last Glacial Maximum (LGM) 1:500000 Ono et al. (2004, 2005)
		Vol. % of coarse fraction at 2 m depth Depth to pedologic bedrock	SoilGrids250m
Indirect proxies specific to either Switzerland or Japan.	Switzerland	SIA 261 (2014) soil class (A-F)	Map of seismic subsoil categories (FOEN)
		Geomorphologic class	Overview of geomorphology map (Swisstopo)
		Thickness of unconsolidated sediments	Thickness model of unconsolidated sediments (Swisstopo)
		Lithological group	SAPHYR (Zappone and Bruijn, 2012)
		Average V_P* and ρ_b* for each lithological group	SAPHYR (Zappone and Bruijn, 2012)
	Japan	Engineering geomorphology class Inferred H800	J-SHIS database
		Lithological group	Basic Geological Map of Japan 1:200000

4 Dataset of experimental amplification functions

The database of site condition indicators illustrated in the previous section was tested against a parallel dataset of empirical Fourier amplification functions derived for the same ensemble of sites (Swiss and Japanese KiK-net stations).

For Switzerland, we obtained the set of experimental amplification functions from the processing of regional seismicity data with the application of a spectral fitting method (Edwards et al., 2013). In brief, the Fourier spectrum observed at an instrumented site is compared with a corresponding simulated spectrum; their difference is ascribed to local site effects. Consequently, for each event and at each station an elastic site response and local attenuation are obtained, both referred to a pre-defined standard rock profile. Averaging over the population of single-event amplification functions available for a given station, we retrieve the mean empirical amplification function representative for that site (as well as its standard deviation).

In our case, we resorted to the database of earthquake waveforms acquired by the national seismic networks of Switzerland (strong-motion and broadband), recorded from 2009 onwards. As output dataset, we derived a set of inelastic Fourier amplification functions for horizontal ground motion, referred to the Swiss rock reference profile as defined by Poggi et al. (2011). Our dataset covers 185 stations (out of a total of 398 sites), as not all sites have a sufficient number of records to constrain a reliable inelastic amplification function. Since the final target of our study is relating site proxies to amplification at the soil surface, we further narrowed down our database to free-field or urban free-field stations, for a final list of 145 sites (excluding stations located in tunnels, borehole, buildings, etc.). Foreseeing the final use of these amplification functions for a neural-network structure and for regression analyses (see following section), we discretized the continuous amplification functions, retaining their mean values and standard deviations at the following ten frequency abscissae: 0.5, 1, 1.67, 2, 3.33, 4, 5, 6.67, 10, 20 Hz.

Figure 18 shows the dataset of empirical amplification functions for the 145 (urban) free-field Swiss stations.

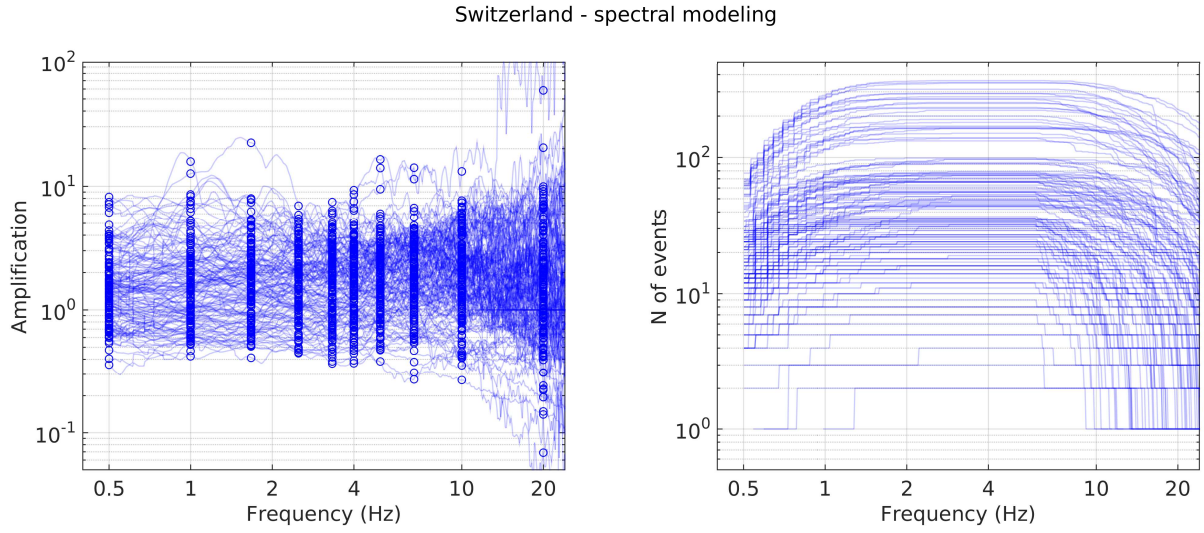

Figure 18: Empirical amplification functions for Swiss (urban) free field stations. Left: Fourier amplification functions. Circles indicate the Fourier amplification factors at selected frequencies (0.5, 1, 1.67, 2.5, 3.33, 4, 5, 6.67,10, 20 Hz). Right: number of events used for the computation of the amplification functions.

As far as Japanese sites are concerned, we followed two parallel approaches to obtain Fourier amplification functions

- The firs approach is that of spectral fitting method, already illustrated above for Switzerland. For Japan, we resorted to the KiK-net waveform database (data 1997-2011), using the recordings from the surface seismometers only. As output dataset, we derived a set of inelastic Fourier amplification functions for horizontal ground motion, referred to the Japanese reference rock profile as defined by Poggi et al. (2013). Our dataset covers 348 stations (out of a total of 698 sites), as not all sites have a sufficient number of records to constrain a reliable inelastic amplification function. According to our knowledge, all KiK-net surface stations can be classified as free field. As final step, for comparability with the Swiss amplification curves, we referred the Japanese functions to the Swiss reference rock profile (Figure 19).
- The second approach exploits the peculiar configuration of KiK-net sites, equipped with a couple of borehole and surface seismometers. The ratios between the Fourier spectrum at surface and borehole receivers for the same events were computed (data 1997-2011), thus providing surface-to-borehole (SB) ratios that portray the local amplification effect between the two seismometers (Cadet et al., 2012). SB ratios from different events recorded by the same station are then averaged to produce a mean ratio representative of that site. We were then able to retrieve SB ratios for 648 sites (out of 698).
  Obviously, these "raw" SB ratios all have a different reference (the rock hosting the borehole receiver), so they are not reciprocally comparable. To do so, they need to be "normalized" to a reference rock profile, besides being corrected for peculiar effects arising from the configuration of the borehole receiver, embedded within the subsurface (Cadet et al., 2012). We therefore applied correction procedures directly derived from or similar to those of Cadet et al. (2012). It should be noted that these procedures require the knowledge of the V_S profile between surface and borehole receivers, which is not entirely available for few KiK-net stations. As outcome, we obtained 637 SB ratios first normalized to the Japanese reference rock profile, then eventually referred to the Swiss reference rock, for compatibility with the Swiss data (Figure 20).

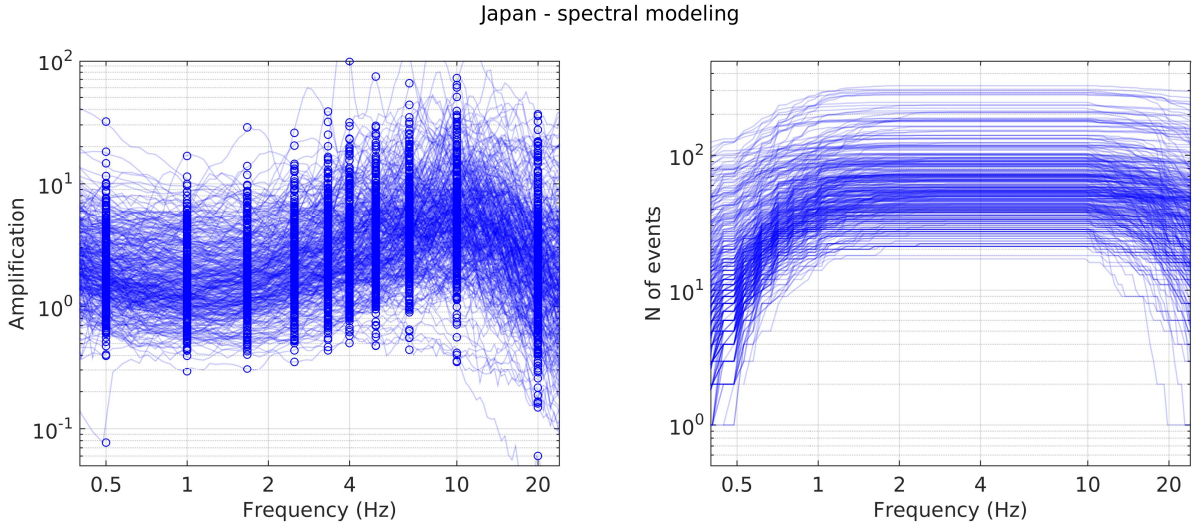

Figure 19: Empirical amplification functions for Japanese KiK-net stations, obtained from spectral modeling technique. Left: Fourier amplification functions. Circles indicate the Fourier amplification factors at selected frequencies (0.5, 1, 1.67, 2.5, 3.33, 4, 5, 6.67,10, 20 Hz). Right: number of events used for the computation of the amplification functions.

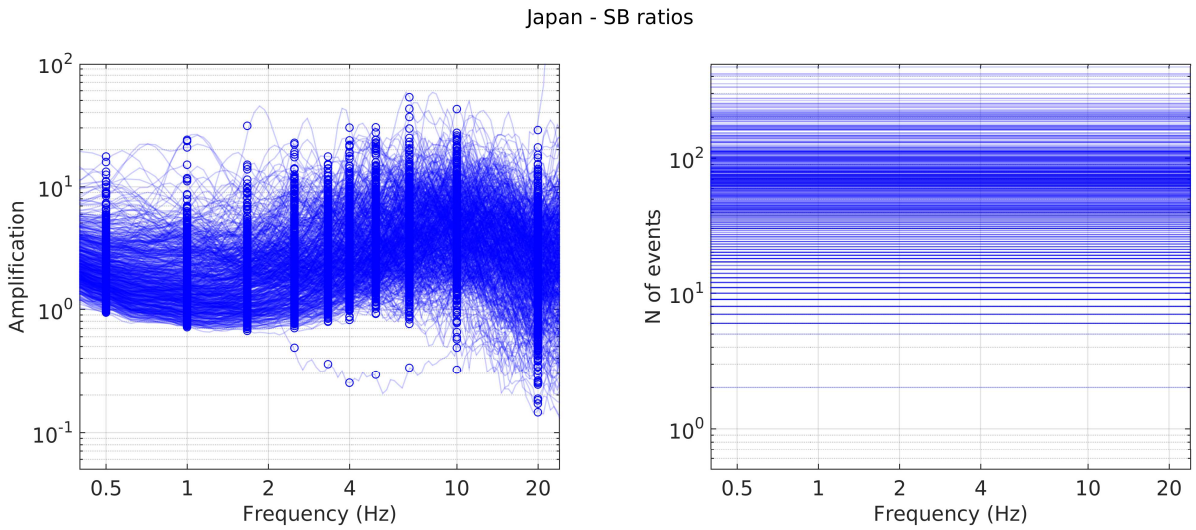

Figure 20: Empirical amplification functions for Japanese KiK-net stations, derived from surface-to-borehole ratios. Left: Fourier amplification functions. Circles indicate the Fourier amplification factors at selected frequencies (0.5, 1, 1.67, 2.5, 3.33, 4, 5, 6.67,10, 20 Hz). Right: number of events used for the computation of the amplification functions.

To obtain a single dataset of empirical amplification functions for Japanese sites, we merged the functions derived from spectral fitting method and those from SB ratios, with the following criteria:

- For any station where an amplification function from spectral fitting method is available (348), that is chosen as representative for the site. In fact, from our point of view, the primary need is to work on a dataset of amplification functions which are reciprocally comparable, i.e. normalized to the same reference profile; the spectral modeling method directly provides this result. Vice versa, the translation of raw SB ratios to commonly referenced amplification curves requires a series of intermediate steps which are based on simplifying assumptions and/or parameters derived from the provided V_S profile (Cadet et al., 2012), which are known to be partly unreliable (Holt et al., 2017);
- For 300 other sites, the amplification functions derived from SB ratios are chosen.

It should be noted that for 50 additional KiK-net sites no amplification function is available.

Figure 21 compares the global distributions of the amplification functions datasets for Switzerland and Japan, at the selected frequency abscissae. The main difference is related to the “hump” exhibited by Japanese stations in the frequency range 4 – 10 Hz, which is just slightly evident for Swiss sites. This discrepancy can be ascribed to the general difference between the near-surface subsoil conditions of the two datasets, summarized in Figure 4 (comparison of the distributions of V_{S30}, V_{Sm}, H800, $V_{Sbedrock}$ for Swiss and Japanese sites). In fact, lower S-wave velocities for the unconsolidated surficial cover and shallower H800 values (Figure 4, see also I_C^{QWL} in bottom row) are indeed compatible with the marked peak of Japanese amplification functions in Figure 21.

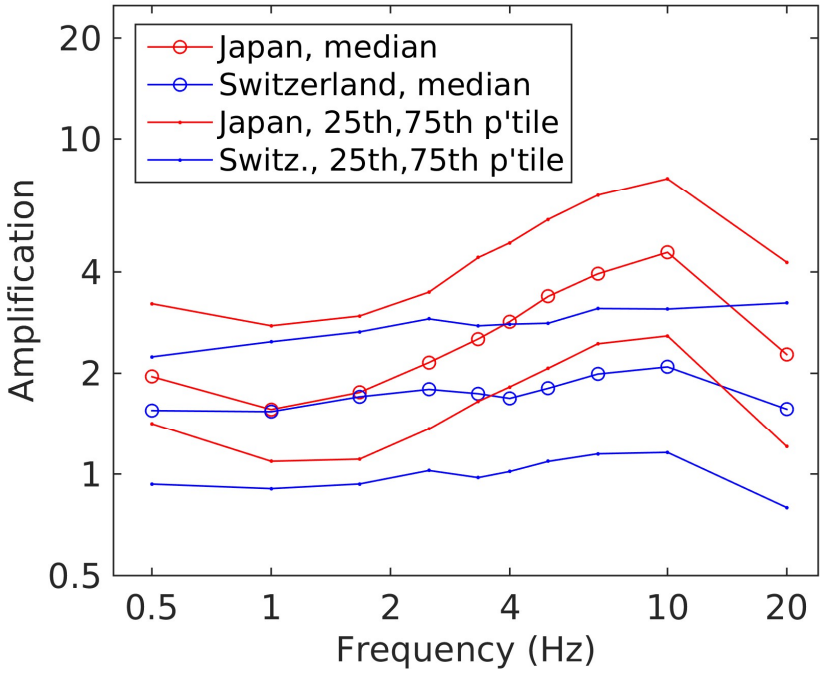

Figure 21: Comparison between the global distributions of the amplification functions datasets for Switzerland and Japan, at the selected frequency abscissae (0.5, 1, 1.67, 2.5, 3.33, 4, 5, 10, 20 Hz).

5 Investigating the correlation between proxies and site amplification through regression analyses and statistical tests

As anticipated in the introduction, in this work the relationship between site condition indicators and site amplification is investigated following two approaches: a neural network structure, attempting to predict amplification factors based on the proxy database (chapter 6), and a series of regression and statistical test analyses, aiming to determine straightforwardly the sensitivity of local amplification to each individual site condition parameter.

This chapter focuses on the second approach. In detail, the targets of our analysis were:

1. To determine the sensitivity of frequency-dependent amplification factors to each continuous-variable proxy; to determine the "strength" and statistical significance of each amplification-proxy correlation. For these goals, we systematically carried out a set of regression analyses (Davis, 2002);
2. For non-continuous variable proxies (e.g. geological/morphological/topographical classes), to determine to what extent the classification they propose actually translates into grouping sites with homogeneous amplification behavior. For this purpose, we adopted as tool statistical tests assessing the significance of the difference of the distribution of the same variable in two populations (Welch, 1947).
3. Based on the results of the regression analyses and statistical tests, to rank the proxies in terms of effectiveness, frequency by frequency;
4. To determine to what extent the behavior of the same proxy is similar at Swiss or Japanese sites.

We highlight that our work aims at correlating site condition parameters and amplification at the free soil surface; therefore, for the analyses presented in this section, we resorted to proxies and amplification data referring to free-field or urban free-field stations (145 out of 398 for Switzerland; all 698 for Japan).

In our opinion, the tools we have selected (regressions, statistical tests), due to their relatively lower level of complexity (with respect to neural network), allow to capture straightforwardly the correlation between site condition parameters and amplification factors. In our intention, some of the expected outcomes of this phase (in particular the ranking of proxies, 3, and the similarity Switzerland-Japan, 4) should provide useful information for or elements of comparison with the neural network. On the other hand, the analyses illustrated in this section do not have any ambition of prediction of amplification factors; this task is entirely left to the neural network (chapter 6).

In the following, we successively focus on each of the goals listed above (1-4).

5.1 Regression analyses between continuous-variable proxies and frequency-dependent Fourier amplification factors.

We systematically investigated the correlation between continuous-variable proxies and Fourier amplification factors through a series of regression analyses. For simplicity, we chose a linear regression model (Davis 2002); although elementary, the linear model has shown to perform adequately for the vast majority of proxies (see Figures 22, 23, 25, 27-29, 31, 32, 34-37). Each proxy was correlated with the dataset of amplification factors at the 10 selected frequencies (0.5 – 20 Hz), separately for Swiss and Japanese data. The continuous-variable parameters we considered are:

- Proxies derived from measured V_S profile: $V_{S10\text{-}20\text{-}30}$, $V_{Sberock}$, V_{Sm}, H800, C_v, C_{v10}, V_S^{QWL}, I_C^{QWL};

- Proxies derived from H/V_{noise} measurement: f_0, A_0, H/V amplitudes at selected frequencies (0.5 – 20 Hz), all available for Swiss sites only;
- Topographical parameters: slope, TPI_{norm} and smoothed topographical curvature (STC) at the seven scales 60 – 2020 m; absolute difference between STC_N and STC_E.
- Common dataset of indirect proxies: ice cover thickness at LGM, % of coarse fraction at 2 m depth, depth to pedologic bedrock;
- Indirect proxies specific to either Switzerland or Japan: thickness of unconsolidated sediments, average V_P and ρ_b for lithological group (Switzerland); inferred H800 (Japan).

In total, we carried out 840 regressions (84 ensembles of proxies – distinguishing between Switzerland and Japan – times 10 frequencies for the amplification factors).

The regression method we implemented is the least-squares method applied to weighted linear regression analyses (Davis, 2002). In brief, we correlate with a linear model two variables, an independent variable X (regressor) versus a dependent (regressed) variable Y. Through least-squares inversion, we identify the best performing values for b_0 (intercept) and b_1 (slope), of the functional form

$$\widehat{y_i} = b_0 + b_1 x_i \qquad (1)$$

where $\widehat{y_i}$ is the modelled value of y_i at specified values of x_i. The best performing couple of b_0, b_1 minimizes the distances between actual and estimated values of y_i in a least-squares sense. Each distance is weighted by the weight w_i (hence weighted linear regression), associated to each y_i. In our case, the independent variable X is the site condition proxy, while the dependent variable Y is the mean Fourier site amplification factor for a chosen frequency abscissa; the weights w_i are the inverse of the variances of the amplification factors (computed over the population of individual-event amplification factors). Since the two variables X,Y should not exhibit a skewed distribution, the amplification factors are translated to the logarithmic scale (as common in literature, e.g. Edwards et al., 2011), and so are many proxies (for each parameter, we evaluated whether its linear or logarithmic form is more suitable for the linear correlation). Figure 22 shows the linear regressions between Fourier amplification factors and V_{S30} (Japanese data) in bi-logarithmic scale.

From each regression, we cared to obtain the following output:

- Least-squares solution for b_0, b_1 and corresponding standard errors (σ_{b0}, σ_{b1}). See Figure 24 (top row) for an example;
- coefficient of determination $r^2 = SS_R/SS_T$, with SS_R = sum of squares due to regression and SS_T = total sum of squares of Y. r^2 expresses the goodness of fit of the linear model (1 = perfect fit; Davis, 2002). See Figure 24 (center row);
- the correlation coefficient $r = sign(b_1) (r^2)^{0.5}$. It is a measure of the strength and direction of the linear relationship between X and Y. r=1 means total positive linear correlation, 0 means no linear correlation, -1 total negative linear correlation;
- the 95% confidence belt around the regression (Davis, 2002; see dashed lines in Figure 22);
- the p-value of the one-way analysis of variance (ANOVA) test evaluating the significance of the goodness of fit of the linear regression (Davis, 2002; see Figure 24, bottom row, circles);
- the p-value of the t-test evaluating the significance of the linear model slope (Davis, 2002; see Figure 24, bottom row, crosses).

We used the two latter values to determine whether the linear correlation between proxy and amplification factor is statistically significant or not. For both tests we assumed a 5% level of significance ($\alpha = 0.05$). If both tests are passed (i.e. both p-values are $< \alpha$, hence both the goodness of fit and the slope coefficient are significant with a 95% or higher confidence level), we then assumed the proxy-amplification correlation to be statistically significant.

As we have described in chapter 3, some site condition parameter datasets for Swiss stations are accompanied by an estimate of the uncertainty on the central proxy values. In these cases, the linear regression method described above must be modified to properly take into account the uncertainty

ranges on the X variable as well. We therefore adopted the weighted linear regression model with errors in bivariate data by Thirumalai et al. (2011), as well as their code. In such a case, the best performing linear model minimizes (in a least-squares sense) the orthogonal distances between the data points and the fitted line; the distances are suitably scaled for the weights of X and Y variables (Figure 25). Also from these orthogonal regressions we cared to obtain the same outputs listed above: b_0, b_1, σ_{b0}, σ_{b1}, r^2, r, 95% confidence belt and p-values.

For direct comparability with the results from the proxies lacking uncertainty information, we ran both ordinary least-squares and orthogonal distance regressions for the site condition parameters accompanied by uncertainty ranges. See Figures 23 and 25-26 for a first comparison between the two regression methods. A systematic collation is illustrated in section 5.4.1.

5.1.1 Proxies derived from measured V_S profile

The datasets of frequency-specific Fourier amplification factors were regressed against the proxies derived from measured V_S profile ($V_{S10\text{-}20\text{-}30}$, $V_{Sberock}$, V_{Sm}, H800, C_v, C_{v10}, V_S^{QWL}, I_C^{QWL}). These are available only for 84 (urban) free-field Swiss stations covered by site-characterization measurements. As for Japan, for 646 stations (out of 698) a complete V_S profile from down-hole seismic test is provided. However, it is known that not all profiles are necessarily correct, or portray the velocity model with a resolution precise enough to properly describe the stratigraphic amplification (Holt et al., 2017, Poggi et al., 2012a, 2013). Therefore, we narrowed down our analysis to a selection of 276 KiK-net sites that we consider to have a reliable velocity profile, based on the collation between the modeled SH-waves transfer function (from the provided V_S model) and the empirical $H/V_{earthquake}$ curve (Poggi et al., 2012a, 2013).

To prevent the proxy variables to have a skewed distribution, we adopted the logarithmic scale for V_{S30} (as is common practice; see for instance Derras et al., 2017), and consequently for all other velocity proxies (V_{S10}, V_{S20}, V_S^{QWL}, V_{Sm}, $V_{Sbedrock}$). When expressed in logarithmic scale, C_v, C_{V10} and I_C^{QWL} are linear combinations of logarithms of velocity quantities, so we used the logarithmic scale for them too. We remark that also in Poggi and Fäh (2015), V_S^{QWL} and I_C^{QWL} are correlated to amplification in a bi-logarithmic scale. Finally, after comparing the distributions of H800 values in linear and logarithmic scale, we adopted the latter (as in Derras et al., 2017).

As examples, Figures 22 and 23 show the regression of amplification factors at f=0.5-20 Hz versus V_{S30} for Japanese and Swiss data, respectively. It is worth remarking that the correlation model we adopted, i.e. a linear model, appears to be generally suitable in describing the relationship between proxy and amplification factors. Secondly, the trend we observe over the frequencies is similar in Switzerland and Japan: the (negative) correlation is more marked in the central frequency range (1.67 – 6.67 Hz) and weaker at very low or high frequencies. This is quantitatively shown in Figure 24: at 1.67 – 6.67 Hz the slope coefficients have larger absolute value (similar for Switzerland and Japan), and r^2 are higher. As for statistical significance, all correlations on Japanese data pass both tests (hence we consider them as significant). For Switzerland, regressions at 0.5 and 20 Hz are not significant, as they fail to pass the t-test for the slope coefficient. In section 5.4.1 we present a systematic comparison for the regressions amplification vs. proxies in Switzerland and Japan.

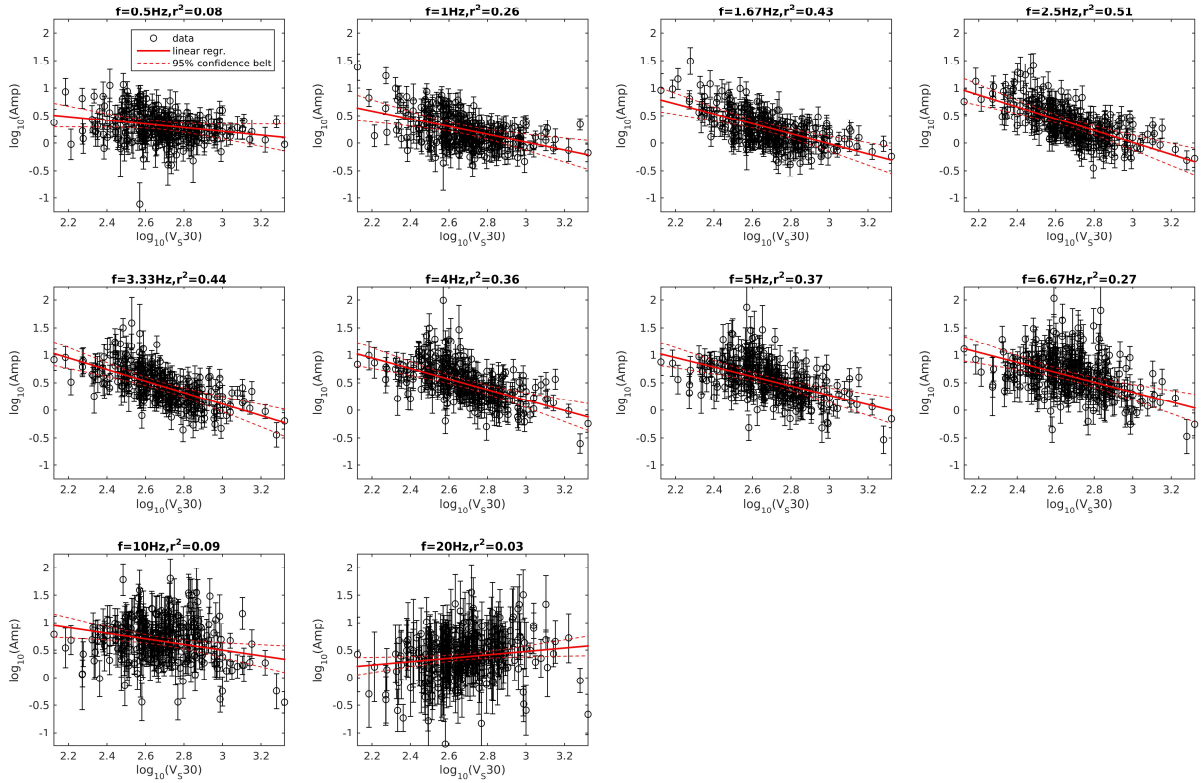

Figure 22: Japanese dataset: linear correlations between Fourier amplification factors at ten frequency abscissae (f=0.5-20 Hz) and V_{S30}, in bi-logarithmic scale. All correlations are statistically significant.

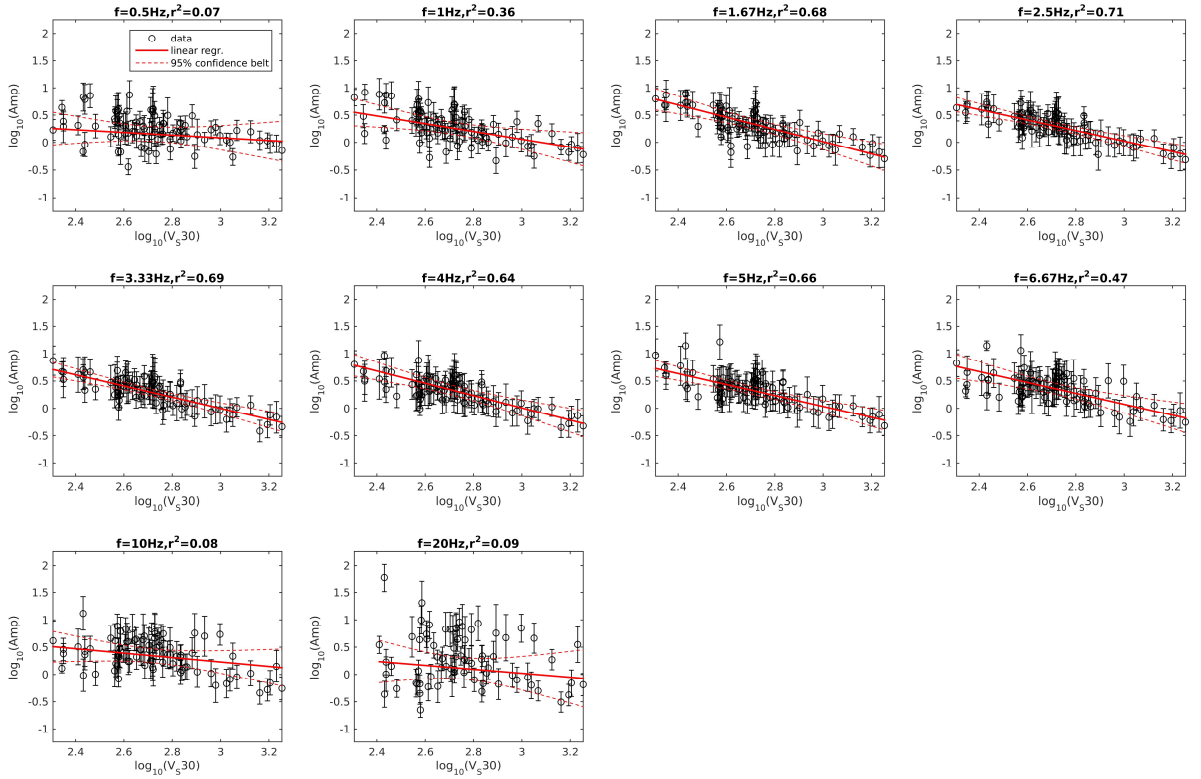

Figure 23: Swiss dataset: linear correlations between Fourier amplification factors at ten frequency abscissae (f=0.5-20 Hz) and V_{S30}, in bi-logarithmic scale. The correlations at f = 0.5 and 20 Hz are not statistically significant.

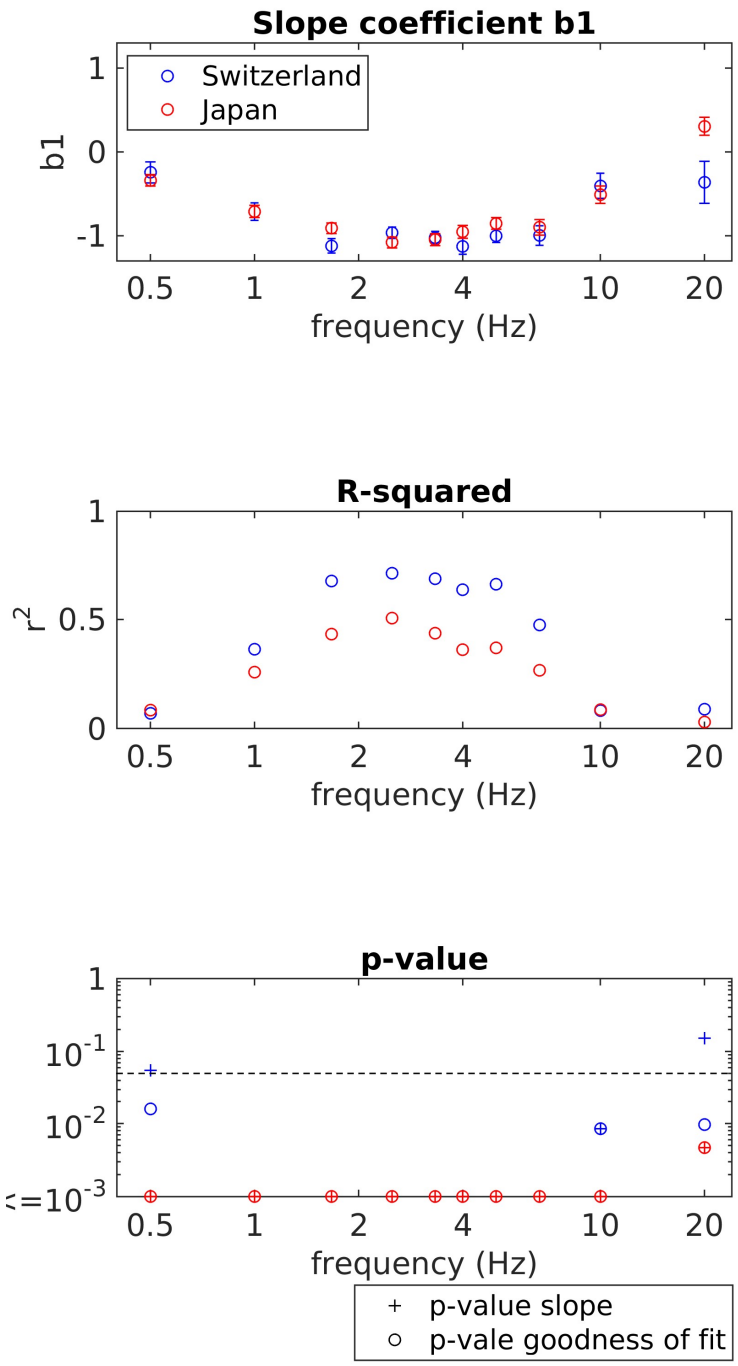

Figure 24: Comparison between parameters in output from the regressions of amplification factors versus V_S30 for Switzerland (blue) and Japan (red). Top: slope coefficients with standard errors. Centre: coefficient of determination r^2. Bottom: p-values of statistical tests for the goodness of fit (circles) and significance of slope coefficient (crosses); the horizontal dashed line represents the adopted significance level (0.05, or 5%)

As anticipated, for the site condition parameter datasets with error estimates (as is the case of V_S-profile proxies for Swiss stations) we computed also the orthogonal linear regression with errors in bivariate data (Thirumalai et al. 2011). Figure 25 shows as example the regressions for V_{S30}.

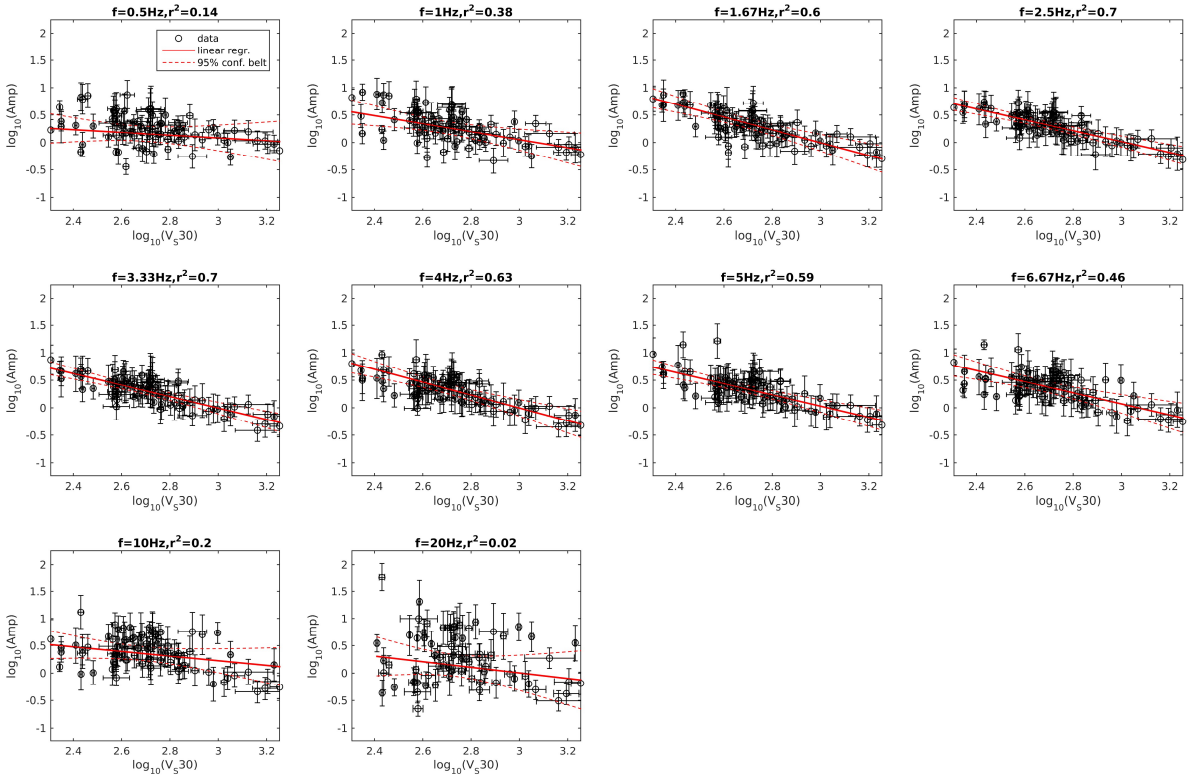

Figure 25: Swiss dataset: orthogonal linear correlations between Fourier amplification factors at ten frequency abscissae (f=0.5-20 Hz) and V_{S30} with relevant uncertainties, in bi-logarithmic scale. Only the correlation for f = 20 Hz is not significant.

At first glance, it appears that introducing errors for the proxy variable and adopting the orthogonal least-squares does not affect considerably the regressions (compare Figures 23-25): in fact, the slopes and the coefficients of determination are similar (Figure 26, top and center). However, when it comes to the statistical tests of significance, the two different fitting strategies start to show some differences (Figure 26, bottom); in particular, the correlation at 0.5 Hz, that for ordinary regression is not statistically significant, passes both tests when orthogonal fitting is adopted. A systematic comparison between ordinary and orthogonal least-squares regressions is shown in section 5.4.1.

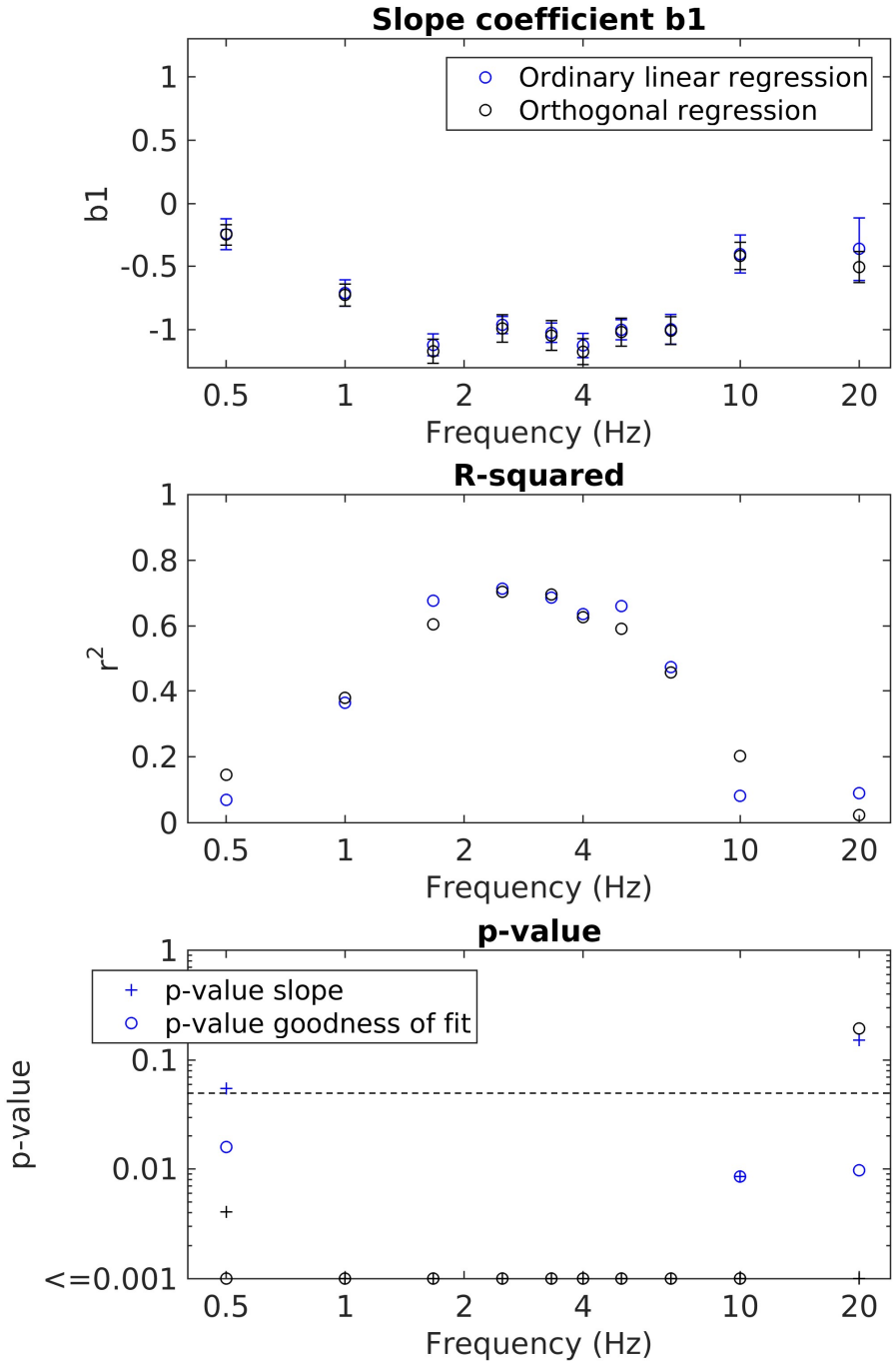

Figure 26: Comparison between parameters in output from the ordinary (blue) and orthogonal (black) linear regressions of amplification factors versus V_{S30} (Swiss data). Top: slope coefficients with standard errors. Centre: coefficient of determination r^2. Bottom: p-values of statistical tests for the goodness of fit (circles) and significance of slope coefficient (crosses); the horizontal dashed line represents the adopted significance level (0.05, or 5%).

As for site-condition proxies in vector form (V_S^{QWL}, I_C^{QWL} and H/V curves in the following paragraph), we correlated each of their frequency-dependent elements to the corresponding set of amplification factors referring to the same frequency. Figure 27 shows the regressions of amplification versus quarter-wavelength velocity for Japanese stations.

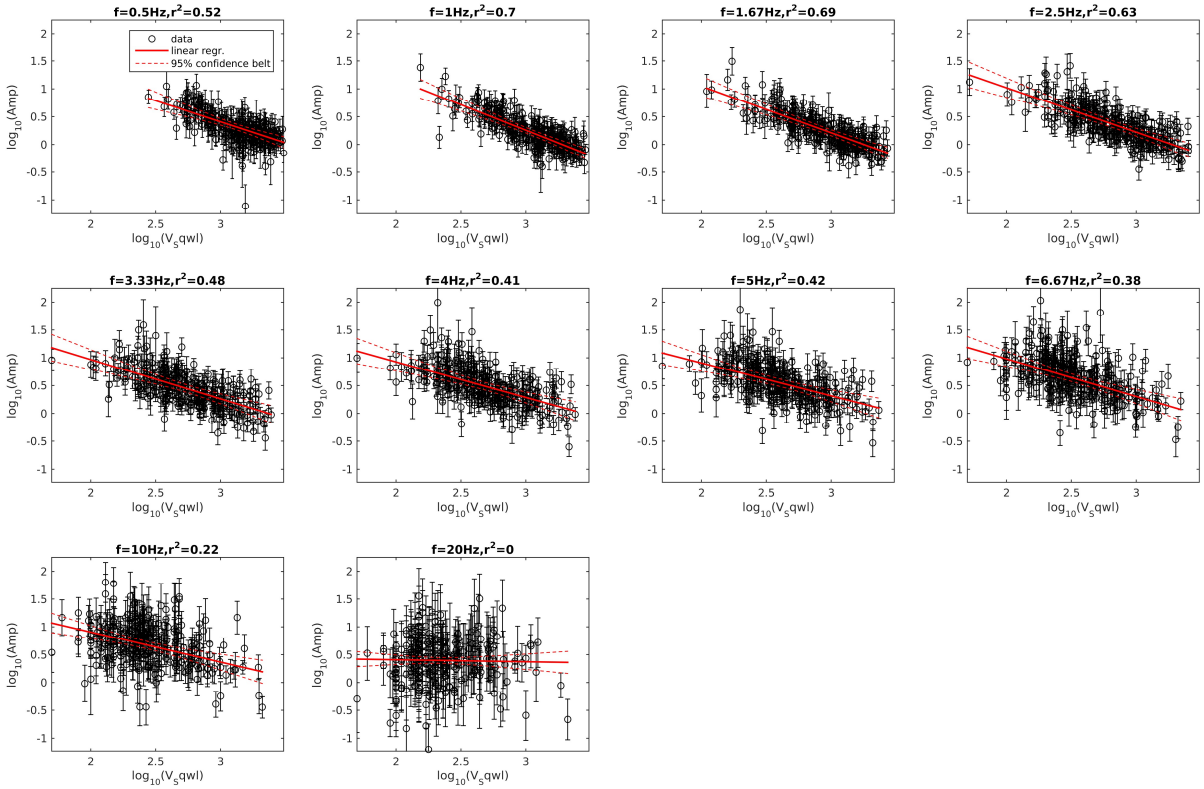

Figure 27 – Japanese dataset: ordinary linear least-squares correlations between Fourier amplification factors at ten frequency abscissae (f=0.5-20 Hz) and V_S^{QWL} values at the same frequencies, in bi-logarithmic scale. All correlations are statistically significant, with the exception of f=20 Hz.

5.1.2 Proxies derived from H/V_{noise} measurements

We evaluated the correlation between Fourier amplification factors and the following proxies derived from H/V_{noise} measurements: fundamental frequency f_0 and corresponding H/V_{noise} ratio A_0, amplitude of the H/V_{noise} curve at ten frequency abscissae (0.5 – 20 Hz). As explained in section 3.2.2, these parameters are available (with relevant uncertainties) for most of Swiss (urban) free-field stations (117 out of 145), but not for Japanese sites. A_0 and the amplitudes of H/V curves at the 10 fixed frequencies were translated to logarithmic scale (as commonly done in literature with H/V data, e.g. Nakamura 1989); as for f_0, the amplification factors at each frequency f_i were regressed versus the absolute distance, in logarithmic scale, between f_0 and f_i ($|\log(f_0/f_i)|$).

As example, we show in Figure 28 and 29 the correlations of amplification factors versus A_0, with ordinary and orthogonal least-squares regressions. Figure 30 collates the slope coefficients, r^2 and statistical significance tests' p-values from the two methods.

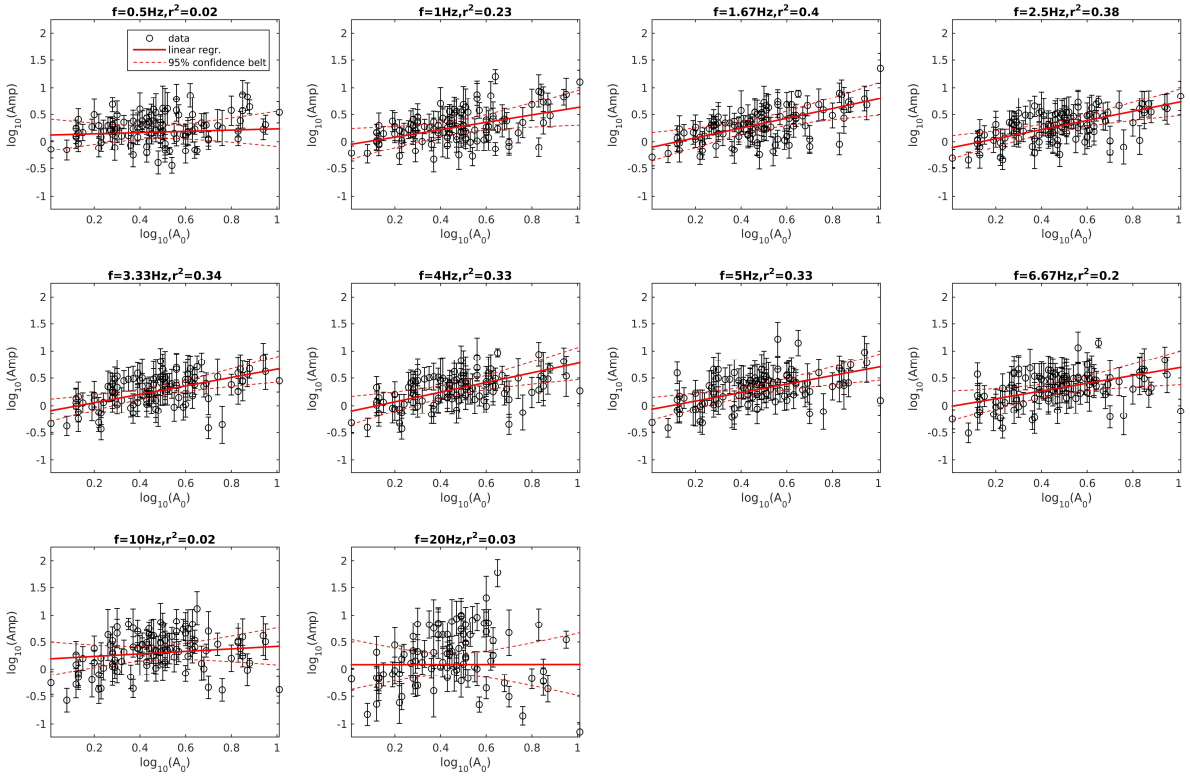

Figure 28: Swiss dataset: ordinary linear least-squares correlations between Fourier amplification factors at ten frequency abscissae (f=0.5-20 Hz) and A_0 values, in bi-logarithmic scale. Regressions at 0.5, 10 and 20 Hz are not statistically significant.

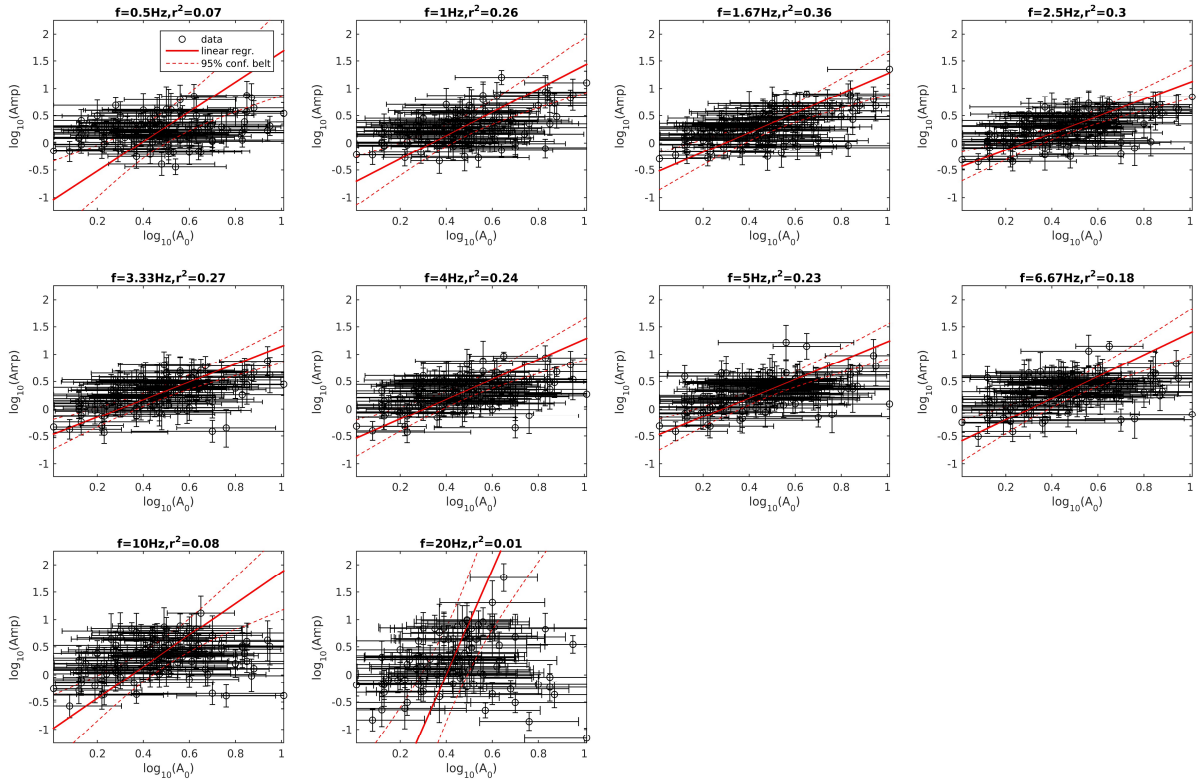

Figure 29: Swiss dataset: orthogonal least-squares correlations between Fourier amplification factors at ten frequency abscissae (f=0.5-20 Hz) and A_0 values, in bi-logarithmic scale. All correlations are statistically significant, with the exception of f=20 Hz.

In this case, differently from Vs_{30} (Figures 23, 25, 26), the wide error intervals for the proxy variable lead the orthogonal regression algorithm to determine steeper slopes for the fitting line, when compared to ordinary least-squares regression (Figure 30, top). In terms of statistical analysis, the correlations at 0.5 and 10 Hz are now statistically significant. Similar considerations (on the comparison ordinary vs. orthogonal regression) apply to the H/V_{noise} amplitudes at the 10 selected frequency abscissae (Figure 31).

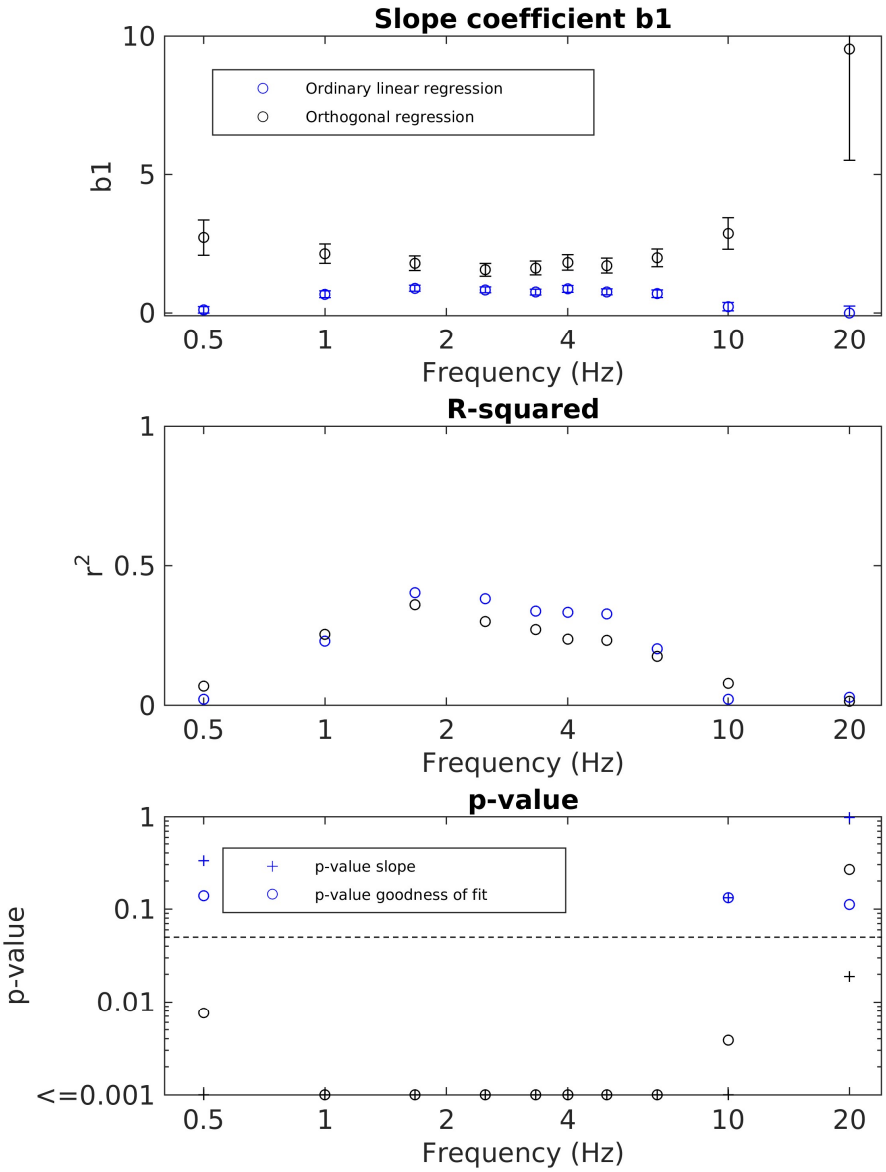

Figure 30 - Comparison between parameters in output from the ordinary (blue) and orthogonal (black) linear regressions of amplification factors versus A_0 (Swiss data). Top: slope coefficients with standard errors. Centre: coefficient of determination r^2. Bottom: p-values of statistical tests for the goodness of fit (circles) and significance of slope coefficient (crosses); the horizontal dashed line represents the adopted significance level (0.05, or 5%).

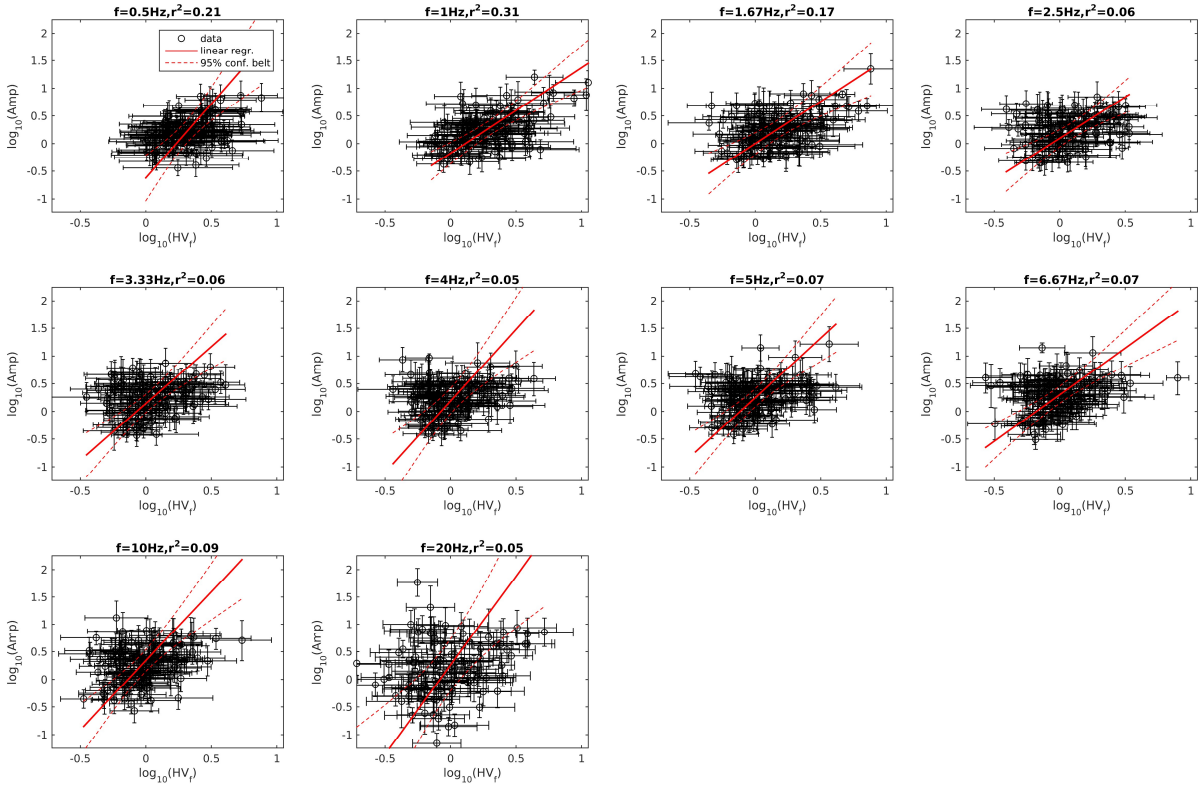

Figure 31: Swiss dataset: orthogonal linear least-squares correlations between Fourier amplification factors at ten frequency abscissae (f=0.5-20 Hz) and H/V_{noise} amplitudes at the same frequencies, in bi-logarithmic scale. All correlations are statistically significant.

5.1.3 Topographical parameters

We evaluated the correlation between Fourier amplification factors and the following topographical parameters, evaluated at seven spatial scales (60 – 2020 m): slope, normalized topographic position index (TPI_{norm}), smoothed topographic curvature (STC) and absolute difference STC along northing minus STC along easting axis. The last two proxies are not available for Japanese stations at the scales 60 and 100 m (see section 3.2.3). The absolute difference STC_N – STC_E aims at identifying 2- or 3D topographical settings (elongated ridges, valleys), where the two curvatures are more likely to exhibit markedly different values.

The whole set of topographical parameters is available for 141 (out of 145) free-field Swiss stations. For Japanese sites, the topographical indexes are available for all stations with empirical amplification function (648).

Slope was translated to logarithmic scale, as is general use in literature (e.g. Wald and Allen 2007). As example, we show in Figure 32 the correlations amplification vs. slope at 180 m scale for the Japanese dataset. At 0.5 – 5 Hz, we observe weak but statistically significant (negative) correlations, with gentler slopes as the frequency increases. Then, the correlation is not significant at 6.67 and 10 Hz (regression lines are basically flat); the correlation is significant again at 20 Hz, this time with a positive slope.

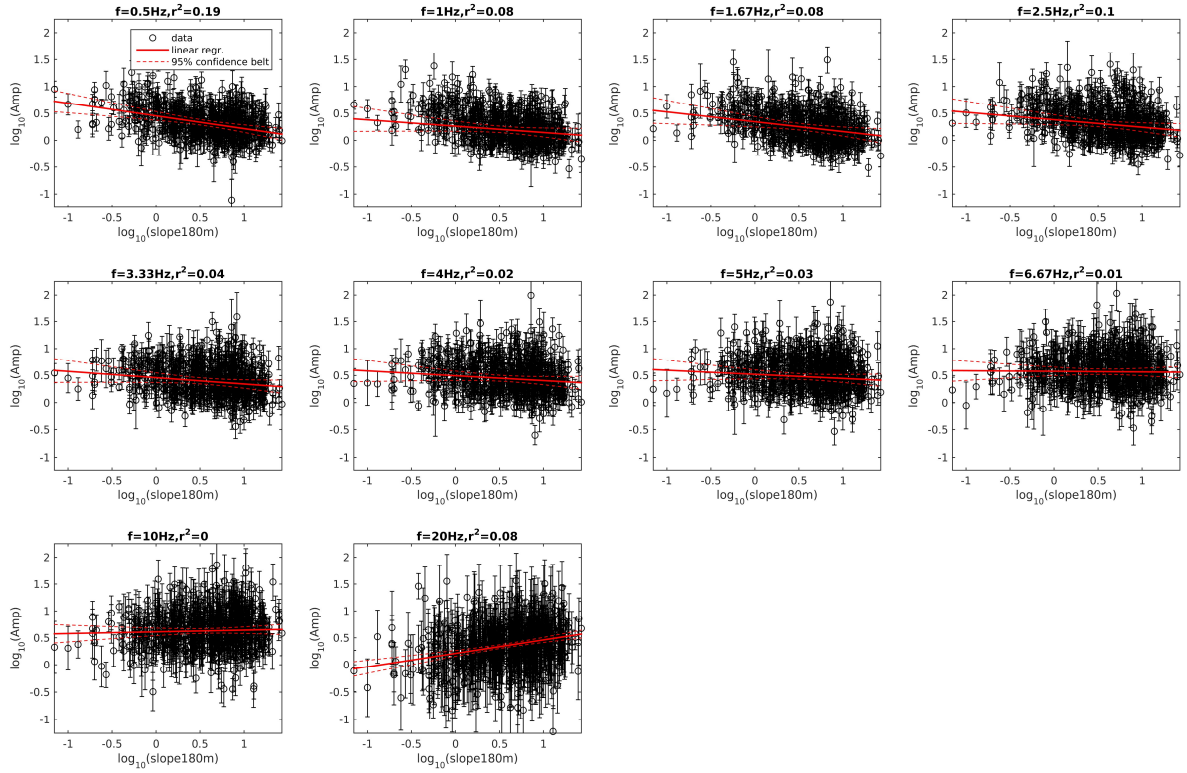

Figure 32: Japanese dataset: linear correlations between Fourier amplification factors at ten frequency abscissae (f=0.5-20 Hz) and topographical slope at 180 m scale, in bi-logarithmic scale. All correlations are statistically significant, with the exception of f = 6.67 and 10 Hz.

The normalized topography position index (TPI_{norm}) and smoothed topographical curvature were kept in linear scale, as they do not exhibit a skewed distribution; besides, they can assume either positive or negative values, so the conversion to logarithm is not possible. Figure 33 shows as example the correlations between amplification and STC at 180 m scale. From Japanese data (black circles, fitted line in red) we obtain weak but significant correlations at all frequencies (positive below 5 Hz; negative above 6.67 Hz). However, after a more in-depth analysis, these correlations appear as artefacts due to the uneven distribution of STC values in the Japanese dataset (lacking positive values, i.e. convex structures; see Figure 7 in section 3.2.3). Indeed, sites with STC very close to 0 are generally characterized by higher amplification factors when compared to sites with negative STC (hence the significant correlations); however, when adding Swiss data (blue circles), with significant coverage of positive STC, it appears clearly that stations with STC close to 0 can amplify more than sites with *either negative or positive curvatures*. Not surprisingly, for Swiss data most of frequencies have insignificant correlations (the lines fitting the data spanning from negative to positive STC values are close to flat). This is the only case (together with TPI_{norm}, exhibiting a similar behaviour) where the linear fitting model proved to be inadequate; probably, a curvilinear fit would have been more in agreement with the data trend.

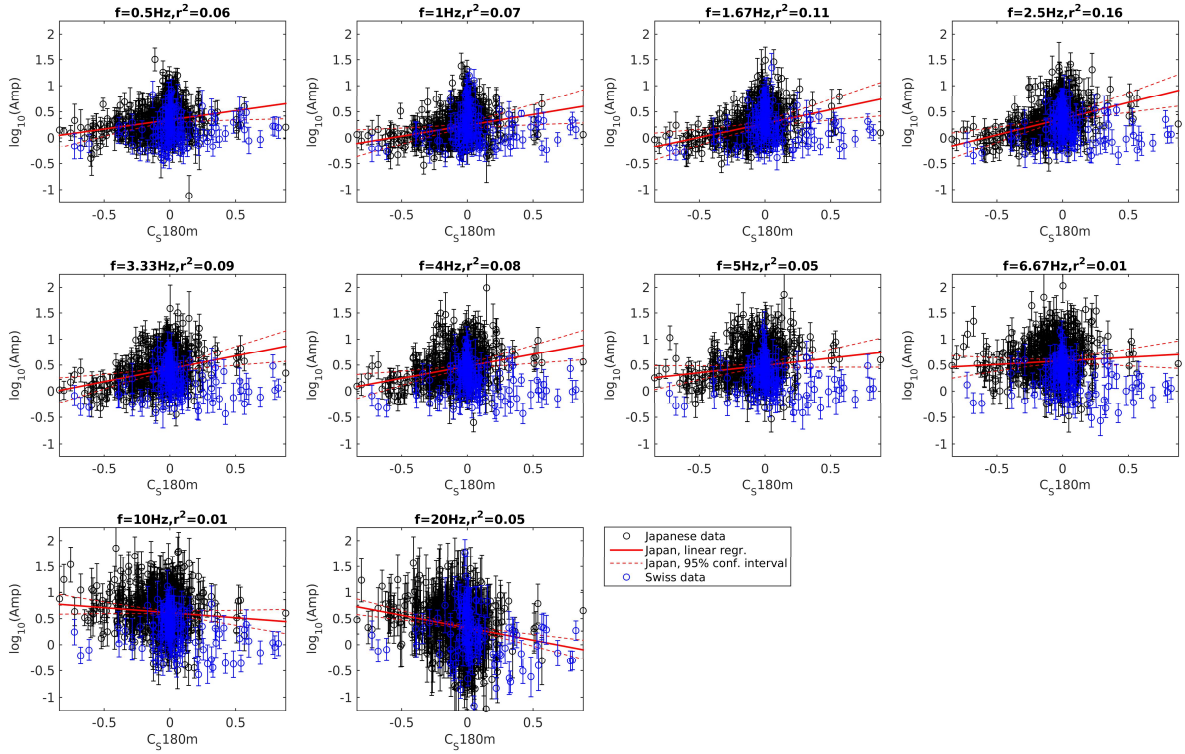

Figure 33: Correlations between smoothed topographical curvature at 180 m scale and amplification factors at 10 frequency abscissae (f = 0.5-20 Hz). Black circles: Japanese data; red line: linear fitting of Japanese data; blue circles: Swiss data.

From a geophysical point of view, the behaviour described above does not fit with the concept of topographical amplification (in this case, we should have amplification factors increasing with the curvature; Maufroy et al., 2015). More probably, the dominant amplification phenomenon we observe is that of stratigraphic amplification, as already argued by Burjanek et al. (2014). In fact, sites with curvature ≈ 0 are more likely to host soft sediments (wide flat alluvial plains, hence the generally larger amplification factors in Figure 33). Vice versa, a curvature ≠ 0 may indicate a more rugged topography, hence stiffer soil, hence lower amplification.

Not surprisingly, we observed for TPI_{norm} the same behavior of STC; in fact, the two indexes both portray the concavity or convexity of the topographical surface.

Similar considerations regarding the geophysical meaning of topographical proxies can be made for the absolute difference between STC_N and STC_E (curvature measured along the northing and easting axis). An example (Swiss data, spatial scale 180 m) is shown in Figure 34. At all frequencies (except f = 20 Hz) we obtain a significant negative correlation between amplification factors and $|STC_N - STC_E|$, in bi-logarithmic scale. We argue that a small difference between the two directional curvatures is likely to identify sites in a 1D depositional environment (e.g. flat alluvial plains), hence characterized by low V_S and high amplification; vice versa, a large difference is likely to occur at sites with pronounced topography, with stiffer soil and hence lower amplification.

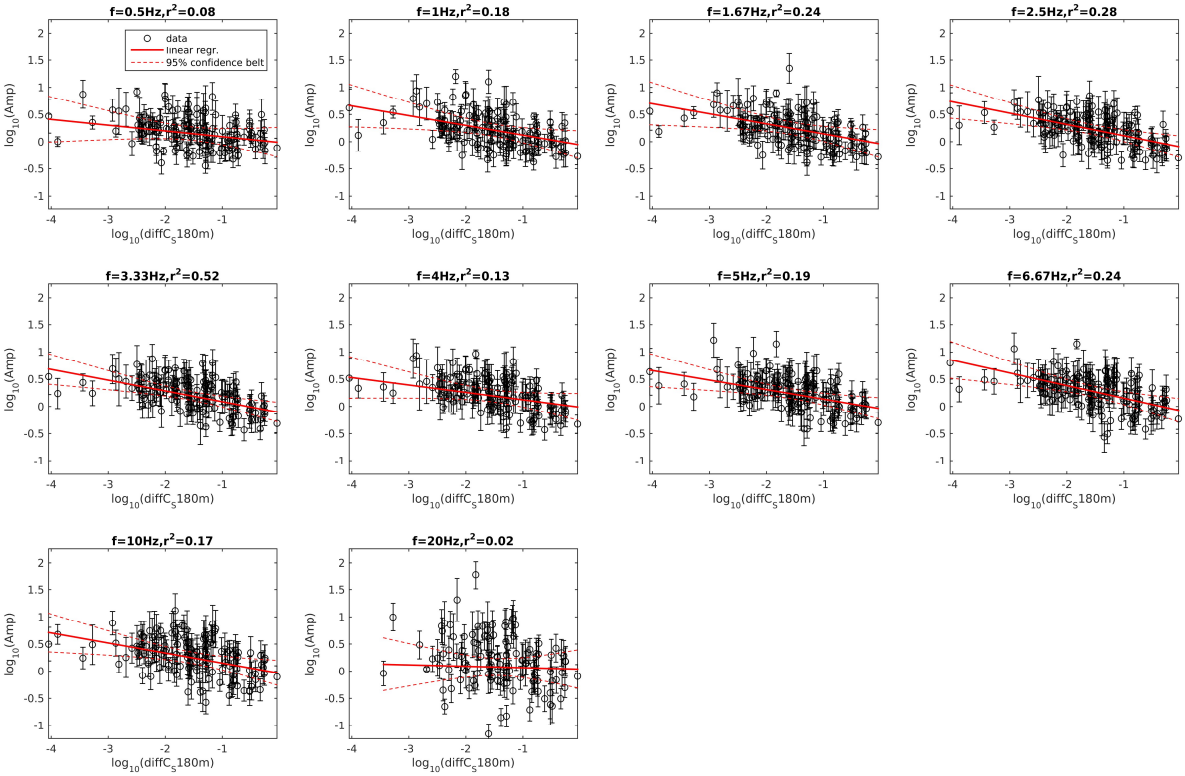

Figure 34: Swiss dataset: linear correlations between Fourier amplification factors at ten frequency abscissae (f=0.5-20 Hz) and the absolute difference of STC_N - STC_E at 180 m scale (bi-logarithmic scale). All correlations are statistically significant, with the exception of f = 20 Hz.

5.1.4 Common indirect proxies

We evaluated the correlation between Fourier amplification factors and the continuous-variable indirect proxies we were able to collect for both Swiss and Japanese sites: the estimated thickness of ice cover at the last glacial maximum (LGM), the inferred volumetric percentage of coarse fraction at 2 m depth and the inferred depth to pedologic bedrock (see section 3.2.4). These parameters are available for all free-field sites with amplification function (145 for Switzerland, 648 for Japan).

As example, Figure 35 shows the regressions of amplification factors versus the thickness of ice cover at LGM. These regressions are available for the Swiss dataset only, as all Japanese sites were estimated to be free of ice at LGM (ice cover = 0 m). Since we adopted the logarithm of the ice thickness as independent variable (to avoid a skewed distribution), the Swiss stations with ice cover = 0 m do not appear in the plot. In the following section (5.2) we will discuss whether there exists a significant difference between stations that were covered by ice and the sites that were not.

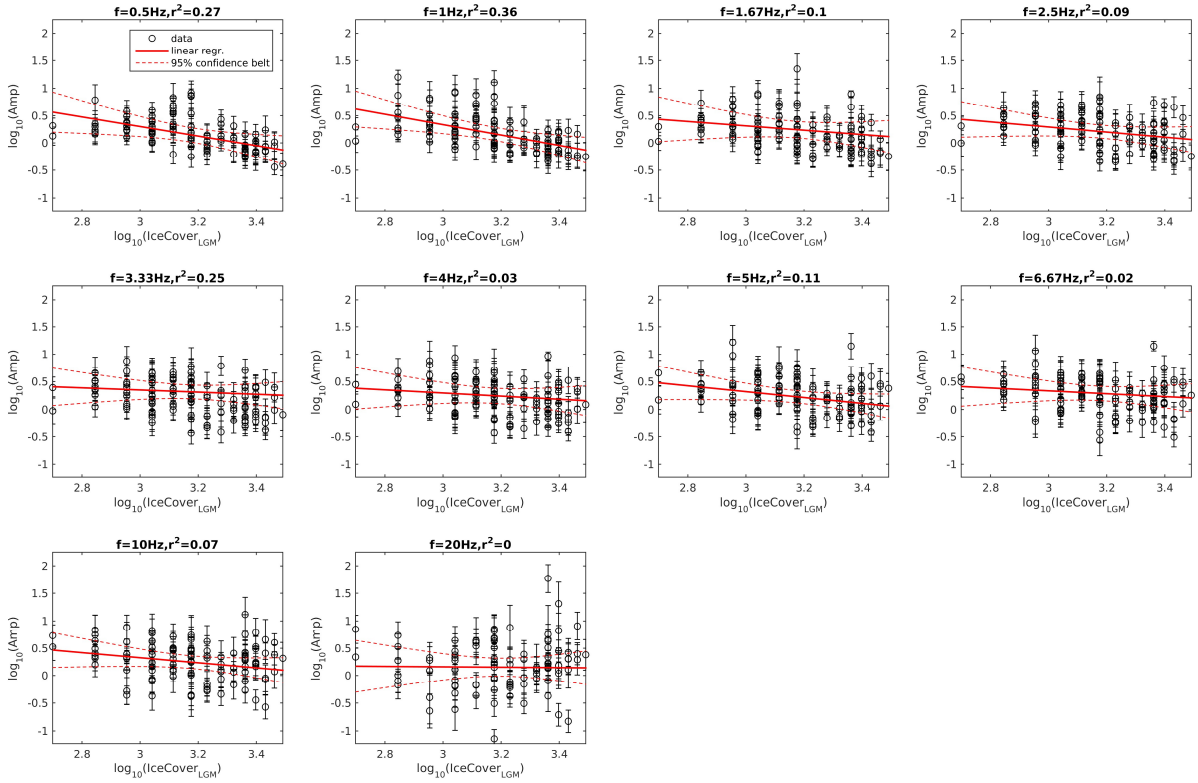

Figure 35: Swiss dataset: linear correlations between Fourier amplification factors at ten frequency abscissae (f=0.5-20 Hz) and the estimated thickness of ice cover at LGM (bi-logarithmic scale). The correlations for f = 0.5, 1, 1.67, 2.5, 5 and 10 Hz are statistically significant.

5.1.5 Indirect proxies specific to either Switzerland or Japan

Finally, we evaluated the correlation between Fourier amplification factors and the continuous-variable indirect proxies we derived from datasets specific to either Switzerland or Japan:

- for Japan, the value of H800 as derived from the JSHIS subsurface model. This parameter is available for all 648 Japanese stations;
- for Switzerland, the thickness of unconsolidated sediments as inferred from the Swiss geological bedrock model, and the average V_P and ρ_b for the lithological group the stations belong to as provided by SAPHYR database (Zappone and Bruijn, 2012). These parameters are available for 104 (sediments thickness) and 133 (SAPHYR physical properties) free-field Swiss stations.

As example, we show here the regressions for estimated H800 (Japan, Figure 36) and attributed bulk density (Switzerland, Figure 37). For the first case, it is worth noting that a clear linear trend is generally evident for H800 > 10 m, and weaker below 10 m.

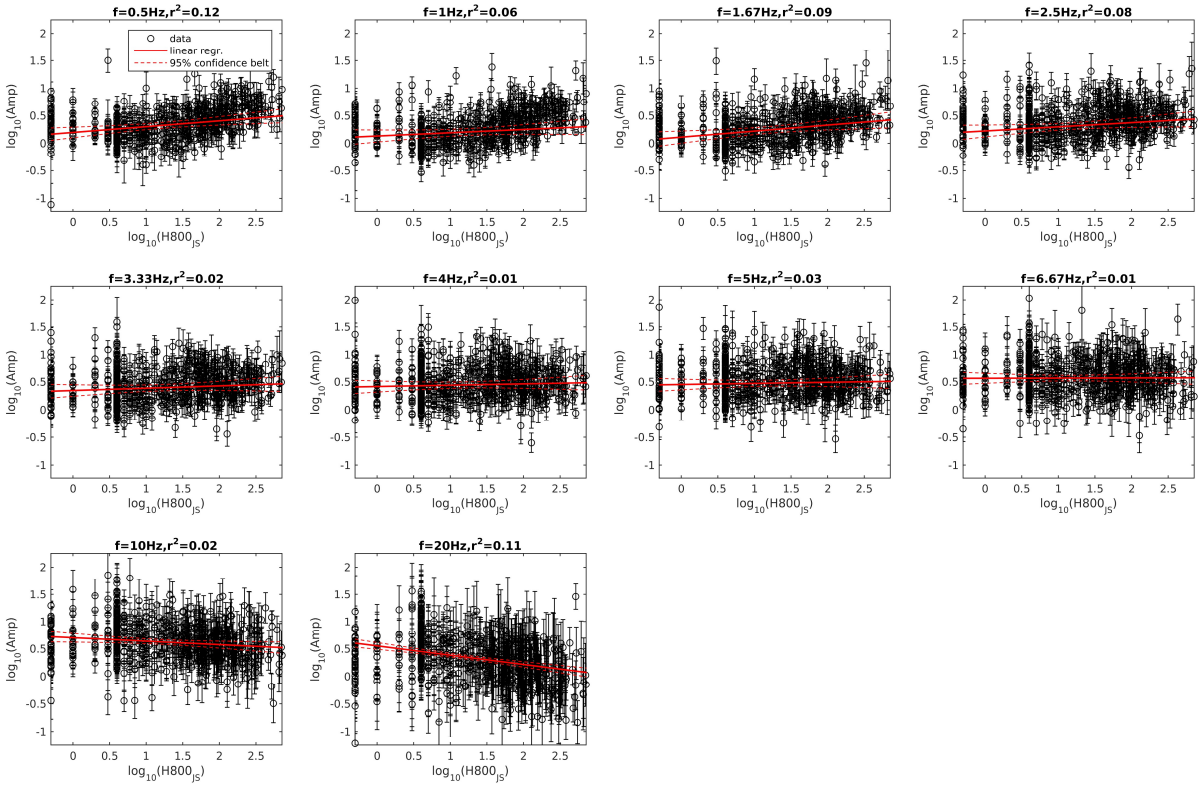

Figure 36: Japanese dataset: linear correlations between Fourier amplification factors at ten frequency abscissae (f=0.5-20 Hz) and the H800 as derived from the JSHIS subsurface model (bi-logarithmic scale). To preserve the completeness of the dataset, an arbitrary value of H800 = 0.5 m was attributed to all stations with H800 = 0 m. The correlations for f = 4, 5 and 6.67 are not statistically significant.

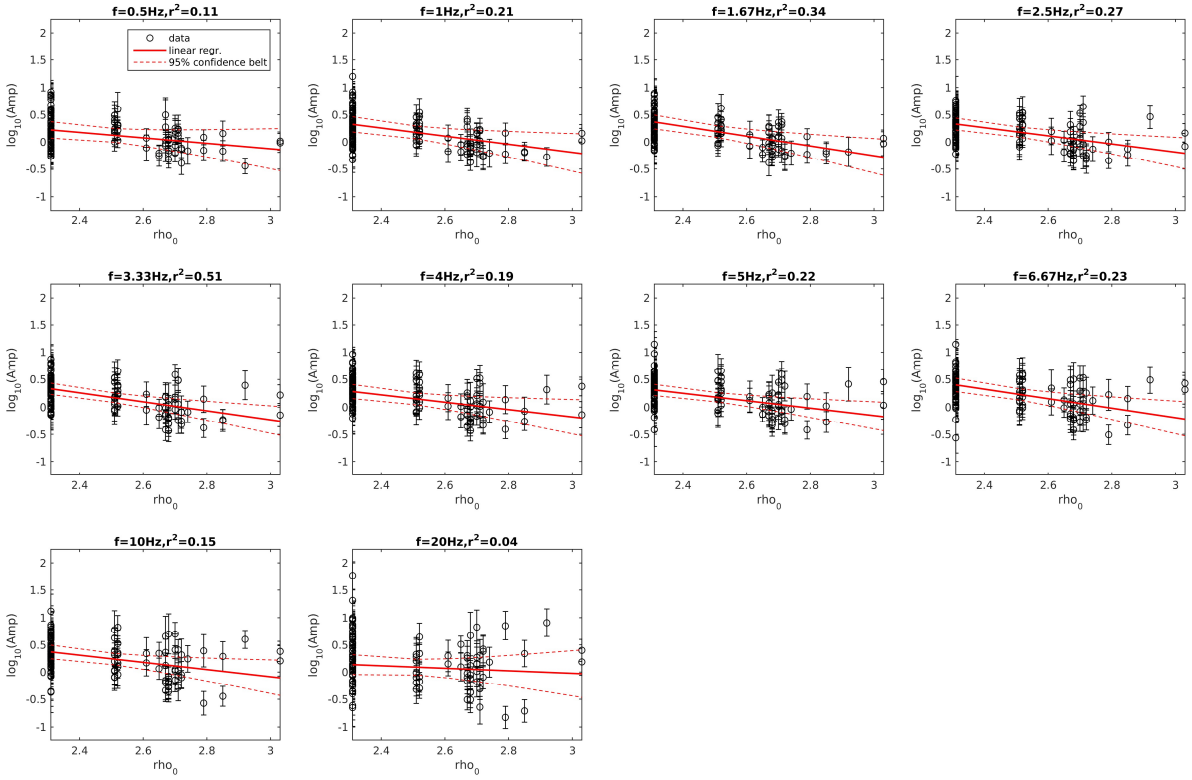

Figure 37: Swiss dataset: linear correlations between Fourier amplification factors at ten frequency abscissae (f=0.5-20 Hz) and the average bulk density value attributed by SAPHYR database to each lithological group (semi-logarithmic scale). All correlations but f=20 Hz are statistically significant.

5.2 Assessment of the statistical significance of the site classifications proposed by category proxies

For all the proxies that do not correspond to a continuous variable (e.g. V_{S30}), but rather provide a category-based classification (e.g. topographical classes), it was meaningless to apply the linear regression strategy illustrated in the previous paragraph. Thus we followed a different approach: first, we group the sites in the categories proposed by the considered proxies (e.g., for topographical classification, valley bottom, flat area, lower/middle/upper slope, ridge). Then, we compute the average amplification factor (for each available frequency abscissa, 0.5 – 20 Hz) for each subpopulation of sites (Figure 38). Finally, using Welch's t-test, or unequal variances t-test (Welch 1947), we establish whether the average amplification factors of each couple of subgroups are statistically equal (i.e. equivalent), or the difference between the two mean values is significant. In the first case, we consider the subdivision proposed by the proxy as not effective; in the second case, as effective. We resort to Welch's test because it does not require the two populations to have equal variances; besides, it is suitable for populations with unequal sample sizes. Regarding its practical implementation, we assumed a 10% level of significance, and we imposed each of the two populations to have at least 10 samples (10 sites; e.g. Figure 39).

We carry out Welch's t-test for each possible couple of subgroups and for each frequency of the amplification factors (Figure 40). To determine the rate of success of each proposed proxy classification, at each frequency, we compute a so-called index of effectiveness:

$$i_e = \frac{number\ of\ unordered\ couples\ of\ populations\ with\ statistically\ different\ average\ amplification\ factors}{total\ number\ of\ unordered\ couples\ of\ populations} \quad (2)$$

The index is therefore 1 when all subgroup pairs have a statistically significant difference in their average amplification values, and 0 when all subgroups have statistically equivalent means (e.g. Figure 41).

The category proxies we analysed are the following

- Topography: topographical classification according to Burjanek et al. (2014) at seven spatial scales (60 – 2020 m);
- Common indirect proxies: rock age and genesis classification;
- Indirect proxies specific to either Switzerland or Japan: SIA soil classification, geomorphology classification, SAPHYR lithological classification (Switzerland), engineering geomorphology classification and lithological classification (Japan).

5.2.1 Topographical classification

The topographical classification according to Burjanek et al. (2014; 6 classes from valley to ridge) is available at seven spatial scales for all Swiss and Japanese (urban) free-field stations with an amplification function (145 and 648, respectively). As example, we show in Figure 38 the subdivision of Japanese sites' amplification factors following the topographical grouping at 100 m scale.

Unfortunately, not all topographical classes are sufficiently represented for our statistical test (i.e. include ≥ 10 sites), in both the Swiss and Japanese datasets (Figure 39). In the first case, only the "ridge", "middle slope" and "flat area" classes have more than 10 sites at all scales; as for Japan, all classes but "ridge" are sufficiently represented.

Continuing with the example of classification of Japanese sites (Figure 38), Figure 39 shows the outcomes of Welch's t-test for each possible pair of topographical categories (100 m scale). As anticipated, all tests involving the "ridge" class are null (black squares), because this group is under-represented. Other than that, we remark that the majority of class couples have statistically different means (green squares), with the exception of frequencies 6.67 and 10 Hz.

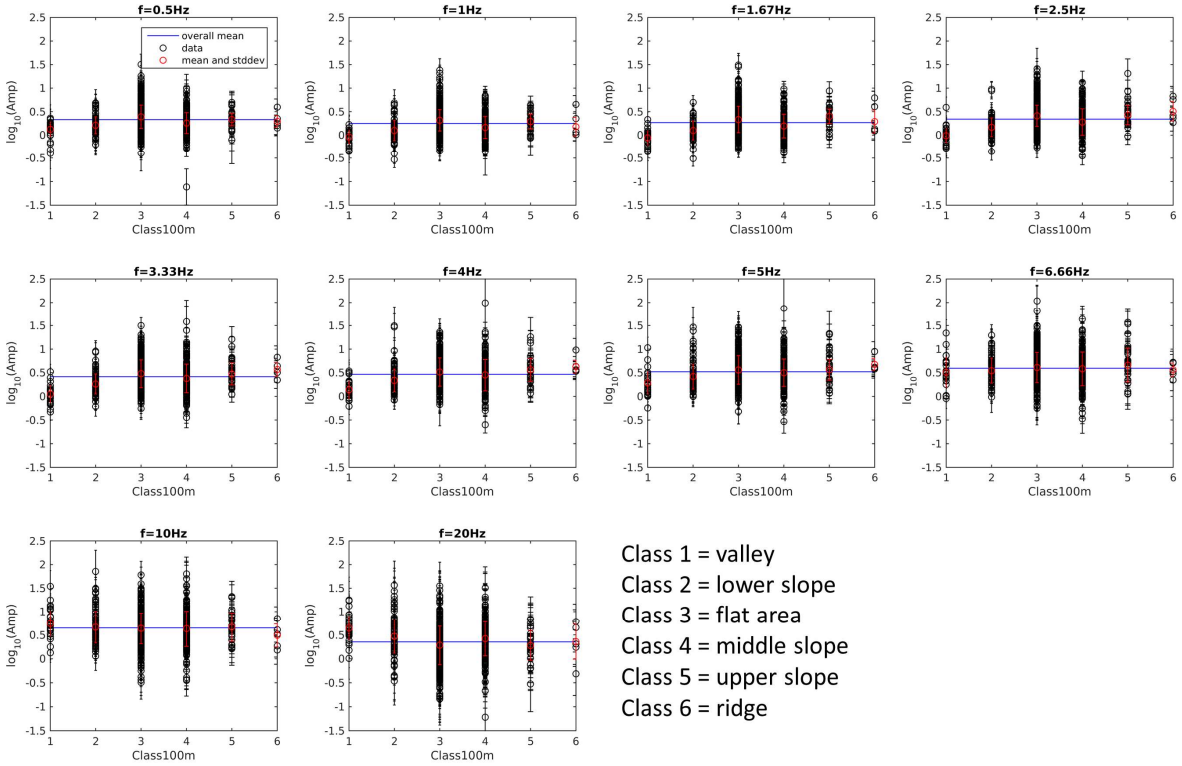

Figure 38: Japanese dataset: grouping of frequency-specific amplification factors according to the topographical class of the corresponding stations (black circles). In red, the mean amplification and standard deviation for each class are represented.

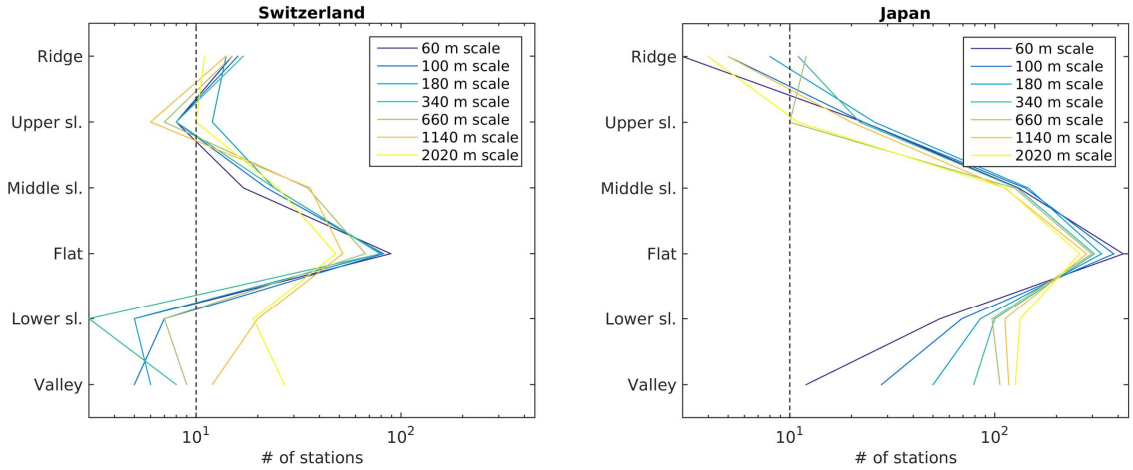

Figure 39: Distribution of Swiss and Japanese stations into the 6 topographical classes of Burjanek et al. (2014) at the seven spatial classes 60 – 2020 m. The vertical dashed line indicates the sample size threshold (10 stations) we imposed to consider a topographical class as adequately represented.

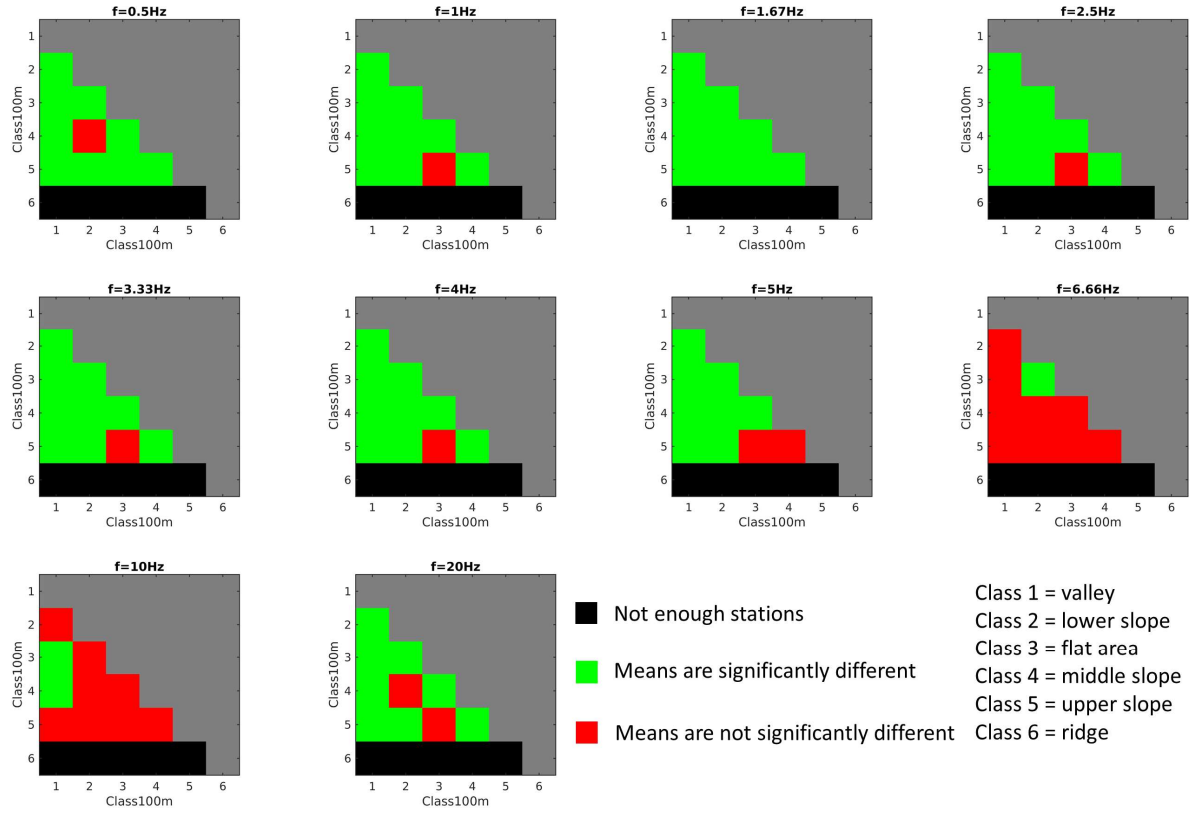

Figure 40: Japanese dataset, topographical classification at 100 m scale. Results of Welch's t-test for the significance of the difference of means of all possible unordered pairs of classes, for the 10 frequency abscissae for which amplification factors are available

To present an overview of the success of the topographical classification in grouping sites with homogenous amplification behavior, we collect in Figure 40 the indexes of effectiveness (i_e , equation 2) for all frequencies and spatial scales, for Switzerland and Japan. In the computation of the indexes, we considered only the classes with sufficient numerosity (i.e. i_e = 1 means that all groups with ≥ 10 samples have statistically different means). We observe an interesting pattern for Japan, where the topographical categorization proves to be more successful at low frequencies and for smaller spatial scales; for Switzerland, the number of considered classes (3, i.e. 3 unordered pairs) is too little to obtain meaningful results.

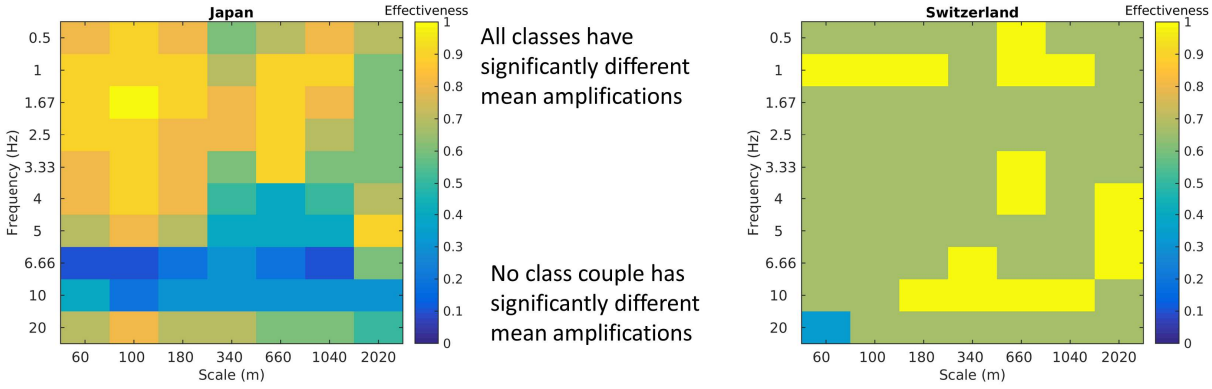

Figure 41: Index of effectiveness (colour scale) of the topographical classification for all scales (x-axis) and frequencies (y-axis), for Japan (left) and Switzerland (right). In the first case, all classes but "ridge" were considered; in the second case only three classes ("ridge", "flat area", "middle slope") were taken into account.

Finally, we analyse the trend of the average amplification factor for each class with respect to the global mean, at all frequencies and all scales (Figure 42). Following the supposed behaviour of topographical amplification (Maufroy et al., 2015), we would expect average amplification factors lower than the global mean at "valley" class, and higher at "ridge". This assumption holds true for "valley" stations, particularly at lower frequencies; on the other hand, "ridge" classes (when represented) exhibit in general amplifications lower than the global mean. Here again (as in subparagraph 5.1.3, Figure 33), we can explain this inconsistency with the fact that topographical parameters do not necessarily identify sites with dominant topographical amplification; rather, the dominant phenomenon appears to be the correlation between topography and geological/sedimentary environment. In fact, we argue that "valley" and "ridge" sites, with rugged topography, are likely to be located on stiffer materials (particularly at smaller spatial scales), hence the lower amplification; vice versa, "flat area" stations are more likely to be hosted in soft sedimentary environments, hence the higher amplifications (see the red "stripes" for class 3 in all subplots of Figure 42).

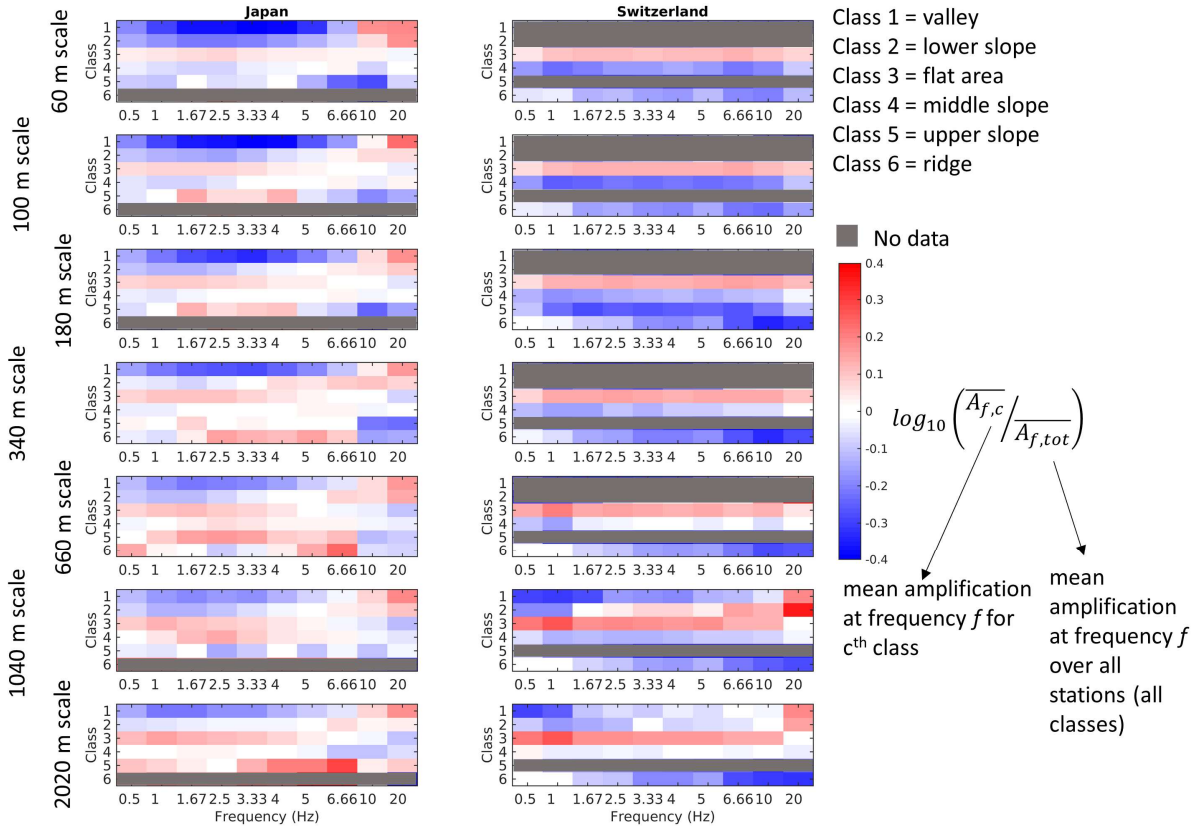

Figure 42: Overview of trend of the average amplification factors for all topographical classes, at all spatial scales, for all frequencies, for the Japanese (left) and Swiss (right) dataset. Every cell in each subplot displays the ratio between the average amplification factor of a given class (y-axis) and the global average amplification, at a given same frequency (x-axis). Grey rows indicate classes with an insufficient number (< 10) of stations.

5.2.2 Classifications from indirect proxies, common to Switzerland and Japan

As illustrated in section 3.2.4, two possible classifications arise from the indirect proxies common to Switzerland and Japan: one based on the age of the rock hosting the station, and one based on the rock genesis. Both classifications are available for all (urban) free-field stations of Switzerland and Japan (145 and 648).

As for the rock age categorization, we show as example in Figure 43 the results of the equivalence-of-means Welch's t-tests for Japan. All classes (Holocene, Pleistocene, Quaternary volcanic, Tertiary and Pre-tertiary) are sufficiently represented (≥ 10 stations). The majority of classes' pairs have significantly

different mean amplifications at low (≤3.33 Hz) and high (≥10 Hz) frequencies. Furthermore, as expected, the sites from quaternary classes (the first three) generally have higher amplifications, while tertiary, and even more markedly pre-tertiary sites amplify less. Similar results were obtained from the Swiss dataset, with one difference: the category "Quaternary volcanic" is empty.

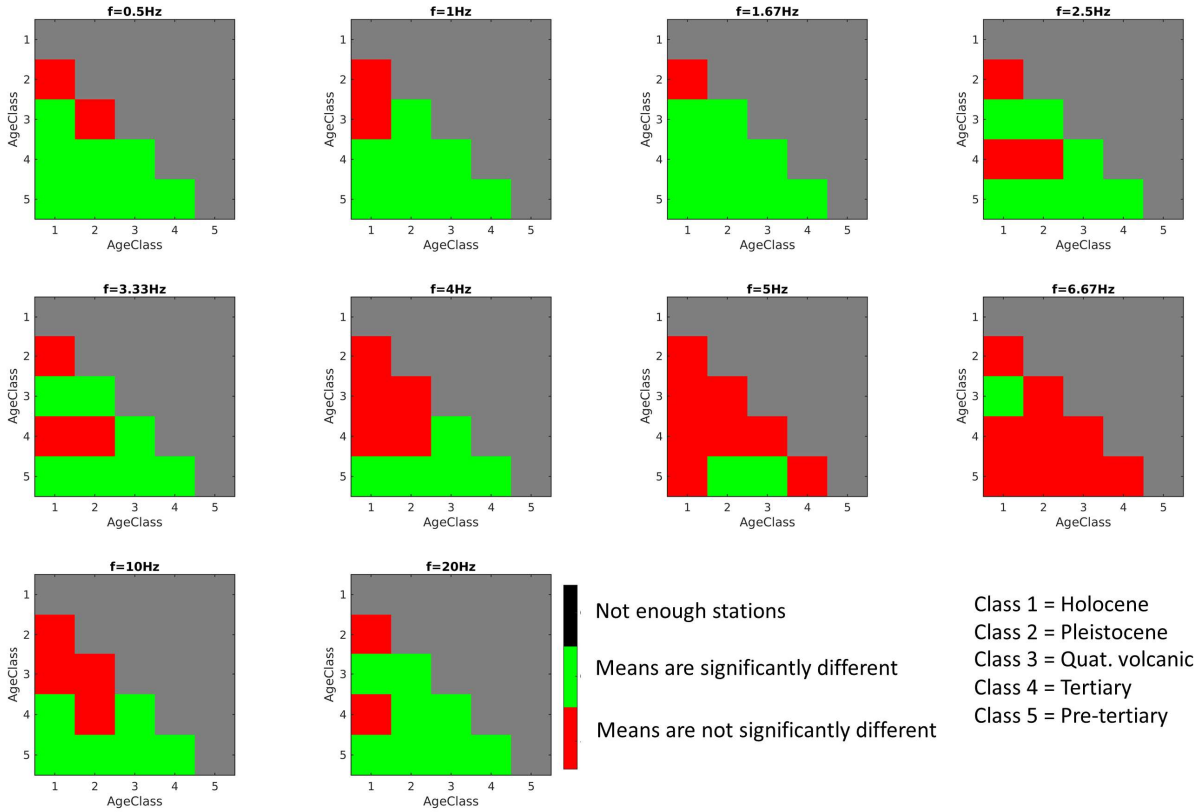

Figure 43: Japanese dataset, rock age classification. Results of Welch's t-test for the significance of the difference of means of all possible unordered pairs of classes, for the 10 frequency abscissae for which amplification factors are available.

Regarding the rock genesis classification, we identified two levels of grouping: a coarse and a detailed one, the latter involving a sub-categorization of the first preliminary classification (section 3.2.4). As for the first-level categorization, in the Japanese dataset all classes are represented: magmatic, metamorphic, sedimentary consolidated rocks, tertiary and quaternary sediments. We show the results of the equivalence-of-means tests in Figure 44. As observed for age categorization (Figure 43), the proposed classification does not perform well in the intermediate frequency range (here 4 – 10 Hz). We highlight that tertiary and quaternary sediments have equivalent average amplifications at all frequencies (lower-right corner of each subplot). In terms of effectiveness of genesis grouping, we obtain similar results from the Swiss datasets, although for fewer number of classes (only 3 categories are represented: metamorphic, consolidated sedimentary rocks, quaternary sediments).

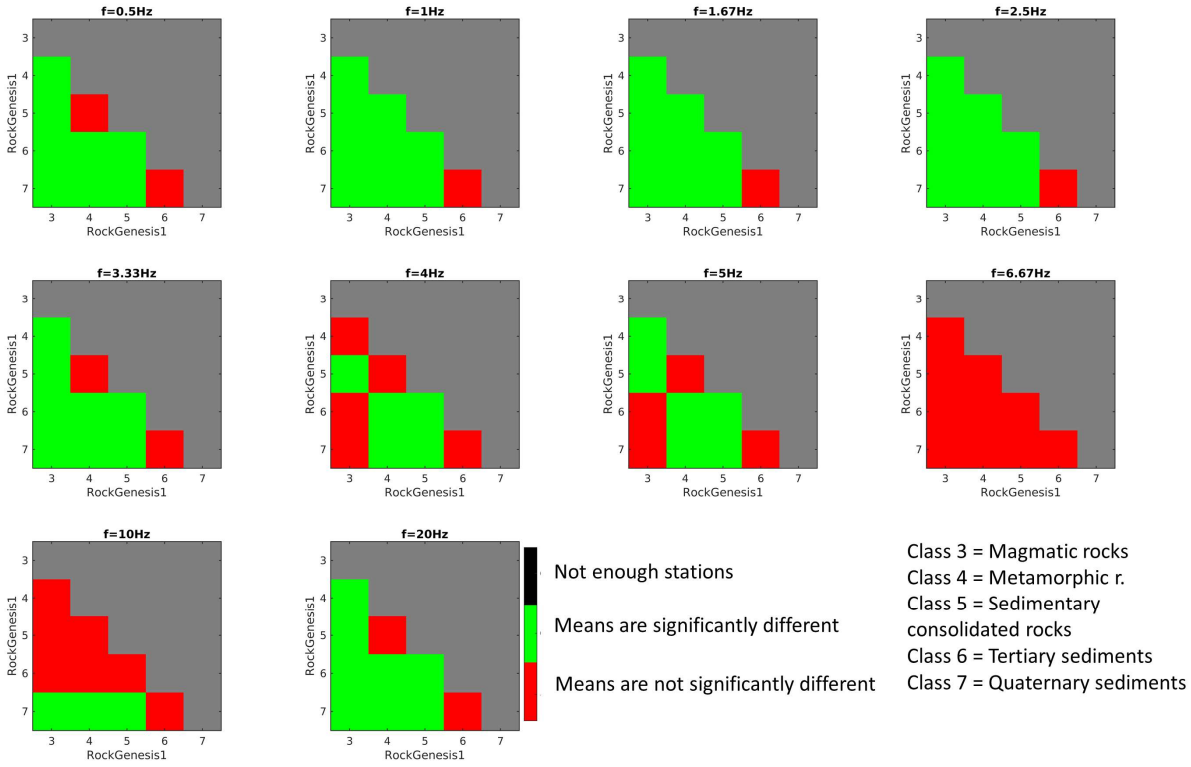

Figure 44: Japanese dataset, first-level rock genesis classification. Results of Welch's t-test for the significance of the difference of means of all possible unordered pairs of classes, for the 10 frequency abscissae for which amplification factors are available.

As for the second-level rock genesis sub-classification, relying only on the classes with sufficient sample size, we were able to evaluate its effectiveness:

- For magmatic rock, in distinguishing between volcanic and plutonic rocks (Japan only);
- For sedimentary consolidated rocks, in distinguishing between clastic and biogenic/evaporitic rocks (Japan and Switzerland);
- For quaternary sediments, in discriminating among a restricted number of subcategories (dejection cone, volcanic debris, gravel terrace, marine and non-marine sediments for Japan; moraine, gravel terrace and alluvia for Switzerland).

The results are shown in terms of index of effectiveness in Figure 45, and appear to be relatively good for compact rocks (two top subplots), but rather poor for quaternary sediments (bottom subplot). For Japan only, we also evaluated the success of the detailed genesis classification by comparing all available pairs of subgroups (11 with satisfactory sample size), without taking into account the 1st level categorization (i.e. collating also e.g. magmatic volcanic rocks with gravel terrace, and so on). The outcome is shown in terms of i_e in section 5.3.2, Figure 55.

Finally, as anticipated earlier on in paragraph 5.1.5, we assessed (for Switzerland only) whether sites that had ice cover at LGM differ significantly from the stations that didn't; the difference between the two average amplifications is significant only at f = 0.5 and 1 Hz (negative difference).

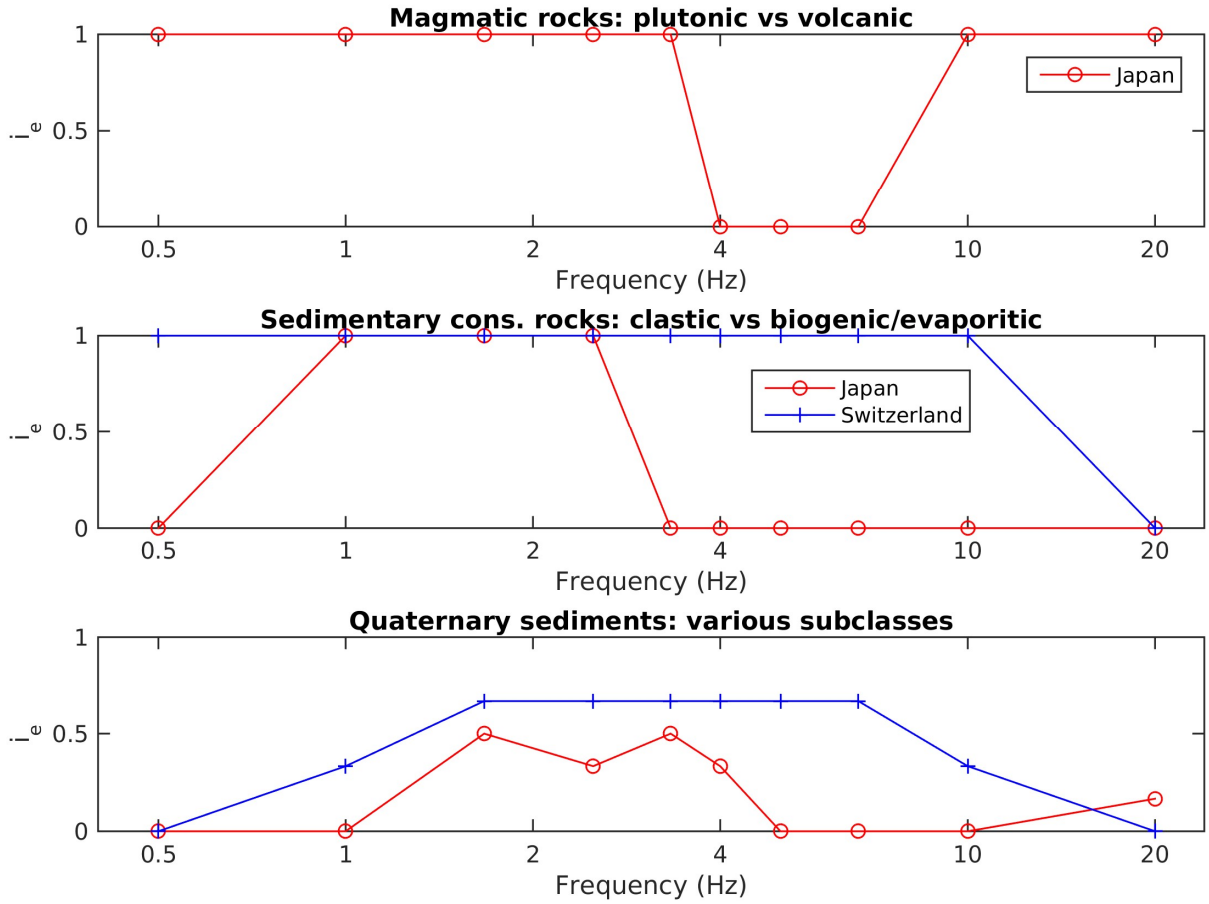

Figure 45: index of effectiveness (i_e) evaluating the possibility to distinguish between volcanic vs plutonic magmatic rocks (Japan only, top), to distinguish between clastic and biogenic/evaporitic sedimentary consolidated rocks (center), to discriminate among various subclasses of quaternary sediments (bottom).

5.2.3 Classifications from indirect proxies, specific to either Switzerland or Japan

As illustrated in section 3.5, three possible stations' classifications arise from the indirect proxies retrieved for Switzerland only:

- One based on the soil class map (A-F, according to SIA 261,2014) produced by the Swiss Federal Office of Environment, covering 57 out of 145 stations. See results of the equivalence-of-means tests in Figure 46 (only three classes have more than 10 sites: A, C, E).
- One based on the geomorphological map produced by Swisstopo, covering all 145 stations. Unfortunately, out of four groups (karstic, denudativ, fluvial, glacial), only the last two have a sufficient number of samples (≥10). The difference between the two average amplifications is significant for all frequencies;
- One based on the lithological groups classification proposed by SAPHYR database. In this case only one class is represented by ≥ 10 sites (unconsolidated debris), so that no equivalence-of-means collation is possible. However, from a visual observation of the distribution of the amplification factors among the various groups, it appears that – at least at low frequencies - the lithological classes collect relatively homogeneous groups of amplification ratios. Therefore, the proposed classification seems promising, although a higher number of sites is required for a full assessment.

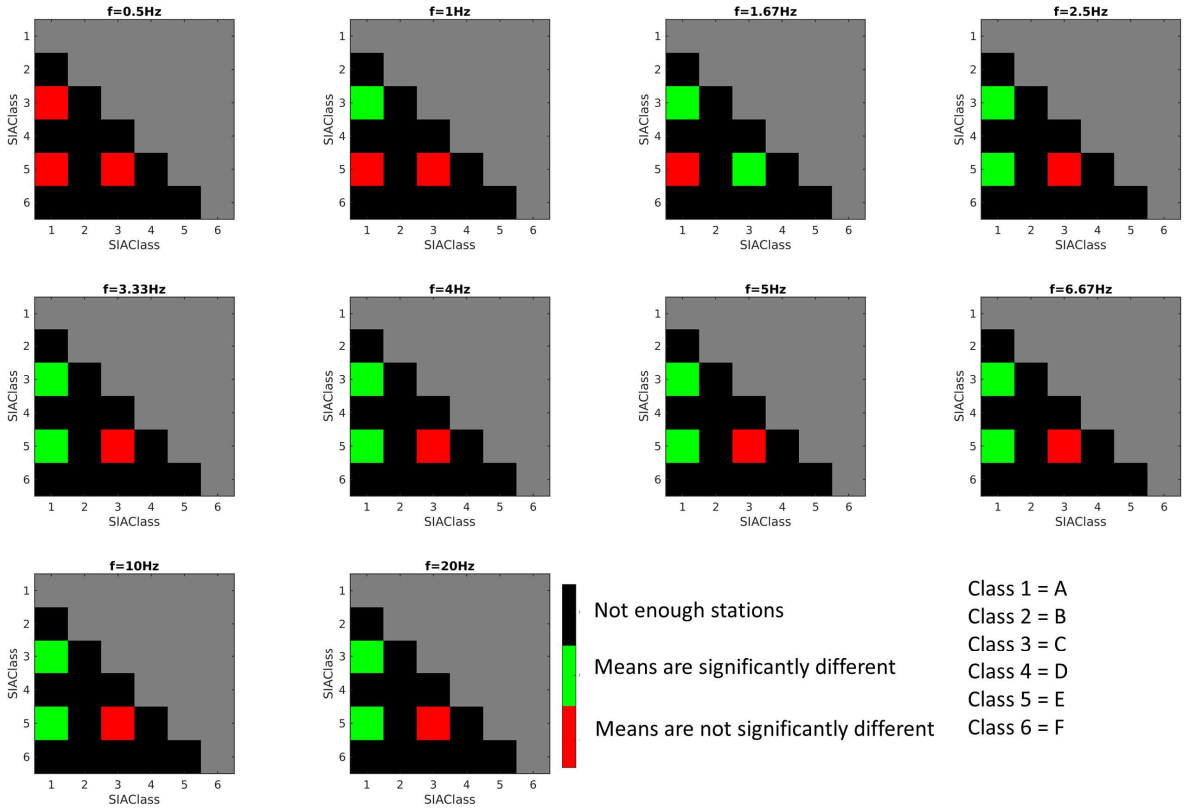

Figure 46: Swiss dataset, inferred soil class from geotechnical map. Results of Welch's t-test for the significance of the difference of means of all possible unordered pairs of classes, for the 10 frequency abscissae for which amplification factors are available.

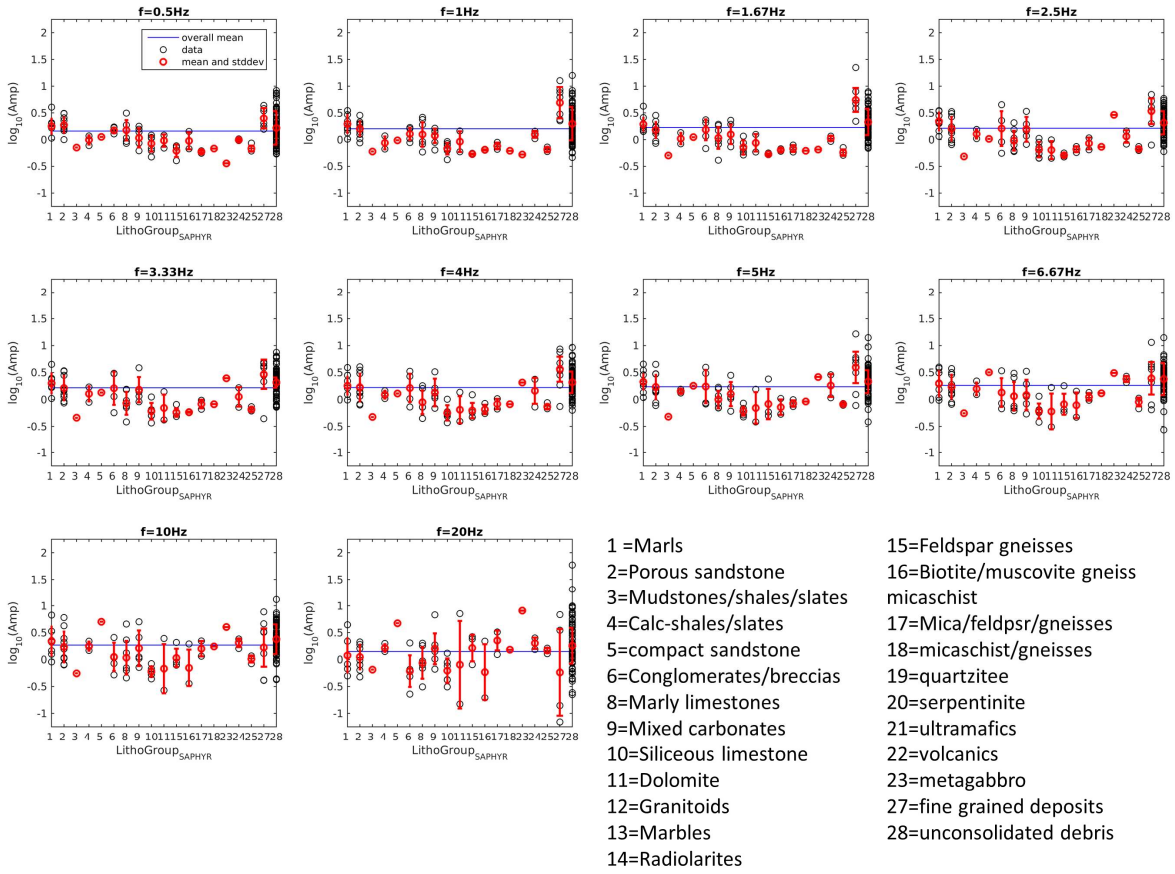

Figure 47: Swiss dataset, distribution of amplification factors from individual stations (black circles) among the main lithological groups proposed by SAPHYR database. The mean amplification and standard deviation for each group are represented in red.

As for Japan, we retrieved two datasets proposing the following classifications (section 3.5):

- One based on the engineering geomorphologic categories issued by JSHIS (Fujiwara et al., 2009), including 22 subgroups (out of which 11 have sufficient sample size). The results of the equivalence-of-means tests are represented in Figure 48.
- One based on a simplified lithological grouping we derived from the geological map of Japan. Only 10 groups (out of 25) have an adequate sample size (Figure 49).

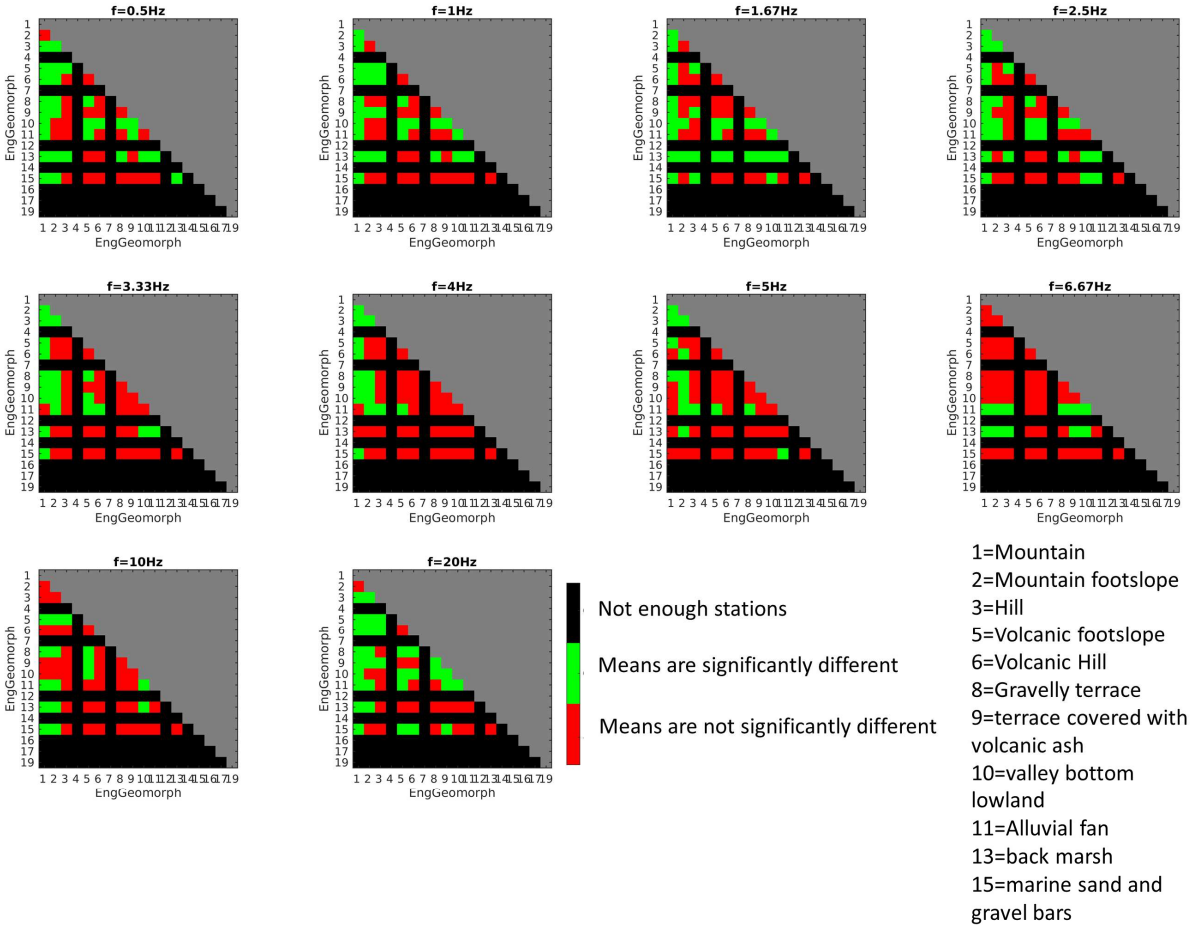

Figure 48: Japanese dataset, engineering geomorphologic classification. Results of Welch's t-test for the significance of the difference of means of all possible unordered pairs of classes, for the 10 frequency abscissae for which amplification factors are available

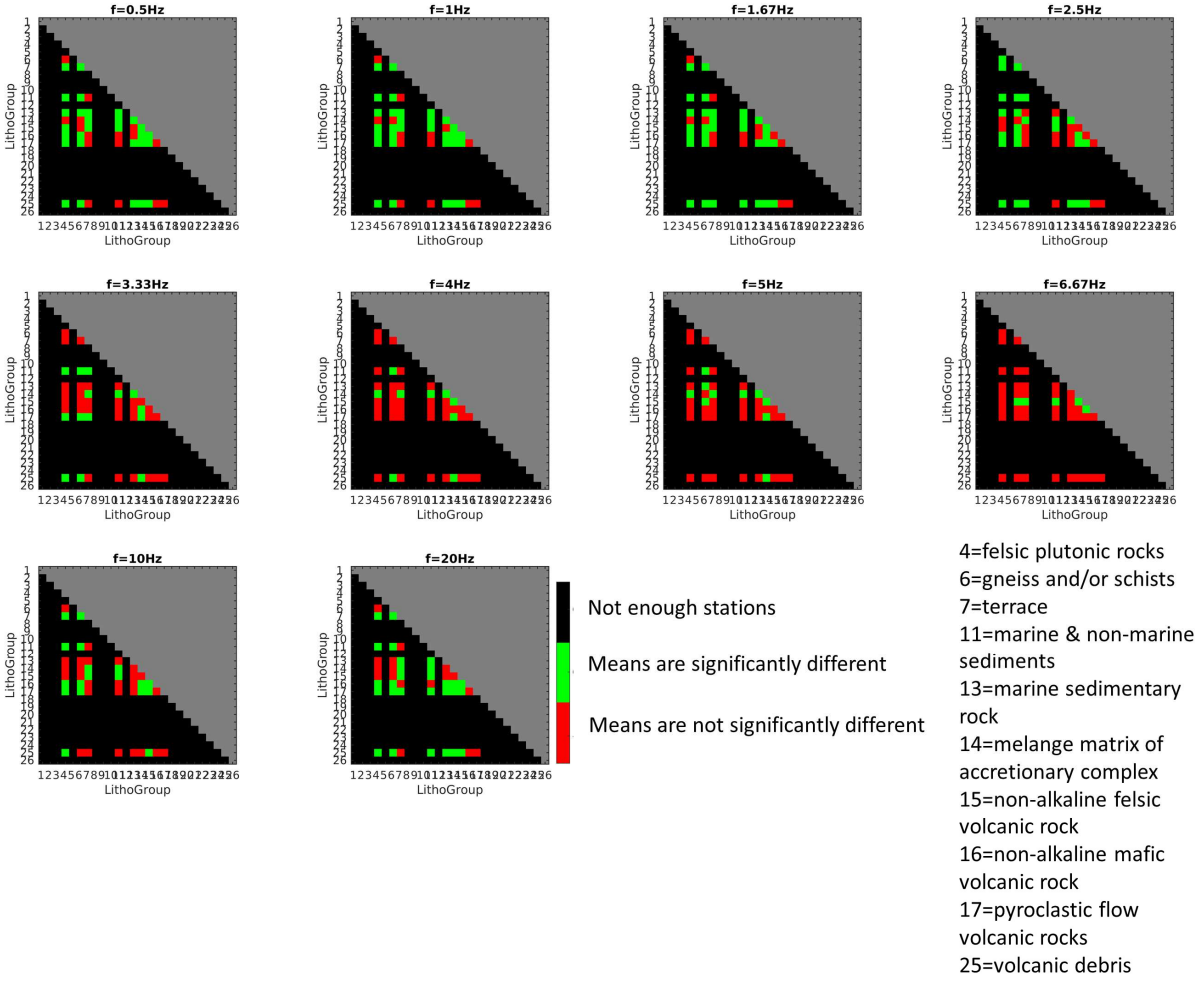

Figure 49: Japanese dataset, lithological classification. Results of Welch's t-test for the significance of the difference of means of all possible unordered pairs of classes, for the 10 frequency abscissae for which amplification factors are available

5.3 Comparing the effectiveness of proxies

The analyses illustrated in the previous sections 5.1 and 5.2 were carried out with the purpose to identify the most "effective" site condition parameters, i.e. the proxies bearing the highest sensitivity, or correlation, with local amplification. This discussion is subdivided into two parts: one dealing with continuous-variable parameters, the other with classification proxies.

5.3.1 Continuous-variable proxies

As described in section 5.1, all continuous-variable proxies were correlated with empirical site amplification factors at 10 frequency abscissae (0.5-20 Hz), through linear regressions. We assume the coefficient of determination r^2, measuring the goodness-of-fit of each regression, as the key parameter to compare the performance of various proxies.

Figure 50 collects all r^2 from the ordinary linear regressions (i.e. without considering possible errors on the proxy variable) of Fourier amplification factors versus proxies derived from the measured V_S profile or H/V_{noise} curve (see earlier subsections 5.1.1, 5.1.2). The following observations can be made:

- In general, proxies show a more marked correlation with amplification in the intermediate frequency range 1 – 6.67 Hz;
- In general, it appears that the correlation amplification-proxy is better for the Swiss data, and weaker for Japanese data (see end of this subsection for a full comment);
- The site condition parameter that "performs" best on a wide frequency band is V_S^{QWL} (quarter-wavelength velocity), followed by V_S30. Also V_S20 and V_S10 show a relatively good sensitivity to amplification, albeit at higher frequencies only. We highlight also the good performance of C_V10 (= $V_S10/V_{Sbedrock}$) and H_{800} at high and low frequencies, respectively. These behaviors apply to both Swiss and Japanese data;
- As for H/V_{noise}-derived parameters (Swiss database only), they generally show higher correlations with amplification at low frequencies. This finding is in agreement with other studies (e.g. Cultrera et al., 2014). A_0 (amplitude of H/V_{noise} curve at the fundamental frequencies) seems to perform better than f_0 or the H/V_{noise} curve sampled at selected frequency abscissae (labelled H/V_f in Figure 50). It is worth highlighting that, differently from the findings of other works (e.g Cadet et al., 2011, Derras et al., 2017) we obtained a relatively poor correlation between f_0 and amplification. We can propose two possible explanations: i) in the papers of Cadet et al. (2011) and Derras et al. (2017), f_0 is obtained from H/V ratios from earthquake recordings, not noise (as in our case); ii) furthermore, the f_0s from the SED H/V_{noise} database derive from an operation of manual picking that was performed by different operators over a period of several years (as and when new measurements were added), and both factors might have compromised the consistency in the criteria for the selection of the f_0 peak. An operation of revision of the fundamental frequency picks is envisaged for the future.

To provide a concise summary of our results, in Table 8 we show the best three V_S profile- or H/V_{noise}-derived proxies for each frequency, for both Switzerland and Japan.

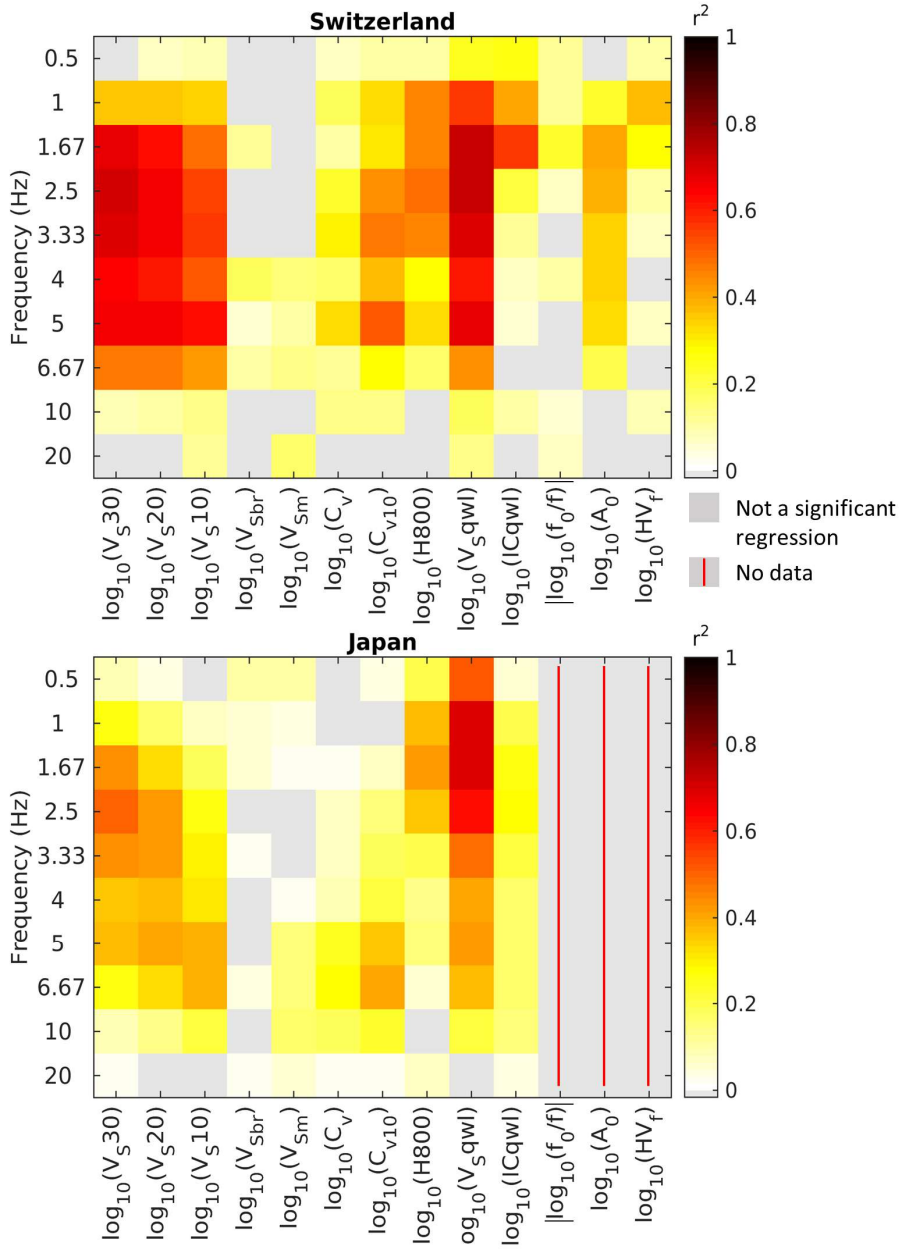

Figure 50: Coefficients of determination r^2 from the statistically significant ordinary linear regressions correlating amplification factors at ten frequencies and proxies derived from V_S profile or H/V_{noise} measurements, for Switzerland (top) and Japan (bottom). The labels on the x-axis refer to the various tested proxies. From left to right: Vs30, Vs20, Vs10, V_S of the bedrock, average V_S above the bedrock, velocity contrast ($C_V = V_{Smin}/V_{Sbedrock}$), Vs10 velocity contrast, ($C_{V10} = V_{S10}/V_{Sbedrock}$), H_{800}, quarter-wavelength velocity, quarter-wavelength impedance contrast, absolute logarithmic distance from fundamental frequency f_0, H/V_{noise} ratio at f_0 (A_0), H/V_{noise} curve sampled at selected frequency abscissae (H/V_f), all in logarithmic scale.

Table 8: The best three V_S profile- or H/V_{noise}-derived proxies for each frequency, for Swiss and Japanese stations, accompanied by their coefficients of determination (between brackets).

	0.5 HZ	1 HZ	1.67 HZ	2.5 HZ	3.33 HZ	4 HZ	5 HZ	6.67 HZ	10 HZ	20 HZ
Switzerland	IC^{QWL}	Vs^{QWL}	Vs^{QWL}	Vs^{QWL}	Vs^{QWL}	Vs30	Vs^{QWL}	Vs30	Vs^{QWL}	Vsm
	(0.26)	(0.57)	(0.73)	(0.73)	(0.70)	(0.64)	(0.67)	(0.47)	(0.18)	(0.16)
	Vs^{QWL}	H800	Vs30	Vs30	Vs30	Vs20	Vs30	Vs20	Cv	Vs^{QWL}
	(0.24)	(0.45)	(0.68)	(0.71)	(0.69)	(0.62)	(0.66)	(0.47)	(0.14)	(0.14)
	f_0/f	IC^{QWL}	Vs20	Vs20	Vs20	Vs^{QWL}	Vs20	Vs^{QWL}	Cv10	Vs10
	(0.12)	(0.41)	(0.63)	(0.67)	(0.66)	(0.61)	(0.66)	(0.44)	(0.13)	(0.12)
Japan	Vs^{QWL}	Vs^{QWL}	Vs^{QWL}	Vs^{QWL}	Vs^{QWL}	Vs^{QWL}	Vs^{QWL}	Cv10	Cv10	H800
	(0.52)	(0.70)	(0.70)	(0.63)	(0.48)	(0.41)	(0.42)	(0.41)	(0.22)	(0.08)
	H800	H800	Vs30	Vs30	Vs30	Vs20	Vs20	Vs10	Vs^{QWL}	Vsm
	(0.20)	(0.38)	(0.43)	(0.51)	(0.44)	(0.37)	(0.4)	(0.39)	(0.22)	(0.05)
	Vsbr	Vs30	H800	Vs20	Vs20	Vs30	Vs10	Vs^{QWL}	Vs10	IC^{QWL}
	(0.10)	(0.26)	(0.42)	(0.42)	(0.42)	(0.36)	(0.38)	(0.38)	(0.21)	(0.03)

The same operation of ranking of proxies was also carried out for the topography-derived parameters (slope, curvature, topography position index, evaluated at various spatial scales, see subsection 5.1.3). The values of r^2 for each frequency and proxy are shown in Figure 51. In this case, we highlight the following key observations:

- Topography-based proxies perform generally better in the low frequency band (≤3.33 Hz), both in Switzerland and Japan;
- Globally, these parameters are more "effective" in Switzerland than Japan (see end of this subsection for a full comment);
- The correlation between smoothed curvature (C_S) or topography position index (TPI_{norm}) and amplification is more frequently significant in Japan than Switzerland. As already observed in section 5.1.3, this feature appears to be an artefact arising from the lack of "convex" sites in the Japanese database; in fact, the trend observed in the more complete Swiss dataset, spanning from negative to positive C_S/TPI_{norm} values, involves higher amplification for stations with $C_S/TPI_{norm} \approx 0$ ("flat" sites), and lower amplification at concave or convex sites (resulting in an almost flat linear regression line, hence not statistically significant).
- In general, large-scale topographical proxies "work" better at very low frequencies, while smaller-scale parameters have higher sensitivity at intermediate-to-low frequencies (1.67 – 3.33 Hz);
- Better correlations are ensured by slope, at least for the Swiss dataset;
- It is also worth remarking the moderate sensitivity of amplification to the absolute value of the difference between curvature along northing minus curvature along easting axis (right side of subplots in Figure 51; for the physical interpretation of this feature see 5.1.3).

Here again, as a summary of these results, we display the best three topographical parameters for each frequency in Table 9.

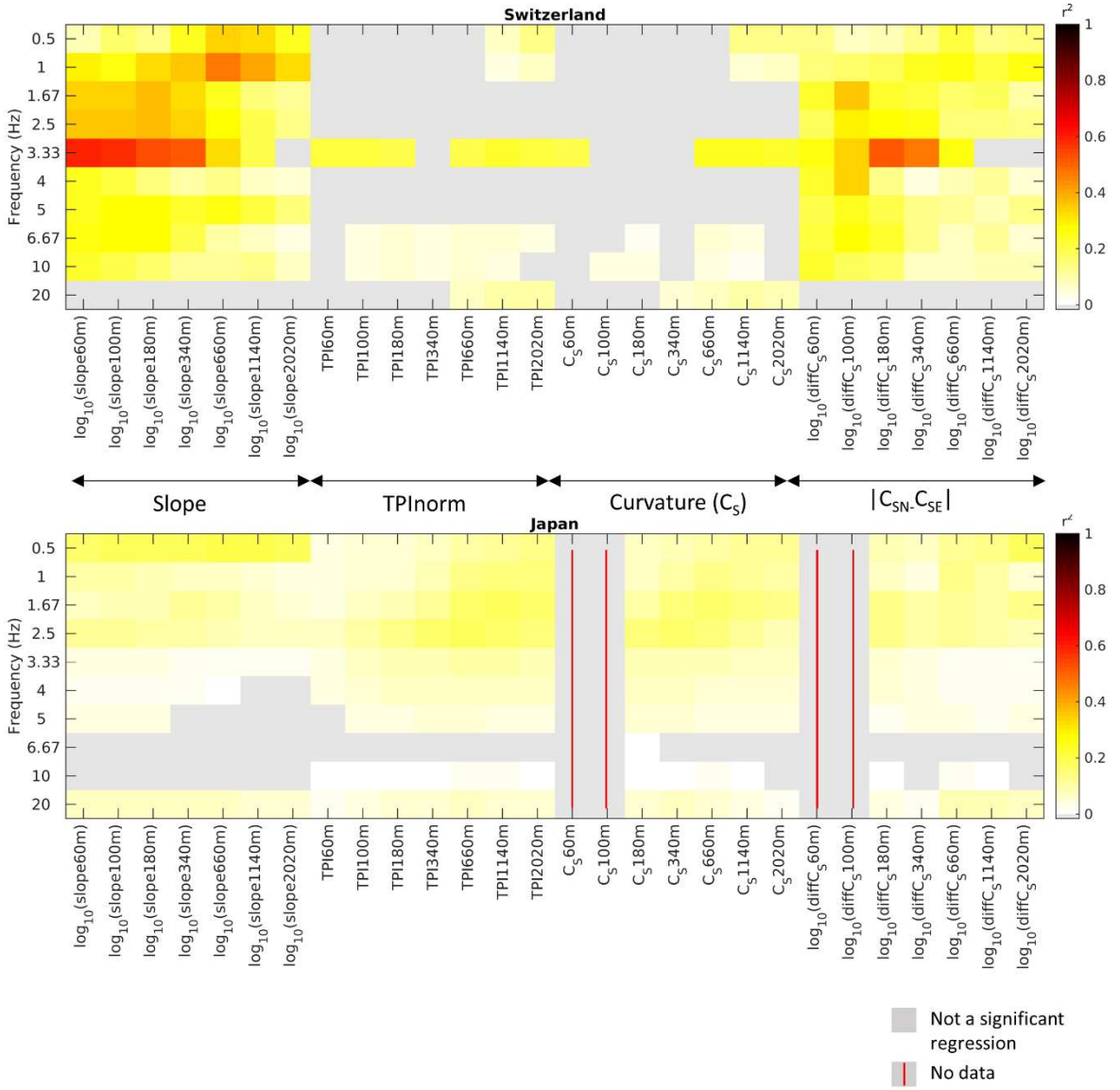

Figure 51: Coefficients of determination r^2 from the statistically significant regressions correlating amplification factors at ten frequencies and proxies derived from topography, for Switzerland (top) and Japan (bottom). The labels on the x-axis refer to the various tested proxies. From left to right: logarithm of the slope at 60, 100, 180, 340, 660, 1140, 2020 m scale, normalized topography position index (TPI_{norm}) at 60 – 2020 m scales, smoothed topographical curvature (C_S) at 60-2020 m scales, logarithm of the absolute difference between curvature along northing minus curvature along easting axis at 60-2020 m scales.

Table 9: The best three topography-based proxies for each frequency, for Swiss and Japanese stations, accompanied by their coefficients of determination. γ = slope, C_S = smoothed topographical curvature, TPI = normalized topography position index, $|C_{SN-E}|$ = absolute difference between curvature along northing minus curvature along easting axis.

	0.5 HZ	1 HZ	1.67 HZ	2.5 HZ	3.33 HZ	4 HZ	5 HZ	6.67 HZ	10 HZ	20 HZ
Switzerland	γ_{660m} 0.34 γ_{1140m} 0.32 γ_{2020m} 0.24	γ_{660m} 0.46 γ_{1140m} 0.4 γ_{340m} 0.36	γ_{180m} 0.37 $\lvert C_{SN-E}\rvert_{100m}$ 0.36 γ_{100m} 0.34	γ_{180m} 0.38 γ_{60m} 0.36 γ_{100m} 0.35	γ_{60m} 0.59 γ_{100m} 0.58 γ_{180m} 0.54	$\lvert C_{SN-E}\rvert_{100m}$ 0.34 γ_{60m} 0.25 $\lvert C_{SN-E}\rvert_{60m}$ 0.24	γ_{100m} 0.29 γ_{180m} 0.27 γ_{660m} 0.27	$\lvert C_{SN-E}\rvert_{100m}$ 0.28 γ_{180m} 0.28 γ_{100m} 0.27	$\lvert C_{SN-E}\rvert_{60m}$ 0.24 γ_{60m} 0.23 γ_{100m} 0.19	TPI_{2020m} 0.11 C_{S1140m} 0.10 TPI_{1140m} 0.10
Japan	γ_{1140m} 0.21 γ_{660m} 0.20 γ_{180m} 0.18	TPI_{2020m} 0.15 TPI_{1140m} 0.15 $\lvert C_{SN-E}\rvert_{660m}$ 0.14	TPI_{1140m} 0.18 TPI_{2020m} 0.17 TPI_{660m} 0.17	TPI_{660m} 0.18 C_{S340m} 0.17 TPI_{1140m} 0.17	TPI_{660m} 0.10 TPI_{1140m} 0.10 C_{S340m} 0.10	C_{S180m} 0.08 TPI_{340m} 0.08 TPI_{660m} 0.08	C_{S340m} 0.05 TPI_{340m} 0.05 TPI_{660m} 0.05	C_{S180m} 0.01	TPI_{1140m} 0.02 $\lvert C_{SN-E}\rvert_{660m}$ 0.02 C_{S660m} 0.02	$\lvert C_{SN-E}\rvert_{1140m}$ 0.09 $\lvert C_{SN-E}\rvert_{660m}$ 0.08 γ_{180m} 0.08

The last set of proxies we analyse is that comprising the parameters we named as "indirect" proxies, i.e. proxies neither based on in-situ measures or topography, but derived from pedologic/geophysical datasets (subsections 5.1.4 and 5.1.5). These are: the depth to pedologic bedrock and % of coarse fraction at 2 m depth inferred from the global SoilGrids250m database, the thickness of ice cover at the last glacial maximum, the average V_P and bulk density attributed by SAPHYR database to each lithological group (Switzerland only), the H800 derived from the JSHIS subsurface model (Japan only). The "strength" of their correlations with site amplification is displayed in Figure 52;

- As already observed for topographical parameters, in general the indirect proxies perform better at low frequencies (≤ 3.33 Hz);
- The only two indirect proxies available for both Switzerland and Japan (depth to pedologic bedrock and % of coarse fraction) work better for Swiss sites (see end of this subsection for a full comment);
- As for Switzerland, the local bedrock model provided by Swisstopo (Swisstopo, 2019) performs better than the global model from the SoilGrids250m database (Hengl et al., 2017). On the other hand, for Japan, the H800 inferred from the national JSHIS subsurface model (Fujiwara et al., 2009) is not more effective than the global SoilGrids250m bedrock model;
- We highlight the relatively good correlations between amplification and physical parameters provided by SAPHYR database (Zappone and Bruijn, 2012) for each lithological group (in particular the bulk density).

To sum up, we present in Table 10 the best 3 non-topography-based indirect proxies at each frequency.

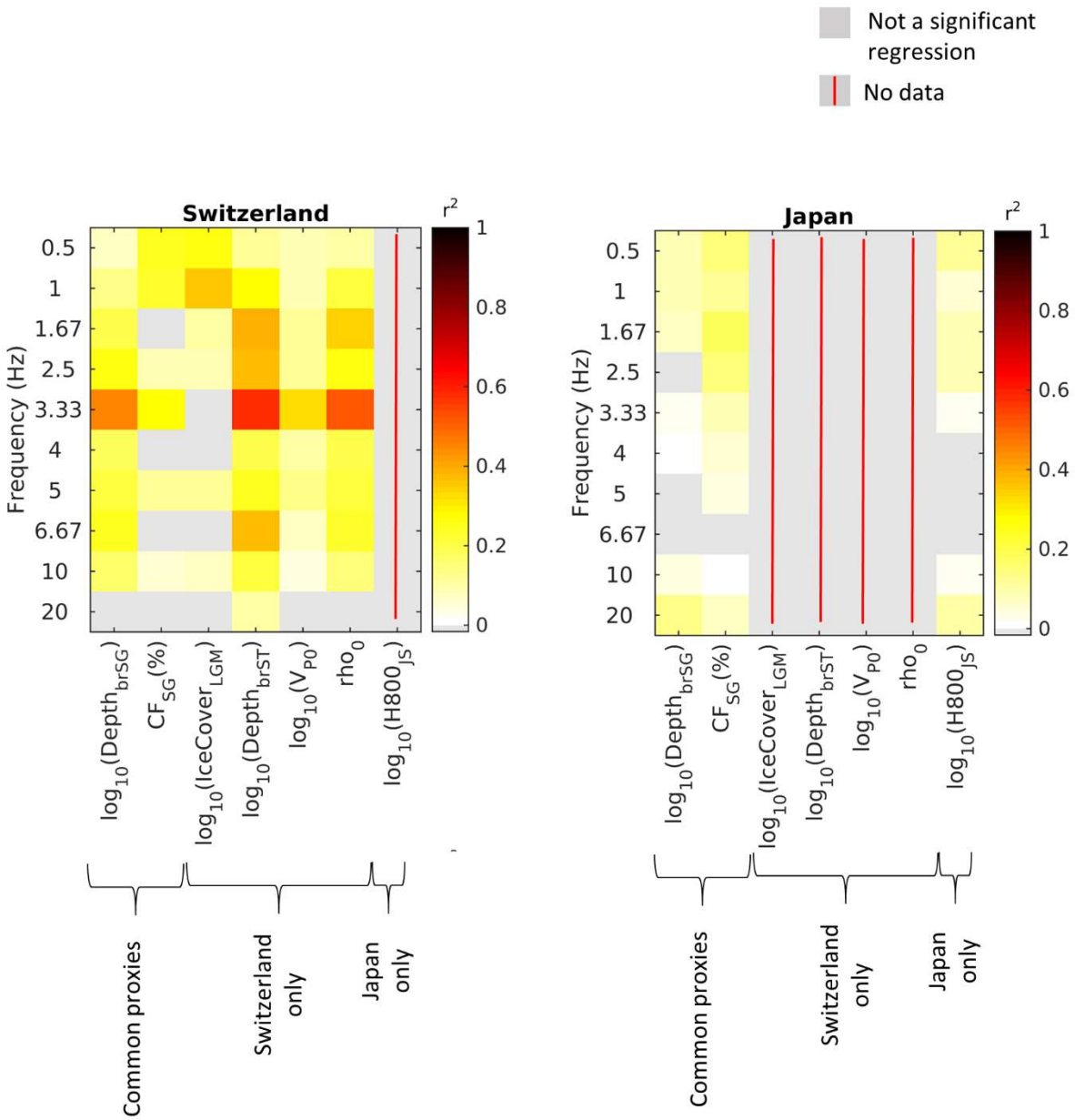

Figure 52: Coefficients of determination r^2 from the statistically significant regressions correlating amplification factors at ten frequencies and indirect proxies not derived from topography, for Switzerland (left) and Japan (right). The labels on the x-axis refer to the various tested proxies. From left to right: logarithm of pedologic bedrock depth from SoilGrids250m database ($\log_{10}(Depth_{brSG})$), % of coarse fraction at 2 m depth from SoilGrids250m database ($CF_{SG}(\%)$), logarithm of the thickness of ice cover at LGM ($\log_{10}(IceCover_{LGM})$), logarithm of bedrock depth from Swisstopo model ($\log_{10}(Depth_{brST})$), logarithm of the average V_P for each lithological group from SAPHYR database ($\log_{10}(V_{P0})$), average bulk density for each lithological group from SAPHYR database (rho_0), logarithm of H800 derived from the JSHIS subsurface model ($\log_{10}(H800_{JS})$).

Table 10: The best three non-topography-based indirect proxies for each frequency, for Swiss and Japanese stations, accompanied by their coefficients of determination. IC_{LGM} = thickness of ice cover at LGM, CF% = percentage of coarse fraction at 2 m depth, $D_{br}SG$ = bedrock depth from SoilGrids250m, $D_{br}ST$ = bedrock depth from Swisstopo, ρ_0 = average bulk density from SAPHYR, $H800_{JS}$ = H800 derived from JSHIS subsurface model.

	0.5 HZ	1 HZ	1.67 HZ	2.5 HZ	3.33 HZ	4 HZ	5 HZ	6.67 HZ	10 HZ	20 HZ
Switzerland	IC_{LGM} (0.27)	IC_{LGM} (0.36)	$D_{br}ST$ (0.39)	$D_{br}ST$ (0.36)	$D_{br}ST$ (0.57)	$D_{br}ST$ (0.20)	$D_{br}ST$ (0.25)	$D_{br}ST$ (0.37)	$D_{br}ST$ (0.21)	$D_{br}ST$ (0.10)
	CF% (0.25)	$D_{br}ST$ (0.29)	ρ_0 (0.34)	ρ_0 (0.27)	ρ_0 (0.51)	ρ_0 (0.19)	ρ_0 (0.22)	$D_{br}SG$ (0.24)	$D_{br}SG$ (0.16)	
	$D_{br}ST$ (0.11)	CF% (0.24)	$D_{br}SG$ (0.20)	$D_{br}SG$ (0.25)	$D_{br}SG$ (0.45)	$D_{br}SG$ (0.18)	$D_{br}SG$ (0.21)	ρ_0 (0.23)	ρ_0 (0.15)	
Japan	CF% (0.16)	CF% (0.12)	CF% (0.18)	CF% (0.16)	CF% (0.08)	CF% (0.06)	CF% (0.05)		$D_{br}SG$ (0.04)	$D_{br}SG$ (0.1)
	$H800_{JS}$ (0.12)	$D_{br}SG$ (0.09)	$H800_{JS}$ (0.09)	$H800_{JS}$ (0.08)	$D_{br}SG$ (0.02)	$D_{br}SG$ (0.02)			$H800_{JS}$ (0.02)	$H800_{JS}$ (0.1)
	$D_{br}SG$ (0.09)	$H800_{JS}$ (0.06)	$D_{br}SG$ (0.06)		$H800_{JS}$ (0.02)				CF% (0.01)	CF% (0.08)

Eventually, we collate the three groups of proxies (V_S profile- or H/V_{noise}-derived, topographical and non-topography-based indirect parameters) to draw some general conclusions:

- As expected, proxies directly derived from a measured V_S profile or H/V_{noise} curve work (in general) better than topographical or indirect geological/geophysical parameters. However – for Switzerland – at very low frequency (0.5 Hz) topography (slope) and geological data (ice cover at LGM) are more effective than quarter wavelength velocity and impedance contrast;
- Topography-based and indirect geology/geophysics-based parameters appear to have comparable levels of correlation with site amplification;
- A key point is the difference in the level of correlation between Japan and Switzerland, always in favor of the latter. We ascribe this feature to the different geographical extent of the two databases (Switzerland has an area that is $1/9^{th}$ of Japan). We argue that the correlations we identified (for instance: amplification vs. slope) are not necessarily the same across the world, and depend heavily on the local geological environment and local pedogenic processes, i.e. a complex reality that is concisely summarized (more or less effectively) by the proxy parameter. In this perspective, our hypothesis is that the correlation amplification-proxies perform better in Switzerland because they refer to a smaller area, more likely to present homogeneous geological features. Vice versa, the regressions we identified for Japan might result from the superposition of more region-specific behaviors, that are somehow smoothed out when stacked in the same statistical population.

A final aspect we intended to address is the relevance of including the uncertainties on the proxy variable, when computing the regressions amplification vs. site condition parameters. As illustrated in section 5.1, when the proxy uncertainties are not taken into account (e.g. because unavailable), the best linear fit minimizes its distances from the data points as measured along the Y (amplification) axis (ordinary linear fit). On the other hand, when introducing the error ranges for the site condition parameter, it is necessary to adopt the orthogonal linear regression method, where the orthogonal distance between data points and linear fit is minimized, and the two components of the distance along X (proxy) and Y (amplification) axes are weighted with the respective uncertainty intervals.

Therefore, in Figure 53 and 54 we collate the coefficients of determination (r^2) and the slope coefficients (b_1), respectively, as obtained from ordinary or orthogonal linear regressions carried out on proxy variables for which a measure of uncertainty is available (Swiss dataset only). In general, the level of data fit (represented by r^2), and the significance of the linear regressions are similar (Figure 53). More significant differences can be observed for the slope coefficients (Figure 54), for the proxies

having wide uncertainty ranges (C_V, C_{V10}, A_0, HV_f, ρ_0, V_{P0}). In these cases, the large error bars on the abscissae (proxy) make it more “convenient” for the orthogonal regression method to yield steeper slopes, with respect to ordinary regression (see for instance Figures 28 and 29). Vice versa, when site condition parameter uncertainties are narrower, the slope coefficients are nearly identical to those obtained from ordinary regression (see for instance V_{S30} in Figure 54, and Figures 23 and 25).

The analyses presented here highlight the importance of a proper computation and handling of the experimental uncertainties, for both the amplification and proxy variables.

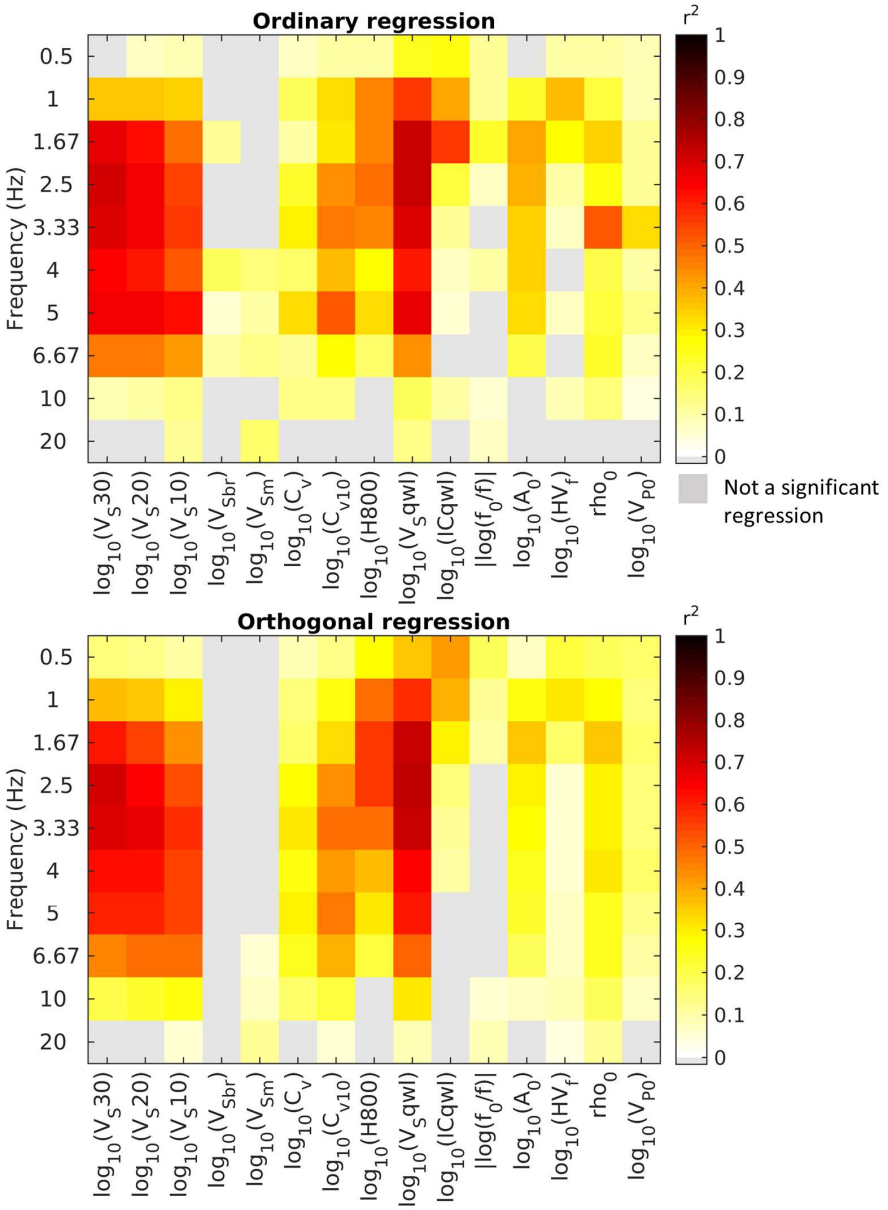

Figure 53: Swiss dataset: comparison between determination coefficients r^2 from amplification vs proxy ordinary (top) and orthogonal (bottom) regressions. In the first case only the uncertainties for the dependent variable (amplification) were taken into account; in the second case, the uncertainties from both variables (amplification and proxy) were considered. The labels on the x-axis refer to the various tested proxies. From left to right: Vs30, Vs20, Vs10, V_S of the bedrock, average V_S above the bedrock, velocity contrast, Vs10 velocity contrast, , H_{800}, quarter-wavelength velocity and impedance contrast, absolute logarithmic distance from fundamental frequency f_0, H/V_{noise} ratio at f_0 (A_0), H/V_{noise} curve sampled at selected frequency abscissae (H/V_f), average bulk density and VP provided by SAPHYR database for each Swiss lithological group.

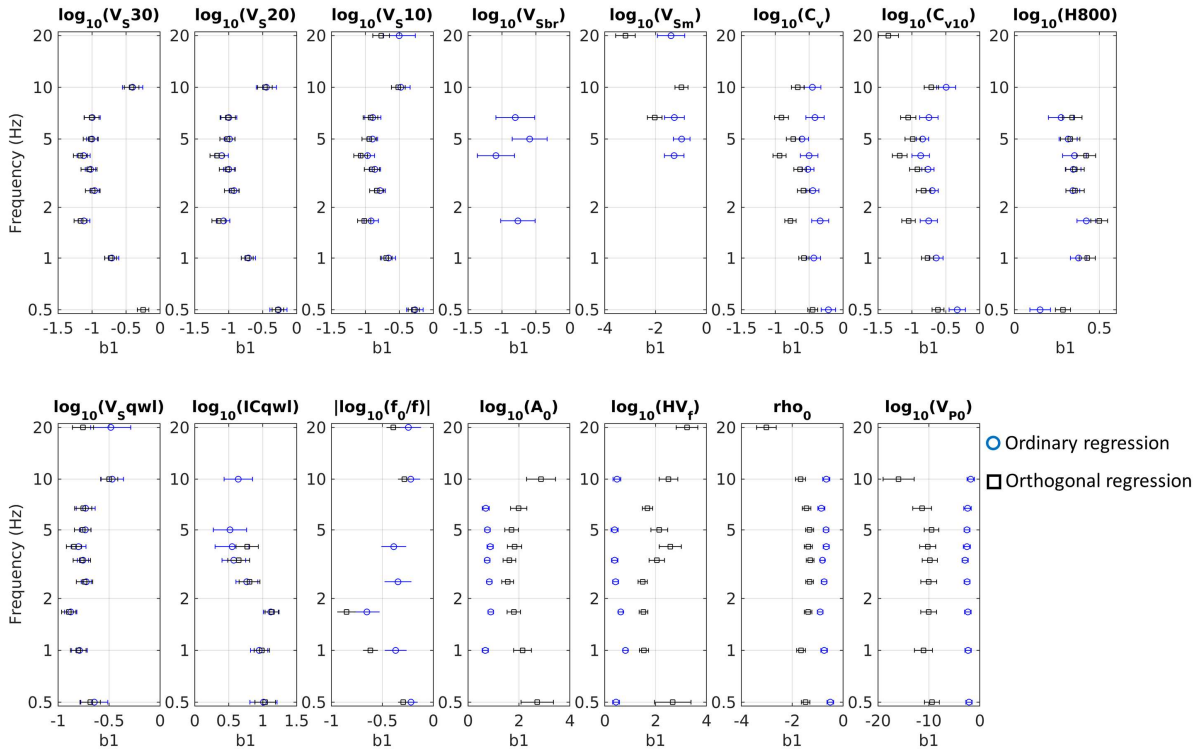

Figure 54: Swiss dataset: comparison between slope coefficients (b1) from amplification vs proxy ordinary (blue circles) and orthogonal (black squares) regressions. In the first case only the uncertainties for the dependent variable (amplification) were taken into account; in the second case, the uncertainties from both variables (amplification and proxy) were considered. Every subplot refers to a different proxy (the same listed in the caption to Figure 53).

5.3.2 Classification proxies

As earlier described in section 5.2, for the proxies that are not continuous variable and propose a classification of the stations into two or more subgroups (e.g. depending on the lithology of the rock formation), we adopted a strategy different than regression to evaluate their performance. We assessed whether the subpopulations proposed by the proxy constitute groups with an internally consistent amplification behaviour, significantly different than that of other classes. Therefore, for such parameters we don't have any coefficient of determination r^2; rather, we base our assessment of the effectiveness of the proxy on a so-called index of effectiveness (i_e, see equation 2 in section 5.2), which is the ratio between the number of unordered class pairs whose average amplification values are not statistically equivalent, divided by the total number of unordered classes couples.

We collect in Figure 55 all the values of indexes of effectiveness, for each proxy-based classification and each frequency:

- For the computation of i_e, we excluded all proposed classes that do not include any station, since we considered them as marginal or not applicable (it is the case, for instance, of the group "quaternary volcanic rocks" for the age classification of Swiss sites);
- The values of i_e are reported for those classifications where more than half of the non-empty subgroups exceeds the sample size (≥10) which we considered sufficient to draw statistical inference; otherwise we assume our population to be too small or too unevenly distributed to evaluate the effectiveness of the proxy.

From the analysis of the proxies' statistical performances, it is possible to draw the following observations:

- In general, the classifications "work" better at low frequencies (≤ 5 Hz). This is particularly evident for the Japanese dataset, where the frequency band 6.67 – 10 Hz shows i_e much lower than those for f ≤ 5 Hz (but at 20 Hz the indexes grow again: this is somehow similar to the trend for continuous proxies in Figure 51, lower subplot);
- As for the topographical classification, this seems to be more effective at smaller spatial scales, at least for Japan (≤180 m; not enough data for Switzerland);
- Coarse categorizations based on the rock age or genesis appear to perform equally well as small-scale topographical classifications;
- Categorizations involving a (relatively) large number of groups (≥ 15) either fail to have a sufficient number of sites in each class (gray columns) or have indexes of effectiveness lower than the classifications described above (topographical classifications, age or rock genesis coarse categorizations have 6 or less groups). The first case (not enough classes with sufficient sample size) applies for instance to the lithological classifications for Switzerland and Japan; the second case (low i_e) applies to the engineering geomorphologic and the detailed rock genesis categorizations for Japan. We argue that these lower i_e arise from the fact that a higher number of classes is likely to define internally homogenous groups, however not necessarily with a distinct amplification behavior with respect to all the other classes (i.e. statistically equivalent means).

To conclude, categorizations based on (smaller-scale) topography or rock age/genesis, involving few subclasses, appear to be effective in defining groups with distinct amplification behaviour. As for more refined classifications, based on lithology or rock age, with our datasets it is not possible to come to a full assessment of their potential, as not enough of the proposed categories collect a statistically significant number of sites. A solution could obviously be the increase of the population of sites; nevertheless, we remark that our databases already include a relatively large number of stations (and, to our knowledge, no network like KiK-net has a such a dense and wide extent, combined with the availability of recorded events and metadata).

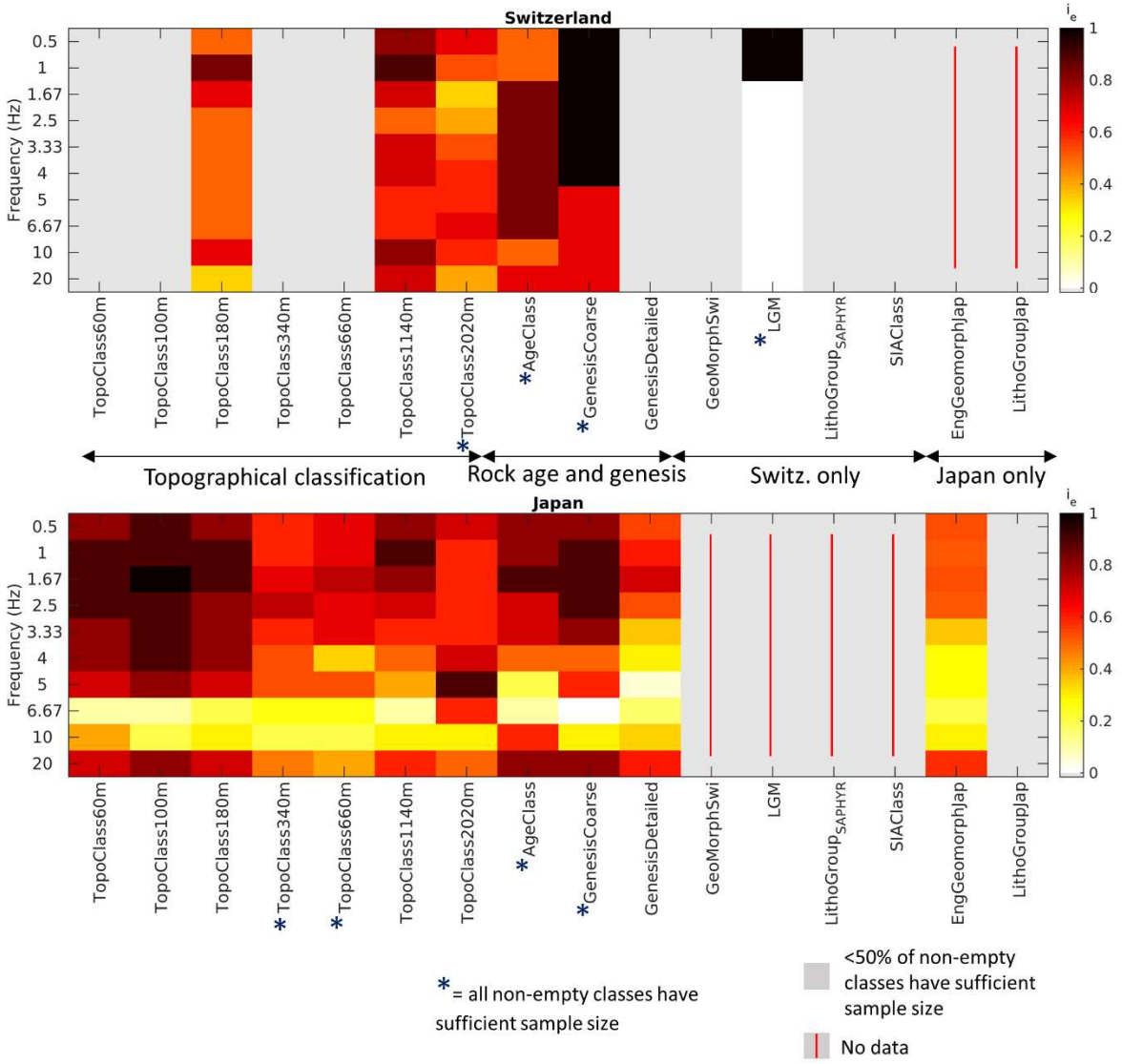

Figure 55: Index of effectiveness i_e for the proxy-based classifications for Switzerland (top) and Japan (bottom). The labels on the x-axis refer to the various tested proxies. From left to right: topographical classification by Burjanek et al. (2014) at the spatial scales 60, 100, 180, 340, 660, 1140, 2020 m, rock age and genesis (coarse and detailed) classification, Swiss geomorphological classification, ice cover at LGM (sites with ice cover vs sites without any ice cover), lithological classification proposed for Switzerland by SAPHYR, soil class grouping according to geotechnical map, engineering geomorphologic classification of Japan, lithological classification of Japan. The blue asterisk denotes the cases where all non-empty groups have sufficient sample size (ideal case).

5.4 Collating the behaviours of proxies in Switzerland and Japan

A key issue we intended to address is assessing whether site condition parameters "behave" in a similar way in Switzerland and Japan.

For continuous-variable proxies, this means understanding to what extent the correlations site amplification vs. proxies are comparable. To answer in a quantitative way, we collated each statistically significant ordinary linear fit from the Swiss database with its companion from the Japanese dataset (same proxy, same frequency), evaluating whether the regression slopes are similar (i.e. equivalent in a statistical way) or not. As suggested by Andrade and Estevez-Perez (2014) for this particular application, we use the Welch's t-test, already described in section 5.2 (assuming a 90% confidence level). If the test null hypothesis of equivalence between the two slopes is to be accepted, we conclude

that for both the Swiss and Japanese datasets the considered proxy determines a similar increase or decrease of site amplification proportionally to its value.

As example, we show in Figure 56 the collation of the regressions amplification vs. V_S30 for Switzerland and Japan. In the frequency band 1 – 10 Hz, both Swiss and Japanese regressions are statistically significant; at the frequencies 1 Hz and 2.5 – 10 Hz, Swiss and Japanese slopes are statistically equivalent. Vice versa, at 1.67 Hz, the difference between the two slope values becomes significant. We underline the role played by the regression coefficients' standard errors when evaluating the significance of their difference through a Welch's t-test: the smaller the standard errors, the smaller their difference needs to be to be considered significant, and vice versa. This is shown, for instance, in the lower-right subplot in Figure 56; at 1.67 Hz, the two slope coefficients are clearly apart, with no overlapping error bars.

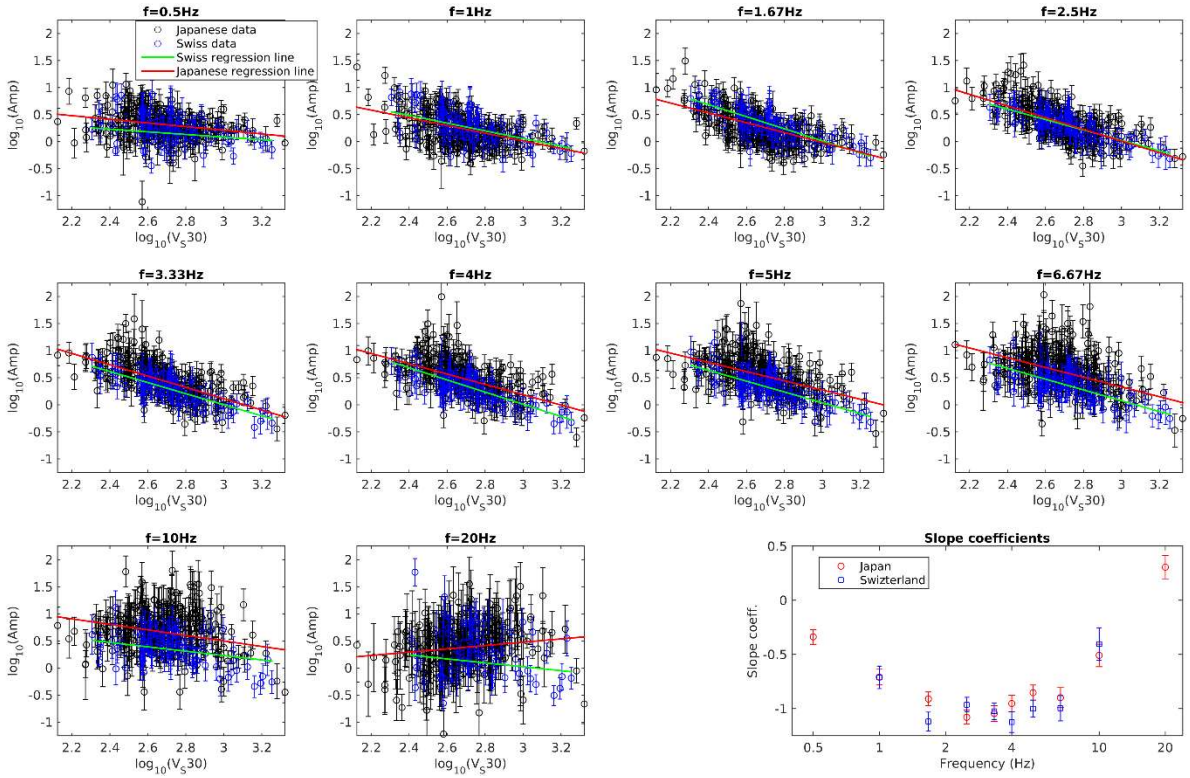

Figure 56: Direct comparison between the regressions amplification vs V_S30 for Switzerland and Japan, for the usual ten frequency abscissae. In the lower-right corner, the subplot displays the slope coefficients for the statistically significant correlations.

Figure 57 offers an overview of the outcome of the statistical tests for all proxies available for both Swiss and Japanese sites. It is important to notice that for the V_S profile-based proxies we frequently obtain "parallel" behaviours for Switzerland and Japan (equivalent slopes, green). On the contrary, for indirect geological proxies (top right) and topographical parameters (bottom), in most of the cases we derive diverging regression lines (red). In fact, V_S profile-related proxies directly refer to a geo-mechanical reality, hence they are likely to be correlated to site amplification in a similar way, in Switzerland or Japan. On the other hand, topographical or indirect geological parameters mirror more or less loosely geo-mechanical quantities, and we argue that the nature of these relationships may heavily depend on local geological features, processes and environments. Hence, it is not surprising that these proxies "work" in different ways in Switzerland and Japan.

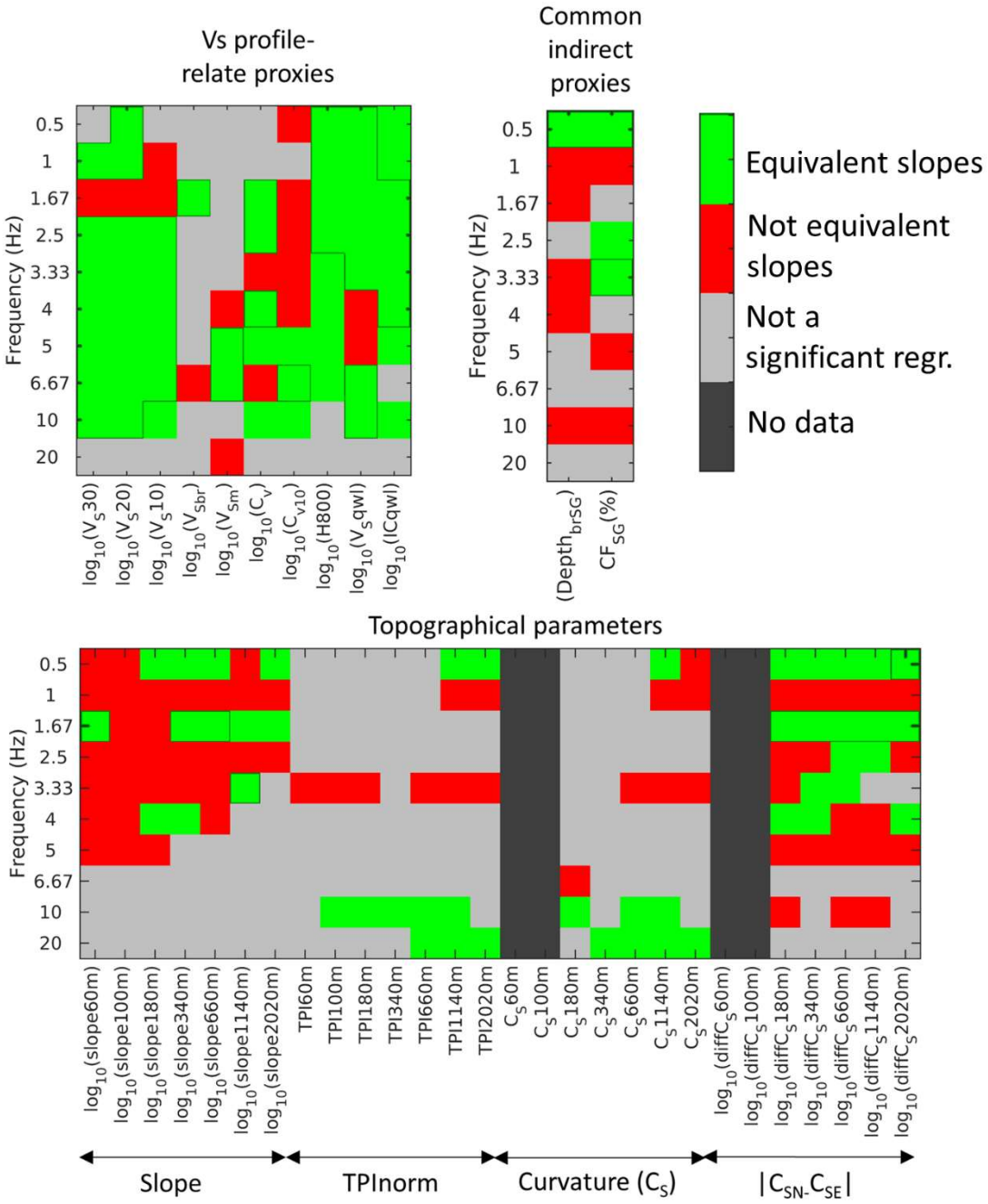

Figure 57: Overview of the results of the statistical tests to compare the regressions amplification vs. proxies from Swiss and Japanese datasets. In each cell, the color code represents the outcome of the tests for each proxy (abscissae) and for each frequency (ordinates). In the top left subplot, the Vs profile-related proxies, from left to right: logarithm of $Vs_{30,20,10}$, V_S of the bedrock, average V_S above bedrock, velocity contrast, Vs_{10} velocity contrast, H800, quarter-wavelength velocity and impedance contrast. Top right: common indirect proxies (depth to pedologic bedrock and % of coarse fraction from SoilGrids250m database). Bottom: topographical parameters (slope, TPI_{norm}, curvature, absolute difference between directional curvatures at 7 spatial scales 60 – 2020 m).

As far as the classification proxies are concerned, we compare the Swiss and the Japanese databases focusing on whether the same categorizations (based on topography, rock age or genesis) classify the sites according to analogous amplification patterns. In other words, we aim to assess if two companion groups of stations, one from Japan and one from Switzerland, belonging to the same category (e.g.

Holocene, from the rock age classification) exhibit similar deviations from the mean amplification behaviour of each respective dataset (Japan and Switzerland).

This analysis can be performed on the categorizations common to Switzerland and Japan, having an adequate number of subgroups with an acceptable sample size (≥ 10 sites). These criteria narrow down our selection to the topographical classing at scales 60 – 2020 m, to the rock age categorization and the coarse rock genesis classification (see subsection 5.2).

Figure 58 shows the mean amplifications and corresponding standard deviations for each rock age group, for Switzerland and Japan, at each frequency abscissa. We observe at low frequencies (0.5 – 2.5 Hz, Figure 58, top) a clear common pattern for Switzerland and Japan, with higher mean amplifications for quaternary deposits (particularly of volcanic origin for Japan), and lower amplifications for tertiary and particularly pre-tertiary classes. In the intermediate frequency range (3.33 – 10 Hz) Japanese sites show little differences depending on the age class, while Swiss stations keep the trend observed at low frequencies. At 20 Hz, for Japanese data the behaviour is the opposite of low frequencies, with lower amplifications for quaternary soils and higher values for tertiary and pre-tertiary groups. Focusing on the standard deviations (Figure 58, bottom), which portray the scatter of each subgroup around the mean value, we notice an increasing trend with frequency for Japan; the same behaviour applies for Swiss sites, with the exception of the anomalous pattern of Holocene sites (high σ at very low frequencies, followed by a trough at 3.33 Hz).

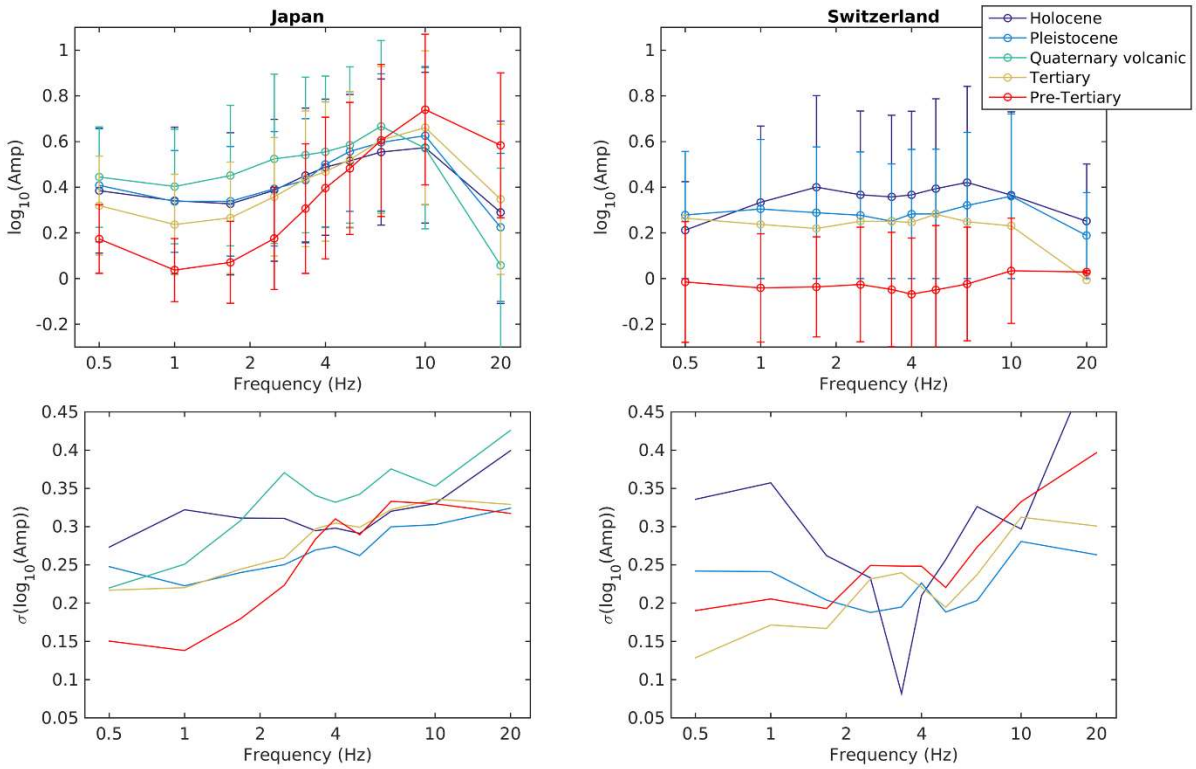

Figure 58: Top: mean amplifications (circles) and standard deviations (error bars) for each rock age class, from Swiss and Japanese data, for each frequency abscissa. Missing data points indicate null or insufficient sample size (<10 sites). Bottom: standard deviations for each rock age class.

An analogous behaviour, with similarities and dissimilarities between Swiss and Japanese data, is also observed for the coarse rock origin classification (Figure 59). Here again, at low frequencies (0.5 – 3.33 Hz, Figure 59 top) we observe a definite trend for Japanese stations: lower amplifications for metamorphic and consolidated sedimentary rocks, intermediate amplifications for magmatic rocks, and higher values for tertiary and quaternary sediments. As for Swiss stations, the same behaviour holds

true for sedimentary rocks and quaternary sediments, while metamorphic rocks amplify significantly less than compact sedimentary rocks. In the intermediate frequency band (4 – 10 Hz) Japanese stations have minor differences depending on the rock genesis class, while for Switzerland we still observe a significant gap between quaternary sediments and compact rocks, but the distance between magmatic and sedimentary rocks decreases with the frequency. At 20 Hz, for Japan the pattern is the opposite of that at low frequencies, and also for Switzerland metamorphic rocks amplify now more than consolidated sedimentary formations. Observing the standard deviations (Figure 59, bottom), as in Figure 58 we have increasing σs with frequency, with the exception of the Quaternary sediments (very high values at low frequency, then a trough at 3.33 Hz).

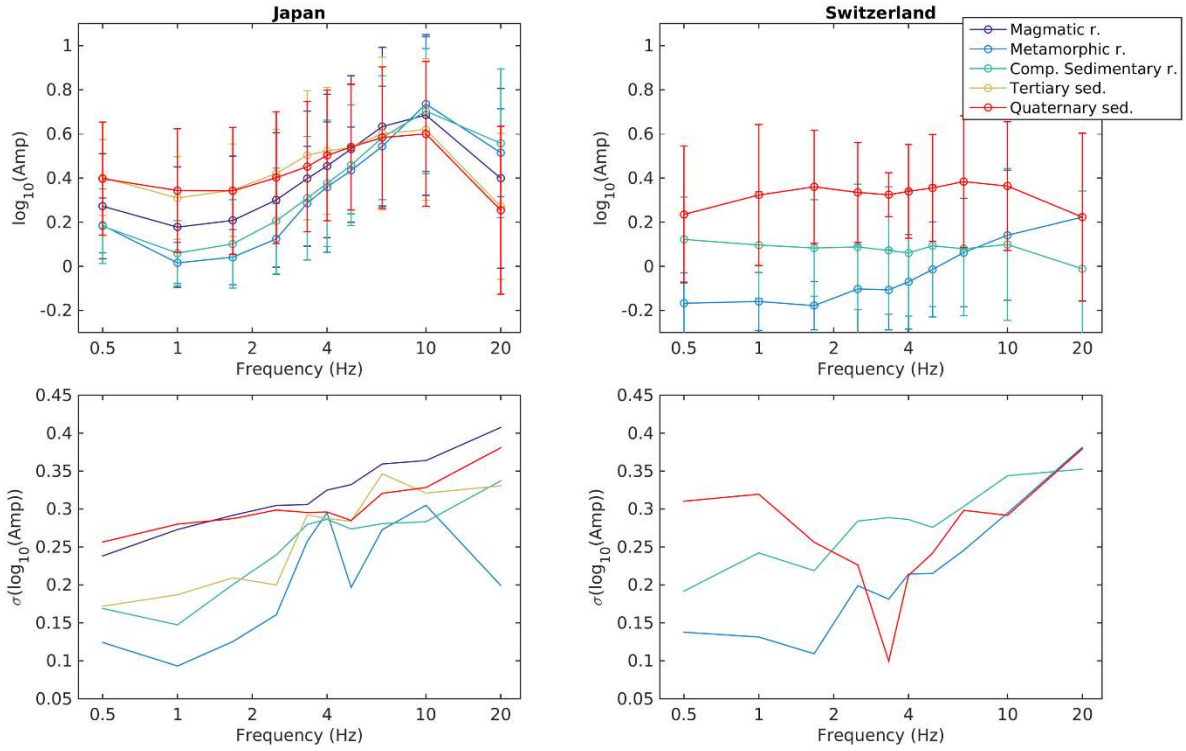

Figure 59: Top: mean amplifications (circles) and standard deviations (error bars) for each rock genesis class (coarse classification), from Swiss and Japanese data, for each frequency abscissa. Missing data points indicate null or insufficient sample size (<10 samples). Bottom: standard deviations for each rock genesis class.

As for the topographical classifications (7 spatial scales, 60 – 2020 m), we show the mean amplification and standard deviation for each category in Figures 60 and 61, denoting generally different patterns for the two regions. For Japanese sites, it is possible to notice a relatively clear trend, approximately consistent for all scales (Figure 60). Below 5 Hz, the highest mean amplifications generally belong to the "flat area" or "upper slope" classes, followed by "middle slope", "lower slope" and finally "valley". When present, the "ridge" category shows high amplification factors, at the levels of "valley" and "upper slope". At 5 Hz, the differences among the various classes are minimal, and beyond this value generally the categories that amplified more at low frequencies now show reduced amplification (e.g. "flat area"), and vice versa. As for Switzerland, here too the highest amplifications are generally related to the "flat area" category, but the "ridge" class shows markedly lower amplification factors. The "middle slope" group lies above "ridge" at low frequencies, and below at higher frequencies. When present, the "upper slope" class has low amplification values across the whole frequency band; the "valley" category, when available, de-amplifies at low-frequency, and then shows increasing amplification factors. The corresponding standard deviations (Figure 61) have the same trend observed for rock age and genesis classifications, i.e. they increase with frequency. Exceptions are the Swiss "flat area" (scales 60 – 340 m)," middle slope" (660 m) and "lower slope" (1140, 2020 m), which show high σ at low frequencies and a trough at 3.33 Hz.

We remark that the observations relevant to Figures 58-61 here are in agreement with the comments on the effectiveness of the classification proxies in subsection 5.3.2.

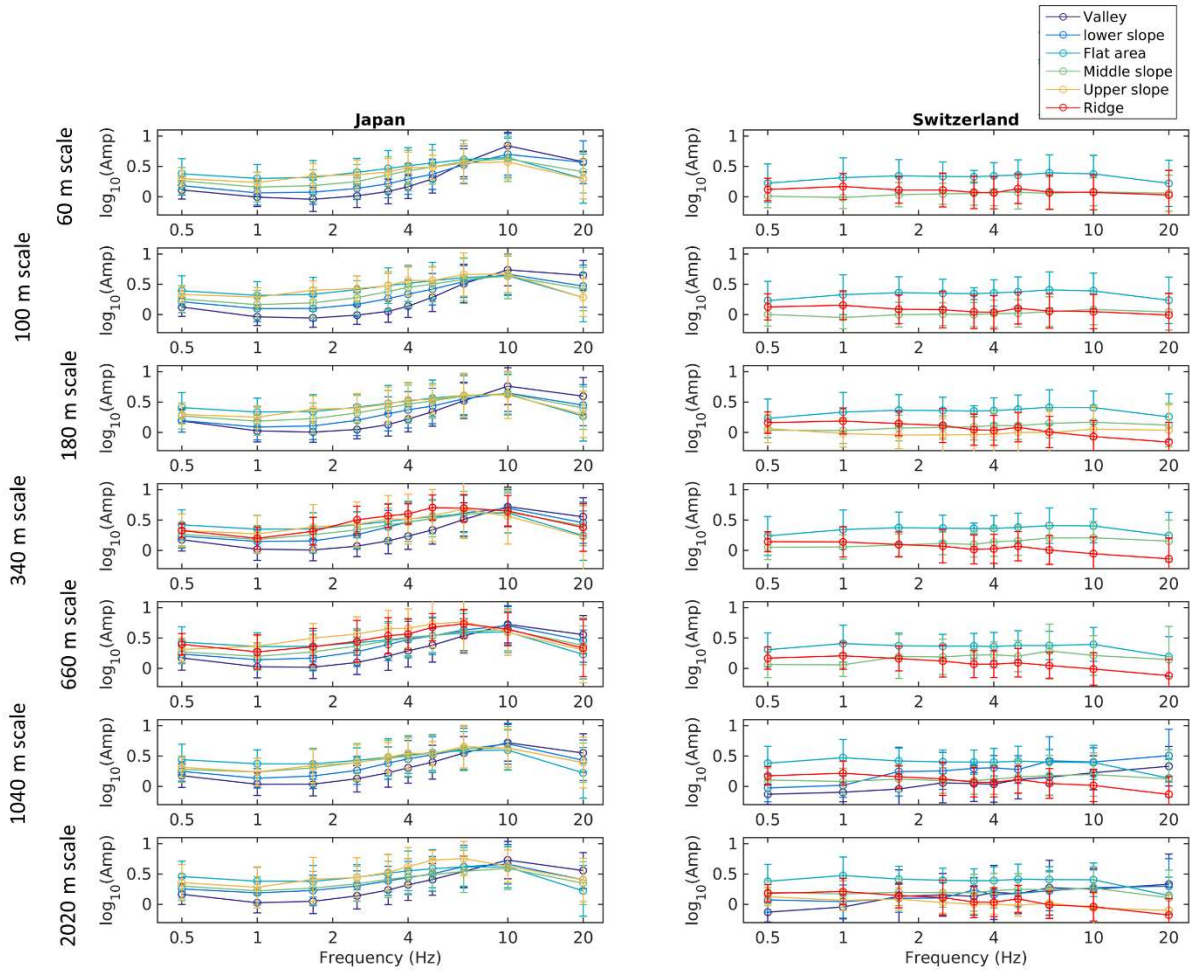

Figure 60 - Mean amplifications (circles) and standard deviations (error bars) for each topographic class, from Swiss and Japanese data, for each frequency abscissa. Missing data points indicate null or insufficient sample size (<10 samples).

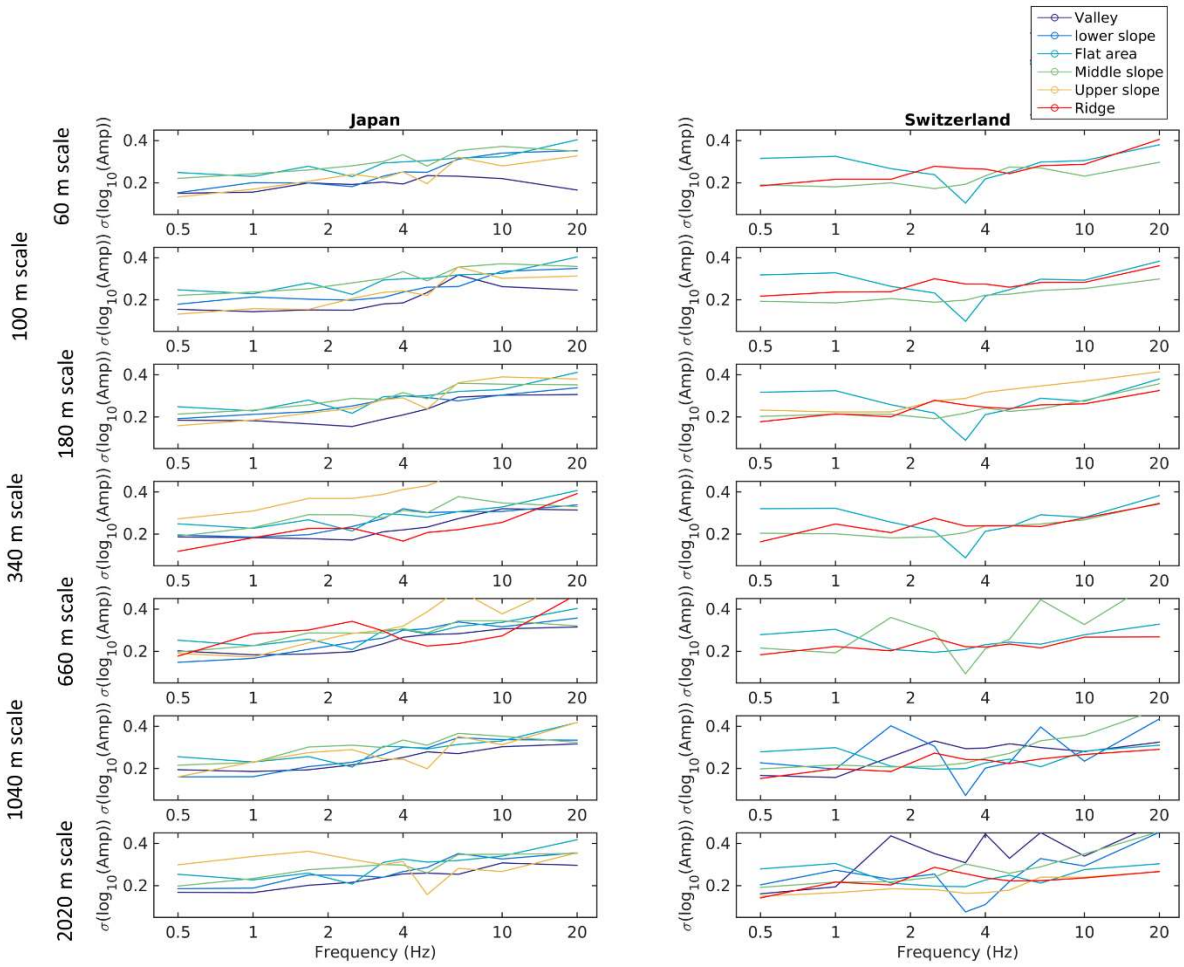

Figure 61 - Standard deviations for each topographic class, from Swiss and Japanese data, for each frequency abscissa. Missing classes indicate null or insufficient sample size (<10 samples).

To conclude, we can affirm that the rock age/genesis and topographical classifications generally do define consistent amplification trends for each of their subcategories, however these trends are in most cases different for Switzerland and Japan, with the exception of some common features. As observed earlier on for the continuous-variable proxies, topographical and geological categories have indeed some correlation with geo-mechanical parameters and hence amplification patterns, but these correlations appear to be region-dependent, i.e. not universally valid.

6 Neural network

As anticipated in previous chapters, in this section the relationship between site condition indicators and site amplification is investigated using a neural network structure, attempting to predict frequency-dependent amplification factors based on the proxy database. In detail, the targets of our analysis were:

1. To determine the prediction performance of various site condition proxies on frequency-dependent amplification factors
2. Based on the results of the neural network analyses, to rank the proxies in terms of prediction performance, frequency by frequency, and to find a 'best' proxy set for predicting frequency dependent amplification factors

The introduction of Neural networks into the science community goes back to the fifties. The perceptron concept was invented by Frank Rosenblatt (1958) as a probabilistic model for information storage in the brain. Interconnections between the neurons are activated or inhibited according to the stimulus arriving at a sensorial layer. The degree of activation (or weights) of the interconnection can be adjusted by comparing the response of the network to some known information ('target'). In the 'untrained' network the weights of the interconnections have some random values and are successively adjusted in a manner that the network finally responds in the desired way. Rosenblatt was able to proof the convergence of the learning, i. e., that – in linear problems - it is possible to adjust the network weights such that its response is close to the desired one. For the intriguing similarity of the computer based processing scheme to learning process encountered in brains those systems of interconnected neurons are often referred to as "Artificial Neural Networks" (hereafter referred to as NNs). However, these somewhat mystical terms lead to overly optimistic expectations, finally reflecting discredit on the whole field of research. Minsky and Papert (1969) reformulated the perceptron approach in rigorous terms of prediction calculus. Their harsh criticism, in particular with respect to limits of the approach in non–linear classification problems (impossibility to resolve the simple XOR problem), brought the perceptron concept almost to an eclipse. In the following decades it turned out that the limits can be overcome by considering more complex configurations and non-linear activation functions. Consequently, the method remains on the screen of researchers working on classification problems.

In seismology NNs are widely used for waveform classification tasks. Falsaperla, et al. (1996) applied NNs to automatically distinguish volcano seismic events recorded at Stromboli volcano. Recently, Spichak and Goidina (2016) applied NNs for establishing cross-correlations between seismic velocities and electric resistivity of rock. In the context of seismic site amplification, Boughdene Stambouli et al (2017) apply NNs to identify C_V (velocity contrast, defined as $V_{Smin}/V_{Sbedrock}$) as the best performing single proxies; Salameh (2016) underline the role of A_{0HV} as a good proxy for the sediments-to-bedrock impedance contrast, hence for site amplification. Motivated by these studies we fed site condition parameters as input to a neural network structure to predict frequency-dependent site amplification factors and to evaluate the relevance of various proxy sets for seismic site amplification prediction.

6.1 Theory

Figure 62 outlines the basic characteristics of a simple linear perceptron. Data are stored in an input vector $\mathbf{x}$, made up of the components x_i. In the jargon of artificial neural networks $\boldsymbol{x}$ is referred to the input layer. A weight w_i is applied to each of the x_i. In the neural network terminology, the lines representing the weights w_i are often referred to "synapses", whereas the nodes (both the input nodes x_i as well as the processing units, such as the "Σ") are "neurons". Finally, the sum of the weighted x_i is further transformed applying an activation function f (in this context f is linear). The output of the perceptron – after applying f – is compared to a desired output. During the learning phase weights w_i are adjusted in order to minimize the difference of the perceptron's output and the target. Training

can consist of an iterative scheme, or just be a simple operation of analytical calculus, as in the case of considering the mean square error.

In the Perceptron approach shown in Figure 62, we assumed that our data groups – at least in principle - can be separated by a linear function. The strategy of minimizing the squared error allows us to account for noise the presence of which may lead to a situation where the data groups cannot be separated linearly in a strict sense, i. e., we have to accept some misclassified samples. However, this strategy fails in problems that are intrinsically not solvable with linear discrimination functions. In case, that two classes cannot be separated by one single linear element, we have to insert a second element as shown in Figure 63. In the architecture of the perceptron this is achieved by adding a new layer of nodes ("neurons") and appropriate "synaptic" weights, obtaining a "Multilayer Perceptron". Here we have one input layer, a second layer – called the "hidden" layer –and the output. The hidden nodes can be referred to as "processing units", which become active under specific conditions. For the moment we assume a threshold or step activation function, and we assign -1 for negative values and 1 for positive values. It can be demonstrated (see Bishop 1995, Theodoridis and Koutrombas, 2009) that, applying the step activation function in the hidden units, at least two hidden layers are necessary for solving an arbitrarily complex classification problem. Even though any classification problem could be solved with a NN having at least two hidden layers (applying the step activation function in the nodes), those schemata are not very popular yet, as they entail many nodes and weights.

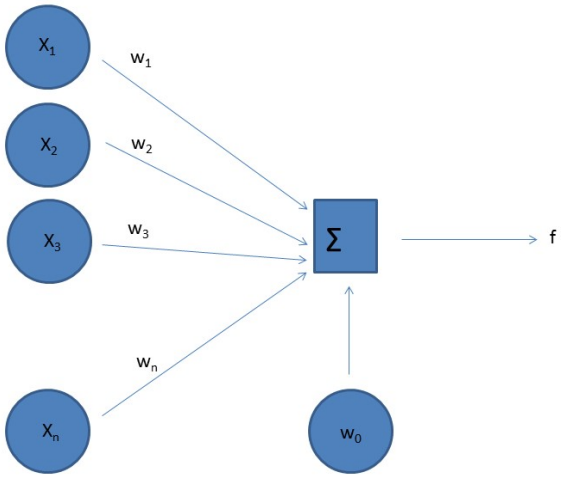

Figure 62 – Flow-chart of the basic perceptron model

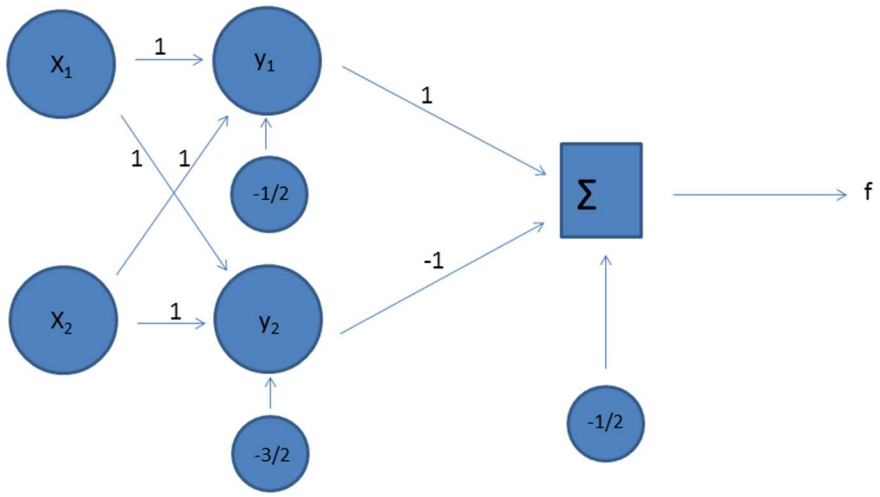

Figure 63 – NN with one hidden layer. Biases (constants) are represented in the smaller circles.

6.2 Assessing site proxies as predictors for site amplification using NNs

The general idea we follow in this approach is the modulation of the seismic action as a function of local geological conditions. By means of NNs we get a fully data driven site characterization without any preconception by the analyst. We are able to analyze a huge amount of proxy combinations, all parameters are correlated together and no prior knowledge on the functional form that describes inherent dependencies is required.

We would like to find the 'best' proxy-set that is most appropriate to predict frequency-dependent seismic site amplification. In order to achieve this goal a NN has to be learned from labelled training data. Having a trained NN, we evaluate the performance in two steps. First the performance of the network can be measured by the coefficient of determination R^2. The variance of the predicted variable is divided in the proportion that is predictable from input variables and the residual. Then R^2 corresponds to the predictable proportion. In the following we use R^2 to get a very rough estimate of the network performance and to estimate if the number of training data is sufficiently large to learn network parameters from available training data. In a second evaluation step we analyze the prediction performance on a test data set, which the network has not seen before. Here, the outputs of standard deviation of errors between target and network output are compared. That network (i.e. proxy-set) which gives the lowest STD performs best.

We use the following network architecture. The network is characterized by one hidden layer which neurons are activated based on the rectified linear unit function. The error between predicted and true target is calculated using the cross entropy criterion. Weights are adjusted using the Adam optimizer and a learning rate of 0.0001. The implementation of the NN is carried out by using PyTorch (www.pytorch.org). PyTorch is an open source, python based, machine learning framework that provides a flexible and comprehensive software library for all NN related task.

6.2.1 Input parameters

All parameters describing the NN (i.e. weights) have to be learned during the training phase from pre-labelled training data. A detailed overview on available training data is given in sections 3 and 4. In Table 11 we give a brief summary on the number of available sites in Switzerland and Japan. Especially for the direct proxies (proxies derived from measurements) the number of available training data is low.

Note, that while for Swiss sites, the full H/V curve is available, for Japanese sites, only f_0 values derived from earthquake data are available.

Table 11: Number of available sites for specific proxies in Switzerland and Japan.

Proxy Sets	Number of available sites in Switzerland	Number of available sites in Japan
Proxies derived from measured V_S profile: $V_{S10\text{-}20\text{-}30}$, $V_{Sberock}$, V_{Sm}, H800, C_v, C_{v10}, V_S^{QWL}, I_C^{QWL}	84	276
Proxies derived from H/V measurement: f_0	117	276
Topographical parameters: slope and TPI_{norm} at the seven scales 60 – 2020 m	145	648
Common dataset of indirect proxies: bedrock depth, % of coarse fraction, geological classifications	142	648

Firsts tests on the direct proxies using available training data result in very unsatisfying predictions. For Japanese sites, the value of R^2 on the training data did not exceed 0.6 while for Swiss sites, the predictions were even worse with an R^2 lower than 0.5 across all frequency ranges. Based on these results we conclude that training data are too sparse to estimate the network parameters reliably. In order to circumvent this problem, we propose two strategies

1. Merge data from Swiss and Japanese sites: Based on the results shown in chapter 5 data sets of direct proxies for Switzerland and Japan can be merged providing a sufficiently large number of training samples for the training NN; merged data set is comprised of 360 sites for proxies from V_S; measurements and 393 sites for H/V proxies. Indirect proxies were not merged as indicated by regression results. An 'indirect' network is learned for Japanese data only, as the number of 650 sites is sufficiently large to learn the network parameters.
2. Generation of surrogate data: For the Swiss sites uncertainties are available for the direct proxies, given by mean and standard deviation. From this information, surrogate data of direct proxies are sampled from a corresponding distribution. However, when using this approach, we may run into the problem of over fitting and further testing is needed.

In order to assess the prediction performance of individual proxies we subdivided the complete proxy set in subsets of proxies. Based on the results obtained in the regression approach we tested 12 different direct proxy subsets and three indirect proxy sets (Table 12). Note that in contrast to the regression approach the NN allows to test any proxy combination. For site-condition proxies in vector form (V_S^{QWL}, I_C^{QWL}), we correlated each of their frequency-dependent elements to the corresponding set of amplification factors referring to the same frequency.

Table 12: Proxy sets used as input for the NN

Type of proxy	Number of proxy set	Contained proxies
Direct proxies	1	V_{S30}
	2	V_{S30}, H800
	3	V_{S10}, V_{S20}, V_{S30},
	4	V_{S10}, V_{S20}, V_{S30}, H800, C_{V10}
	5	V_{S30}, f_0
	6	V_{S30}, H800, f_0
	7	V_{S10}, V_{S20}, V_{S30}, f_0
	8	V_{S10}, V_{S20}, V_{S30}, H800, C_{V10}, f_0
	9	V_{S10}, f_0
	10	V_{S10}, V_{S20}, f_0
	11	V_S^{QWL}, I_C^{QWL}
	12	V_S^{QWL}, $I_C^{QWL}f_0$
Indirect proxies	1	Rock genesis code, rock age, bedrock depth, % of coarse fraction
	2	TPI_{norm}, slope
	3	Combination of indirect proxy set 1 + 2

6.2.2 Output parameters

As anticipated, we conduct a systematic assessment of the sensitivity of the various site condition indicators towards local amplification at 10 selected frequency abscissae in the range 0.5 – 20 Hz. The target we aim to predict is frequency-dependent site amplification. We use a discretized version of the continuous amplification function (chapter 4). The amplification range 0.2 - 20 is subdivided in 25 bins, logarithmically spaced. Figure 64 shows the distribution of the amplification functions after the binning.

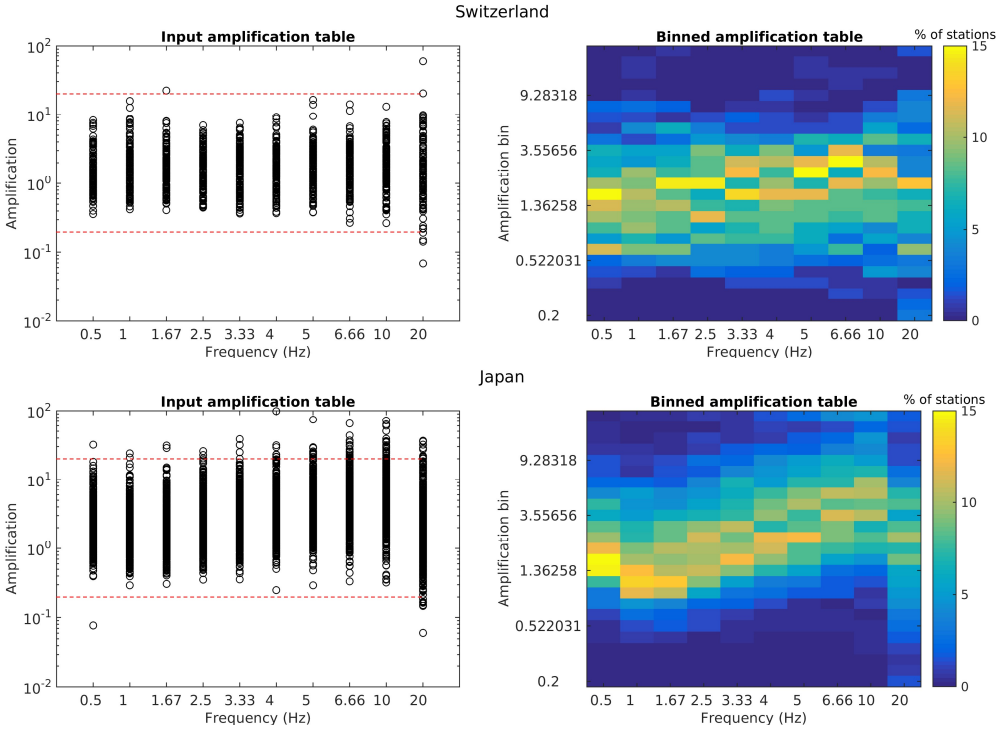

Figure 64 – Binning of empirical amplification functions for Switzerland and Japan.

Using this representation, the amplification function can be traced while crossing the frequency and amplification bins as shown in Figure 65. For each frequency band a separate network is trained. The 'activity' of each amplification bin is predicted by the NN, i.e. the probability that the corresponding bin is passed by the amplification function. Thus, in terms of Figure 65, the gray value of each bin at a specific frequency is predicted.

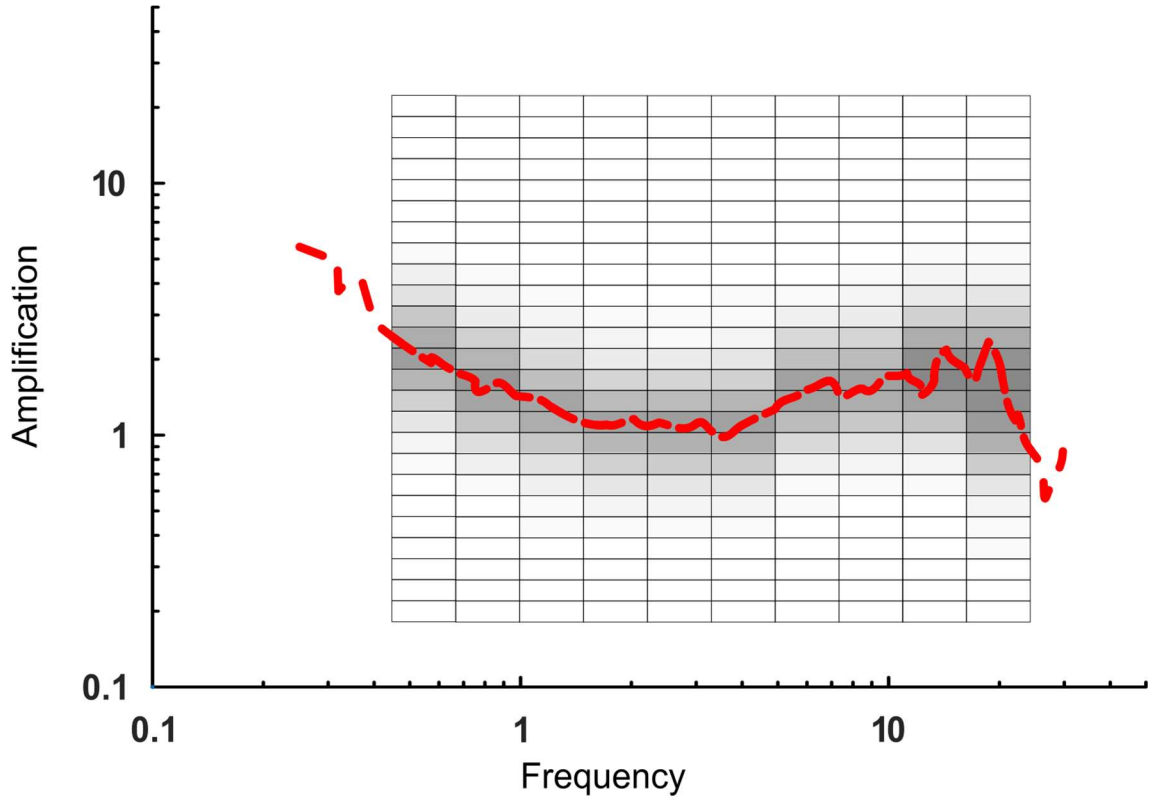

Figure 65 - Amplification function is binned in 25 logarithmically spaced amplification bins at each frequency band. Gray values of bins correspond to probability that the bin is actually crossed by the amplification function.

6.3 Results

Both data sets (direct and indirect) are divided in a training and validation data set and the performance of the NN is evaluated using cross validation. Here, 80 % of all data are used for training the NN and 20 % are used for testing the NN. For each tested proxy subset 100 runs, consisting of a training and a testing cycle, are carried out. For each run, the training data are selected randomly from the full data set. The non-selected sites are used as validation data set.
For the direct proxies, we present in the following the results using the merged data set (Swiss sites + Japanese sites) only. The work on the surrogate data is still in progress in order to ensure that data are independent and represent the true underlying data distribution.
For indirect proxies, we present results from Japanese data only, as for Switzerland the number of training samples is not sufficient.

6.3.1 Direct proxies

Figure 66 and summarize the results for the direct proxies. For each frequency band the prediction performance is shown for all proxy sets by means of deviation from the true bin. The deviation is multiplied by the probability of hitting this bin, obtaining a weighted distance measure.

The following conclusions can be drawn from Figure 66:

- The site condition parameter set that "performs" best on all frequencies is V_S^{QWL} (quarter-wavelength velocity) and I_C^{QWL} (quarter-wavelength impedance contrast). V_S30 performs acceptably in the medium frequency range (1.67Hz-6.66Hz). We highlight also the good performance of proxy set 8 (all direct proxies, except V_S^{QWL} and I_C^{QWL}) in the low and medium frequency bands.

- At high frequencies (10 Hz and 20 Hz), amplification is always overestimated from available proxies.
- For most proxy sets and frequency bands, the inclusion of f_0 does decrease the variance of amplification predictions, therefore it appears to better constrain the problem.
- The variance in amplification predictions is lowest in the intermediate frequency bands and increases at low and high frequencies.

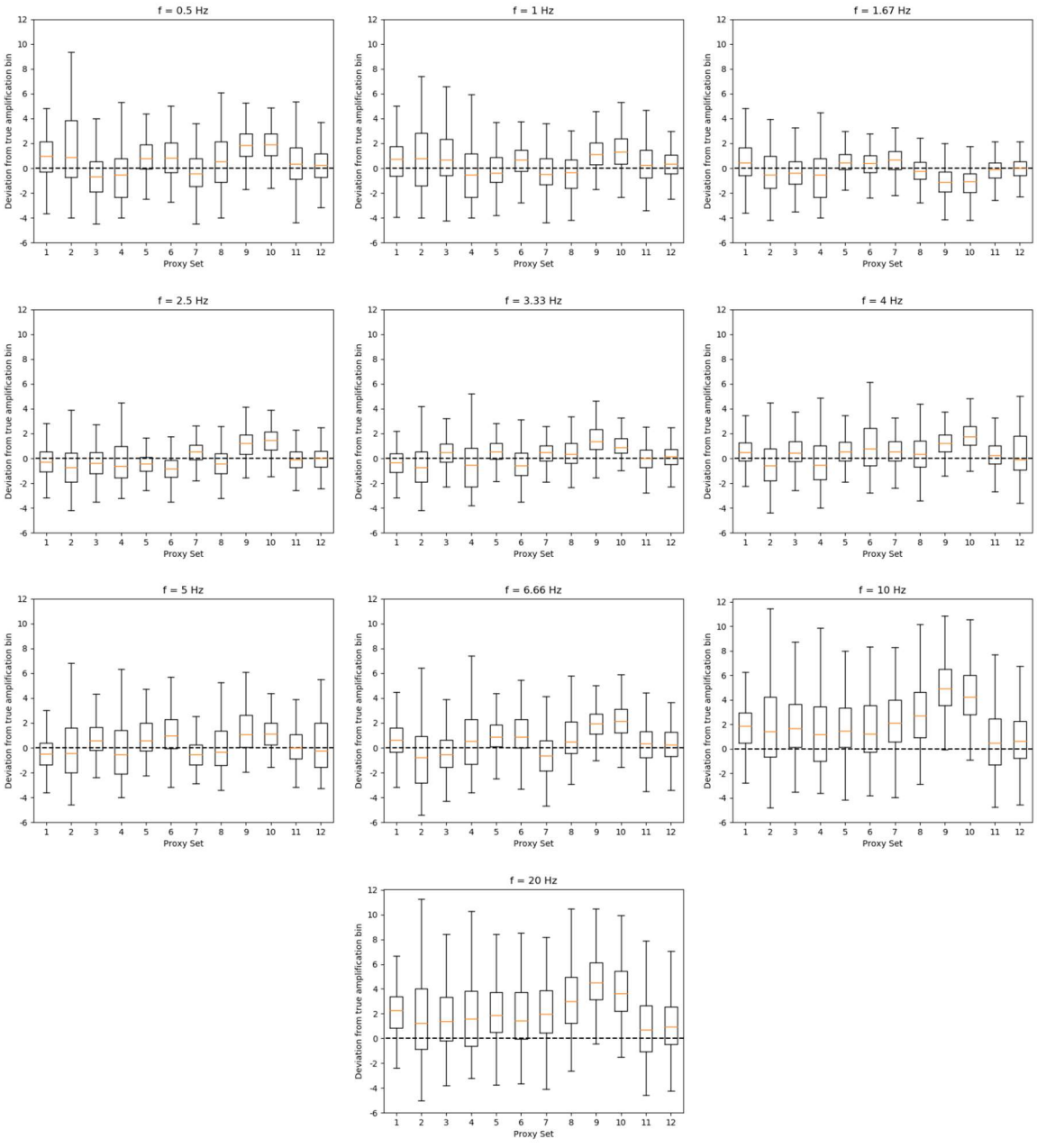

Figure 66 - Prediction performance of direct proxy sets (Table 12), represented as boxplots. The box extends from the lower to upper quartile values of the data, with a line at the median. The whiskers extend from the box to show the range of the data.

6.3.2 Indirect proxies

Figure 67 summarizes the results of prediction for the indirect proxies for Japan. For each frequency the prediction performance is shown for all proxy sets by means of deviation from the true bin. The deviation is multiplied by the probability of hitting this bin, obtaining a weighted distance measure.

The following conclusions can be drawn from Figure 67

- The site condition parameter set that “performs” best on a wide range of frequencies is the full available proxy set. Predictions from topographical proxies are in an acceptable range for low and medium frequency bands. From common indirect proxies (coarse fraction, geology) amplification is highly overestimated at all frequency bands.
- Predictions from common indirect proxies cover a very narrow amplification range at all frequencies.
- For all proxy sets there is no systematic decrease or increase of variance in prediction performance across all frequency bands.

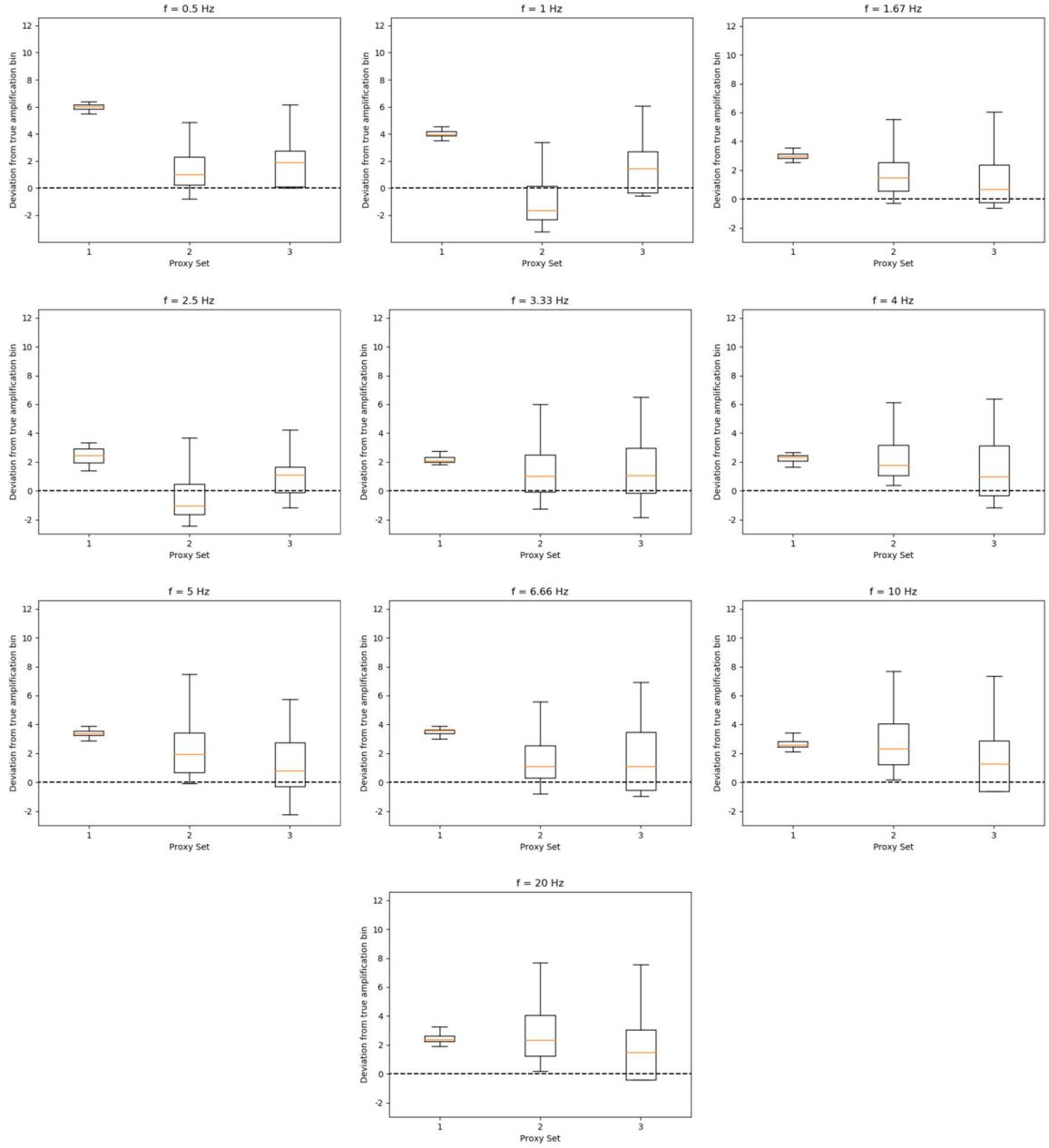

Figure 67 - Prediction performance of indirect proxy sets (Table 12), represented as boxplots. The box extends from the lower to upper quartile values of the data, with a line at the median. The whiskers extend from the box to show the range of the data.

We remark that all the results shown in this chapter are preliminary outcomes. Further testing is needed in order to verify the prediction performance.

7 Conclusions

This deliverable summarizes the work carried out in the framework of the task 7.4 of SERA project, "Towards improvement of site characterization indicators". We have tackled the broad topic of site condition parameters with a comprehensive approach; i) firstly, we have reviewed the state of the art and tracked the present research trends in the use of proxies; ii) secondly, to test their applicability at a wide scale, we have compiled an extensive database of site condition parameters, covering more than 1000 instrumented sites, and paired it with a companion dataset of empirically-derived local

amplification functions. In this phase of data collection, particular attention was dedicated to the harmonization of information derived from disparate sources and referring to different geological and geographical contexts; iii) in a third step, we have systematically assessed the sensitivity of site condition indicators towards local seismic amplification, ranking and collating their behaviour (also in different environments); iv) lastly, we have attempted to assess their potential for the prediction of local site response, resorting to a neural-network structure.

Each of the four phases of our work has yielded interesting outcomes.

- The *literature review* has evidenced the variety of site condition indicators introduced so far, the diversity of their sources (e.g. digital elevation models, geological maps, databases of geophysical measurements) as well as their purposes (e.g. for the prediction of local response, or the prediction of another indicator) and methods of applications (e.g. statistical correlation, spatial extrapolation, neural network).
- In the successive stage of *proxy database compilation* particular effort has been devoted to homogenizing site condition information deriving from different sources and referring to different territories (in our case, Switzerland and Japan). While in some cases the harmonization is quite straightforward (e.g. digital elevation models analysis), in others it requires thoughtful, and at times subjective, expert work (e.g. the definition of a common geological classification from maps with different origins and scales; in our case, we tackled the issue by relying on the lowest common denominator of rocks' age and genesis). This is a key aspect to bear in mind when planning the implementation of site condition indicators at the scale of Europe, where, for instance, no common geological description of the near-surface layers exists to this day – at least at an adequate resolution.
- The third part of our work consisted in *evaluating systematically the sensitivity of local amplification towards the collected sets of indicators*. The most relevant take-home messages are the following: i) as expected, proxies derived from in-situ geophysical measurements (e.g. V_{S30}, H800, f_0, A_0) perform in general better than parameters derived from local topography or geology (i.e. they are more "strongly" correlated with amplification). For the first group of indicators, the highest correlation is generally achieved with amplification factors in an intermediate frequency band (1.7 – 6.7 Hz); for the second group, at lower frequencies (0.5 – 3.3 Hz). Furthermore, proxies derived from in-situ measurements show similar correlations with local amplification even in different geological and geographical contexts; for topographical and geological indicators these correlations appear to have a local validity; ii) we recommend the extraction of topographical parameters at a set of increasing spatial scales. Larger scales are more closely related to amplification at low frequencies, smaller scales to higher frequencies. From our study it also appears that topographical proxies do not capture topographical amplification, but they are indirectly related to the local geophysical properties (and hence to stratigraphic amplification); iii) parameters derived from local geological models or databases generally show a stronger correlation with site amplification when compared to indicators from global models/databases; iv) Topographical and geological categorizations can be successful in classifying instrumented sites into subgroups with distinct amplification behaviors, particularly at low frequencies (≤3.3 Hz). Here again, these classifications seem to have local validity. The possibility to evaluate the effectiveness of categorization proxies depends on an adequate coverage of all classes (this condition was achieved in our case only by coarse classifications with less than 10 subgroups).
- Finally, we evaluated the prediction performance of various site condition parameter sets for frequency-dependent site amplification using a *neural network* structure. The most appropriate proxies to predict local site amplification across all frequency ranges are the quarter-wavelength parameters. Predictions based on V_S30 give satisfying results in intermediate frequency bands (1.67

– 6.66 Hz). The combination of all direct site condition indicators except the quarter-wavelength parameters performs well in low and intermediate frequency bands (≤6.66 Hz). Furthermore, including f0 seems to better constrain the prediction problem; the problem is best constrained in the intermediate frequency bands. The consistent overestimation of site amplification in high frequency bands (≥ 10 Hz) across all direct proxy sets needs to be further analyzed in the future. For indirect proxies, the prediction performance at all frequency bands shows best results when using all information that is available. While geologic site condition parameters alone highly overestimate the true amplification across the complete frequency range, topographic proxies perform acceptable in low and intermediate frequency bands. The prediction performance of indirect information (topography and geology) needs to be further assessed in the future.

As evidenced in the list above, the robustness of our inferences was limited in some cases (classification proxies, neural network) by the size of our joint proxy-empirical amplification database (collecting anyway around 800 sites). Therefore, a possible development of the present work could be constituted by the search and inclusion of additional sites, maybe broadening the geographical horizon to other European countries and the United States, with a focus on large-scale seismic hazard assessment. Obviously, this would require a further effort in harmonizing different data sources.

8 Acknowledgements

The authors would like to acknowledge a number of researchers that have contributed to the work presented herein. Colleagues from partner institutions of WP7 have indeed assisted in the preliminary phase of literature review, and offered their feedback and suggestions at the SERA meetings in Bucharest (April 2018), Thessaloniki (December 2018) and L'Aquila (March 2019), as well as via email: Pierre-Yves Bard, Cécile Cornou, Giovanna Cultrera, Giuseppe di Giulio Émeline Maufroy, Kyriazis Pitilakis, Evi Riga. We also thank Sean Ahdi (UCLA) and Alan Yong (USGS) for their recommendations on proxy-related publications. Finally, we thank our colleagues at ETH Vincent Perron and Francesco Panzera for their help in the compilation of fundamental frequencies dataset; Franziska Glüer for assisting in the interpretation of the Japanese geological map; Alba Zappone for providing the SAPHYR database.

9 References

Abrahamson N., G. Atkinson, D. Boore, Y. Bozorgnia, K. Campbell, B. Chiou, I. Idriss, W. Silva, and R. Youngs, 2008. Comparison of the NGA ground-motion relations. Earthquake Spectra 24(1), 45 – 66.

Ahdi S. K., Stewart, Ancheta, Kwak, and Mitra, 2017. Development of VS Profile Database and Proxy-Based Models for VS30 Prediction in the Pacific Northwest Region of North America. BSSA 107(4), 1781–1801

Andrade J.M., and M.G. Estevez-Perez, 2014. Statistical comparison of the slopes of two regression lines: A tutorial. Analystical Chimica Acta, 838, 1-12.

Bard P. Y. and M. Bouchon, 1985. The two-dimensional resonance of sediment-filled valleys. BSSA, vol. 75, no. 2, 519-541.

Bindi D., S. Parolai, F. Cara, G. Di Giulio, G. Ferretti, L. Luzi, G. Monachesi, F. Pacor and A. Rovelli, 2009. Site Amplifications Observed in the Gubbio Basin, Central Italy: Hint for Lateral Propagation Effects. BSSA, vol. 99, no. 2A, 741-760.

Bishop, C. M. (1995). Neural Networks for Pattern Recognition. Oxford University Press, Oxford, 482 pp.

Bo M., D. Bergamo, E. Calvi, M. Iacovino, Y. Falcone, E. Grisoglio and S. Salizzoni, 2019. Role of comprehensive geriatric assessment in low surgical risk older patients with aortic stenosis. Aging Clinical and Experimental Research. https://doi.org/10.1007/s40520-019-01228-0.

Boore D.M., E.M. Thompson, and H. Cadet, 2011. Regional Correlations of Vs30 and velocities averaged over depths less than and greater than 30 meters. BSSA, vol. 101. No. 6, 3046 – 3059.

Borcherdt, R. D., 1994. Estimates of Site-Dependent Response Spectra for Design (Methodology and Justification). Earthquake Spectra, vol. 10, no. 4, 1994.

Boughdene Stambouli A., P.Y. Bard, E. Chaljub, P. Moczo, J. Kristek, S. Stripajova, C. Durand, D. Zendagui, and B. derras, 2018. 2D/1D aggravation factors: from a comprehensive study to estimation with a neural-network model. 16th European Conference on Earthquake Engineering, Thessaloniki 18-21 June 2018.

Boughdene Stambouli A., D. Zendagui, P.Y. Bard and B. Derras, 2017. Deriving amplification factors from simple site parameters using generalized regression neural networks: implications for relevant site proxies. Earth, Planet and Space 69:99

Burjánek J., B. Edwards and D. Fäh, 2014. Empirical evidence of local seismic effects at sites with pronounced topography: a systematic approach. GJI, 197, 608-619.

Cadet H., P.Y. Bard, A.M. Duval, and E Bertrand, 2012. Site effect assessment using KiK-net data: part 2 – site amplification prediction equation based on f_0 and Vsz. BEE, vol. 10, no. 2 , 451-489.

Cadet H., P.Y. Bard, A. Rodriguez-Marek, 2010. Defining a Standard Rock Site: Proposition Based on the KiK-net Database. BSSA, vol. 100 no. 1, 172-195.

Cadet H., P.Y. Bard, A. Rodriguez-Marek, 2012. Site effect assessment using KiK-net data: Part 1. A simple correction procedure for surface/downhole spectral ratios. BEE, 10, 421-448

Cauzzi C., B. Edwards, D. Fäh, J. Clinton, S. Wiemer, P. Kästli, G. Cua, and D. Giardini, 2015. New predictive equations and site amplification estimates for the next-generation Swiss ShakeMaps. GJI, 200, 421-438.

Cauzzi, C., D. Fäh, J. Clinton and S. Wiemer, 2018. Calibration of global empirical models for real-time liquefaction prediction in Swizterland. 16th European Conference on Earthquake Engineering, Thessaloniki, 18-21 June 2018.

Cauzzi, C., D. Fäh, D.J. Wald, J. Clinto, S. Losey, and S. Wiemer, 2018. Shake Map-based prediction of earthquake-induced mass movements in Switzerland calibrated on historical observations. Natural Hazards, vol. 92, no.2, 1211–1235

CEN, 2004. Eurocode 8 (EC8): design of structures for earthquake resistance (EN 1998).

Cultrera G., V. De Rubeis. N. Theodoulidis, H. Cadet, and P.Y. Bard, 2014. Statistical correlation of earthquake and ambient noise spectral ratios. BEE, 12: 1493-1514

Davis, J. C., 2002. Statistics and Data Analysis in Geology. John Wiley and Sons, Inc.

Derras B., P.Y. Bard and F. Cotton, 2016. Site-condition proxies, Ground Motion Variability, and Data-Driven GMPEs: Insights from the NGA-West2 and RESORCE Data Sets. Earthquake Spectra, vol. 32, no.4 2027-2056.

Derras B., P.Y. Bard and F. Cotton, 2017. Vs30, slope, H800 and f0: performance of various site-condition proxies in reducing ground-motion aleatory variability and predicting nonlinear site response. Earth, Planet and Spaces, 59:133.

Edwards B., C. Michel, V. Poggi, and D. Fäh, 2013. Determination of Site Amplification from Regional Seismicity: Application to the Swiss National Seismic Networks. Seismological Research Letters, vol. 84, no. 4, 611-621.

Ermert L., V. Poggi, J. Burjánek J., and D. Fäh, 2014. Fundamental and higher two-dimensional resonance modes of an Alpine Valley. GJI, vol. 198, issue 2, 795-811.

Fäh, D., F. Kind and D. Giardini, 2001. A theoretical investigation of average H/V ratios. GJI, 145, 535-549.

Fäh, D., and G. Gassner-Stamm, 2014. Soil Classes (http://map.bafu.admin.ch) compared with Geophysical measurements (Vs30 and f0). Report SED/BAFU_Site/R/004/20140107.

Falsaperla, S., Graziani, S., Nunnari, G., Spampinato, S. (1996). Automatic classification of volcanic earthquakes by using Multi-Layered neural networks. Nat Hazards (1996) 13: 205. doi:10.1007/BF00215816.

Federal Office for the Environment (FOEN), 2017. Map of seismic subsoil categories according to the standard SIA 261.

Federal Office for Topography (Swisstopo), 2005. DHM25, Le modèle de terrain de l'ensemble de la Suisse.

Federal Office for Topography (Swisstopo), 2005. Geological Map of Switzerland 1:500000 (GK500).

Federal Office for Topography (Swisstopo), 2008. Overview of geomorphology, based on Atlas of Switzerland, Sheet 8, Geomorphology (1975)

Federal Office for Topography (Swisstopo), 2009. La Suisse Durant le dernier maximum glaciaire (GK500-LGM), by A. Bini, J. G. Buoncristiani, S. Couterrand, D. Ellwanger, M. Felber, D. Florineth, H.R. Graf, O. Keller, M. Kelly, C. Schluchter and P. Shoeneich.

Federal Office for Topography (Swisstopo), 2018. swissALTI3D, Le modèle de terrain à haute résolution de la Suisse.

Federal Office for Topography (Swisstopo), 2019. Thickness model of unconsolidated deposits.

Fujiwara H. et al., 2009. A study on Subsurface Structure Model for Deep Sedimentary Layers of Japan for Strong-motion Evaluation. Technical Note for the National Research Institute for Earth Science and Disaster Prevention. no. 337.

Geli L., P.Y. Bard, and B. Julien, 1988. The effect of topography on earthquake ground motion: A review and new results. BSSA, vol. 78, no. 1, 42 – 63.

Geological Survey of Japan, 2017. Seamless Digital Geological Map of Japan (1:200000). Copyright 2003-2017 Geological Survey of Japan, AIST.

GeoExpert ag, 2009. Seismic Shear Wave Velocity Determination and Hybrid Seismic Surveying at 20 Swiss Seismological Service Stations in Switzerland. Report for PEGASOS Refinement Project: SP2 – Ground Motion Characterization. Contract no. PMT-VT-1032.

Hassani B. and G. M. Atkinson, 2016. Applicability of the Site Fundamental Frequency as a VS30 Proxy for Central and Eastern North America. BSSA, vol. 106 (2), 653–664

Hengl T., J. Mendes de Jesus, G.B.M. Heuvelink, M. Ruiperez Gonzalez, M. Kilibarda, A. Blagotic et al., 2017. SoilGrids250m: Global gridded soil information based on machine learning. PLoS ONE 12(2) e0169748.

Hollender F., C. Cornou, A. Dechamp, K. Oghalaei, F. Renalier, E. Maufroy, C. Burnouf, S. Thomassin, M. Wathelet, P.Y. Bard, V. Boutin, C. Desbordes, I. Douste-Bacqué, L. Foundotos, C. Guyonnet-Benaize, 2017. Characterization of site conditions (soil class, V_{S30}, velocity profiles) for 33 stations from the French permanent accelerometric network (RAP) using surface-wave methods. BEE, vol. 16, no. 6, 2337-2365

Holt J., et al., 2017. Improvement of 1D Site Velocity Profiles for yje KiK-net network. SED PSHA Workshop, Lenzburg, Switzerland, 5-7th September 2017.

Holzer T.L., A. C. Padovani, M.J. Bennet, T.E. Noce, and J.C. Tinsley. Mapping NEHRP Vs30 Site Classes. Earthquake Spectra, vol. 21, no. 2 , 253-370.

Joyner, W.B., 2000. Strong Motion from Surface Waves in Deep Sedimetary Basins. BSSA, 90, 6B, S95-S112.

Kuo C. H., K.L. Wen, H. H. Hsieh, C.M. Lin, T. M. Chang, and K.W. Kuo, 2012. Site classification and Vs30 estimation of free-field TSMIP stations using the logging data of EGDT. Engineering geology, 129-130, 68-75.

Kwak D., S. J. Brandenberg, A. Mikami, J. P. Stewart, 2015. Prediction Equations for Estimating Shear-Wave Velocity from Combined Geotechnical and Geomorphic Indexes Based on Japanese Data Set. BSSA; 105 (4): 1919–1930.

Kwok O. L. A., J.P. Stewart, D.Y. Kwak, P.L. Sun, 2018. Taiwan-specific Model for Vs30 Prediction Considering Between-Proxy correlations. Earthquake Spectra, vol. 34, issue 4, 1973-1993.

Lee S.J., Y.C. Chan, D. Komatitsch, B.S. Huang, and J. Tromp, 2009. Effects of Realistic Surface Topography on Seismic Ground Motion in the Yangminshan Region of Taiwan Based Upon the Spectral-Element Method in the LiDAR DTM. BSSA, vol. 99, no. 2A, 681-693.

Lemoine, A., J. Douglas and F. Cotton, 2012. Testing the applicability of correlations between topographic slope and Vs30 for Europe. BSSA, vol. 120, no. 6, 2585-2599.

Lovati S., M.K.H. Bakavoli, M. Massa, G. Ferretti, F. Pacor, R. Paolucci, E. Haghshenas, and M. Kamalian, 2011. Estimation of topographical effects at Narni ridge (central Italy): comparisons between experimental results and numerical modeling. BEE, 9, 1987-2005.

Martin G.R. and R. Dobry, 1994. Earthquake site response and seismic code provisions. NCEER Bull. 8 (4) 1-6.

Matsuoka M. and K. Wakamatsu, 2013. Nationwide 7.5 Arc Second Japan Engineering Geomorphologic Classification Map and Vs30 Zoning. Journal of Disaster Research, vol. 8 no. 5 904-911.

Maufroy, E., V. M. Cruz-Atienza, F. Cotton, and S. Gaffet, 2015. Frequency-scaled curvature as proxy for topographic site-effect amplification and ground-motion variability. BSSA, vol. 105, no. 1, 354-367

Minsky, M. L., Papert, S. A. (1969). Perceptrons. MIT Press, Cambridge, MA., U.S.A (1990).

Nakamura S., 1989. A Method for Dynamic Characteristics Estimation of Subsurface using Microtremor on the Groud Surface. Quarterly Report of RTRI, vol. 30 no. 1, 25-33.

Nejad M. M., M. S. Momeni, and K. N. Manahiloh, 2018. Shear wave velocity and soil type microzonation using neural networks and geographic information system. SDEE, 104, 54-63.

Ono Y., J. Schulmeister, F. Lehmkuhl, K. Asahi, and T. Aoki, 2004. Timings and causes of glacial advances across the PEP-II transect (East Asia to Antarctica) during the last glaciation cycle. Quaternary International, 118/119, 55-68.

Ono Y., T. Aoki, H. Hasegawa, and L. Dali, 2005. Mountain glaciation in Japan and Taiwan at the global Last Glacial Maximum. Quaternary International 138-139, 79-92.

Peel N., and S. Kuys, 2012. Gait Speed as a Measure in Geriatric Assessment in Clinical Settings: A Systematic Review. Journal of Gerontology, 68 (1), 39-46.

Pessina V., and E. Fiorini, 2014. A GIS procedure for fast topographic characterization of seismic recording stations. SDEE, 63, 248-258.

Pitilakis K. D., K.A. Makra, and D.G. Raptakis, 2001. 2D vs 3D site effects with potential applications to seismic norms: the case of EUROSEISTEST and Thessaloniki. In: Proceesings of the XVth ICSMGE, Istanbul, 123-133.

Poggi V., J. Burjanek, C. Michel and D. Fäh, 2017. Seismic site-response characterization of high-velocity sites using advanced geophysical techniques: application to the NAGRA-net. GJI, vol. 210, no. 2, pp. 645-659.

Poggi V., B. Edwards and D. Fäh, 2011. Derivation of a Reference Shear-Wace Velocity Model from Empirical Site Amplification. BSSA, vol. 101, no. 1, 258-274.

Poggi V., B. Edwards and D. Fäh, 2012a. Characterizing the vertical to horizontal ratio of ground-motion at soft sediment sites. BSSA, 102, 2741-2756.

Poggi V., B. Edwards and D. Fäh, 2012b. The quarter-wavelength average velocity: a review of some past and recent application developments. 15th WCEE, Lisbon 2012.

Poggi V., B. Edwards and D. Fäh, 2013. Reference S-wave velocity profile and Attenuation Models for Ground-Motion Prediction Equations: Application to Japan, BSSA, vol. 103, no. 5, 2645-2656.

Poggi V. and D. Fäh, 2010. Estimating Rayleigh wave particle motion from three component array analysis of ambient vibrations. GJI, 180, no. 1, 251-267.

Poggi V. and D. Fäh, 2015. A proposal for horizontal and vertical elastic design spectra: input for the new Swiss code for dams. SED Technical Report SED/BFE/R/01/30072015

Reigner, J., B. Derras, P.Y. Bard, and H. Cadet, 2018. Non-linear modulation of site response: sensitivity to various loading parameters and site proxies using a neural network approach. Abstract S29-1033, ESC 2018 Malta.

Rey S., Agathe Roullé, T. Dewez, A. Hohmann, S. Auclair, et al.., 2011. Cartographie automatique des classes de sol á l'échelle régionale á partir d'un modèle numérique de surface. 8ème Colloque AFPS, Vers une mâıtrise durable du risque sismique, Sep 2011, Champs-sur-Marne, France.

Rodriguez-Marek A, J.D. Bray, N. A. Abrahamson, 2001. An empirical geotechnical seismic site response procedure. Earhquake Spectra, 17 (1) 65-87.

Rosenblatt, F. (1958) The Perceptron: A Probabilistic Model for Information Storage and Organization in the Brain. Cornell Aeronautical Laboratory, Psychological Review, 65, 386-408.

Salameh C., P.Y. Bard, B. Guillier, J. Harb, C. Cornou and M. Almakari, 2016. Using Ambient Vibration Measurements for Risk Assessment at an Urban Scale: from Numerical Proof of Concept to a Case Study in Beirut (Lebanon). 5th IASPEI/IAEE International Symposium: Effects of Surface Geology on Seismic Motion, August 15-17 2016.

Savvaidis A., K. Makr, N. Klimis, E. Zargli, A. Kiratzi, N. Theodoulidis, 2018. Comparison of Vs30 using measured assigned and proxy values in three cities in Northern Greece. Engineering Geology, 239, 63 – 78.

Società svizzera degli ingegneri e degli architetti (SIA), 2014. SIA 261 Azioni sulle strutture portanti. Copyright © 2014 by SIA Zurich

Spichak, V. and Goidina, A. G. (2016). Neural Network Estimate of Seismic Velocities and Resistivity of Rocks from Electromagnetic and Seismic Sounding Data. Izvestiya, Physics of the Solid Earth, 52, 371-381. doi: 10.1134/S1069351316030125.

Stolte A. C., B. R. Cox, and R.C. Lee, 2017. An Experimental Topographic Amplification Study at Los Alamos National Laboratory Using Ambient Vibrations. BSSA, vol. 107, no. 3, 1386-1401.

Thompson E. M., D. J. Wald, and C. B. Worden, 2014. A Vs30 Map for California with Geologic and Topographic Constraints. BSSA, vol. 104, no. 5, 2313-2321

Thirumalai K., A. Singh and R. Ramesh, 2011. A Matlab code to perform weighted linear regression with (correlated or uncorrelated) errors in bivariate data. Journal Geological Society of India, vol. 77, 377 – 380.

Vilanova S. P., J. Narciso, J. Carvalho, I. Lopes, M. Quinta-Ferreira, C. C. Pinto, R. Moura, J. Borges, and E. S. Nemser, 2018. Developing a Geologically Based Vs30 Site-Condition Model for Portugal: Methodology and Assessment of the Performance of Proxies. BSSA, vol. 108, no. 1, 322-337

Wakamatsu K., M. Matsuoka and K. Hasegawa, 2006. GIS-based nationwide hazard zoning using the Japan engineering geomorphologic classification map. Proceedings of the 8th US National Conference on Earthquake Engineering, April 18-22, 2996, San Francisco, Paper no. 849.

Wald D. J. and T. I Allen, 2007. Topographic Slope as a Proxy for Seismic Site Conditions and Amplification. BSSA, vol. 97, no. 5, 1379-1395.

Welch, B. L., 1947. The generalization of Student's problem when several different population variances are involved. Biometrika, 34, (1-2), 28 – 35.

Willis C.J., M. Petersen, W.A. Bryant, M. Reichle, G.J. Saucedo, S. Tan, G. Taylor and J. Treiman, 2000. A Site-condition map for California based on geology and Shear wave velocity. BSSA, 90, 6B, S187-S208.

Xie J., P. Zimmaro, X. Li, Z. Wen, and Y. Song, 2016. VS30 empirical prediction relationships based on a new soil-profile database for the Beijing Plain Area, China. BSSA. 106(6), 2843–2854

Yong A., S. E. Hough, J. Iwahashi, and A. Braverman, 2012. A Terrain-Based Site-Conditions Map of California with Implications for the Contiguous United States. BSSA vol. 102, no. 1, 114-128.

Zappone A. and R. H. C. Bruijn, 2012. The Swiss Atlas of Physical Properties of Rocks (SAPHYR). Rapport Annuel 2012, Commission Suisse de Géophysique

Zhu J., L. G. Baise, E. M. Thompson, 2017. An Updated Geospatial Liquefaction Model for Global Application. BSSA; 107 (3): 1365–1385

Zhu J., D. Daley, L. G. Baise, E. M. Thompson, D. J. Wald, and K. L. Knudsen, 2015. A geospatial Liquefaction Model for Rapid Response and Loss Estimation. Earthquake Spectra, vol. 31, no. 3, 1813-1837.

Contact

Project lead	ETH Zürich
Project coordinator	Prof. Dr. Domenico Giardini
Project manager	Dr. Kauzar Saleh
Project office	ETH Department of Earth Sciences
	Sonneggstrasse 5, NO H-floor, CH-8092 Zürich
	sera_office@erdw.ethz.ch
	+41 44 632 9690
Project website	www.sera-eu.org